LASERLAB Amsterdam

Advances in OCT for biological imaging

Johannes F. de Boer*,

Physics Department, VU University, Amsterdam
and Rotterdam Ophthalmic Institute, Rotterdam
Director LaserLaB Amsterdam

Formerly Harvard Medical School and Wellman Center
of Photomedicine, Massachusetts General Hospital,
Massachusetts Eye and Ear Infirmary

*Commercial interest: Intellectual property

Wellman Optical Diagnostics Group

R.O.I.
rotterdams oogheelkundig instituut
rotterdam ophthalmic institute

vrije Universiteit amsterdam

In this lecture:

- **Introduction into OCT**
- **Signal to noise ratio**
- **Spectral/Fourier domain sensitivity advantage**
- **OFDI/Swept Source OCT – Laser designs**
- **Doppler OCT**
- **Polarization Sensitive OCT**
- **Clinical Examples**

The impact of physics on imaging in healthcare

Anna Berthe Röntgen: Hand mit Ringen
Wilhelm Röntgen's first "medical" x-ray,
of his wife's hand,
taken on 22 December 1895

X-Ray, CT, MRI, PET, Ultrasound

These techniques are a mainstay of medical imaging

Translational Research

Translating discoveries to other fields

Röntgen immediately translated the discovery of X-rays to medicine

Nowadays, that takes a long path through ethical and safety regulations

The key to success is a good knowledge of outstanding problems and

Close collaboration with clinicians

Optics in Medicine

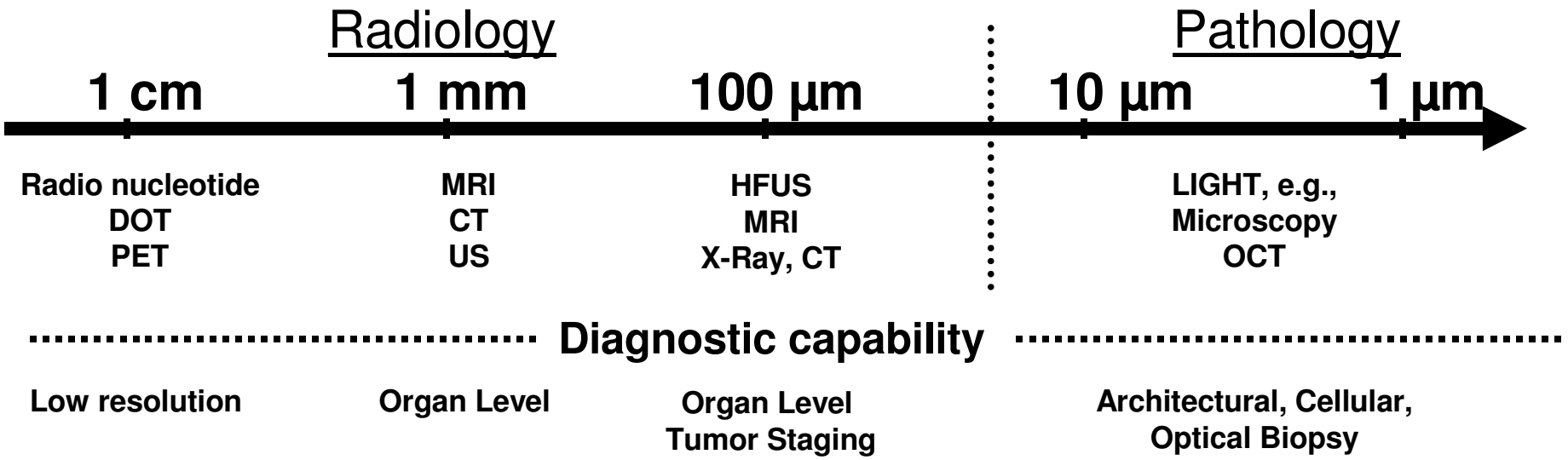

Histopathology is the golden standard especially for cancer diagnosis

Only optical technique approach cellular resolution

DOT: Diffuse Optical Tomography; PET: Positron Emission Tomography;
MRI Magnetic Resonance Imaging; CT: Computed Tomography; US: Ultra Sound;
HFUS: High Frequency Ultra Sound; OCT: Optical Coherence Tomography.

Currently used medical imaging methods

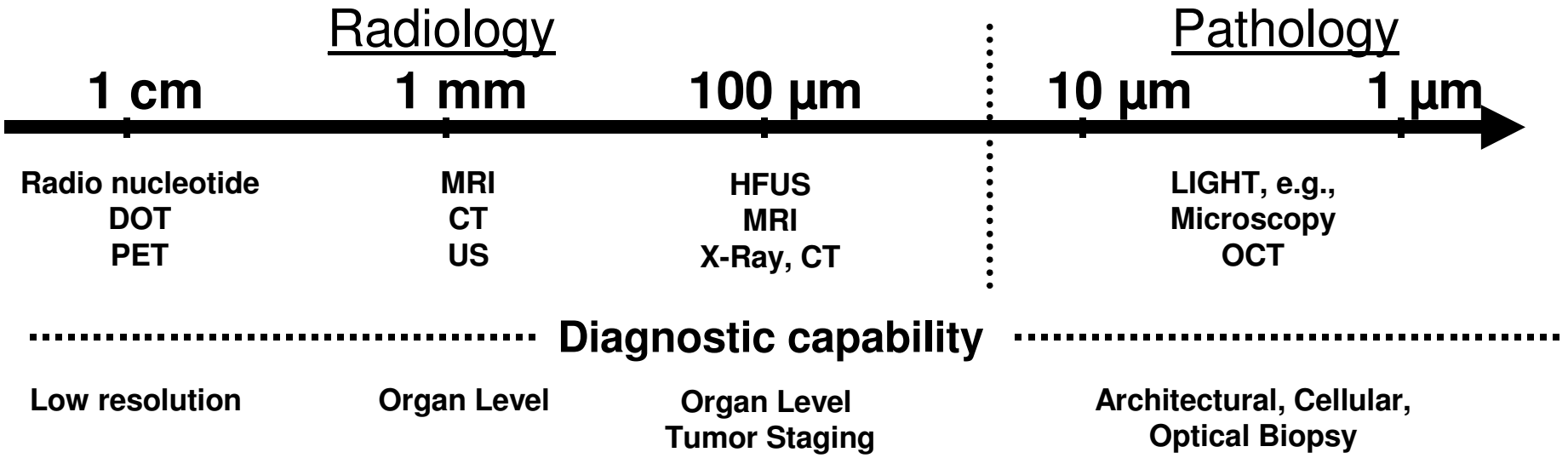

Histopathology is the golden standard especially for cancer diagnosis

DOT: Diffuse Optical Tomography;
PET: Positron Emission Tomography;
MRI Magnetic Resonance Imaging;
CT: Computed Tomography;
US: Ultra Sound;
HFUS: High Frequency Ultra Sound;
OCT: Optical Coherence Tomography.

Measurements

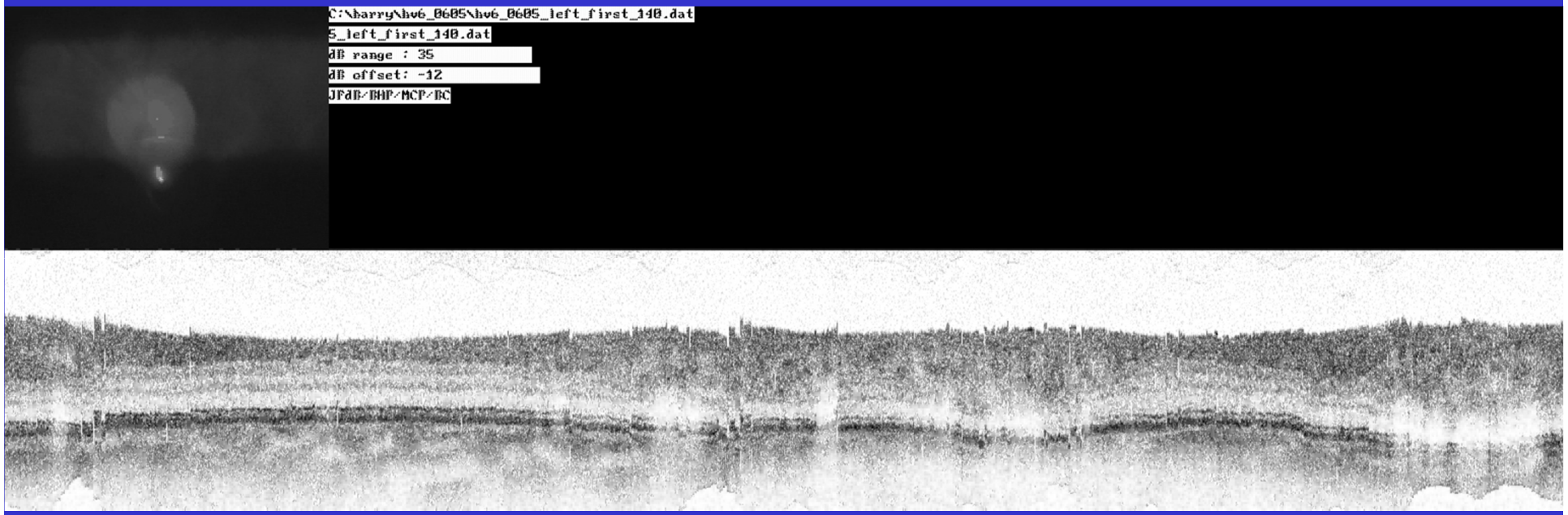

Example:

- 1 OCT B-scan in 6 s
- 1536 A-lines per B-scan
- 1024 pixels / A-line
- dynamic range ~35 dB

- resolution in depth 6 µm
- resolution in width ~ 20-30 µm
- 32 video frames / 6 s
- B-scans post processed to remove motion artifacts

First video rate images of the human retina (2003-2004)

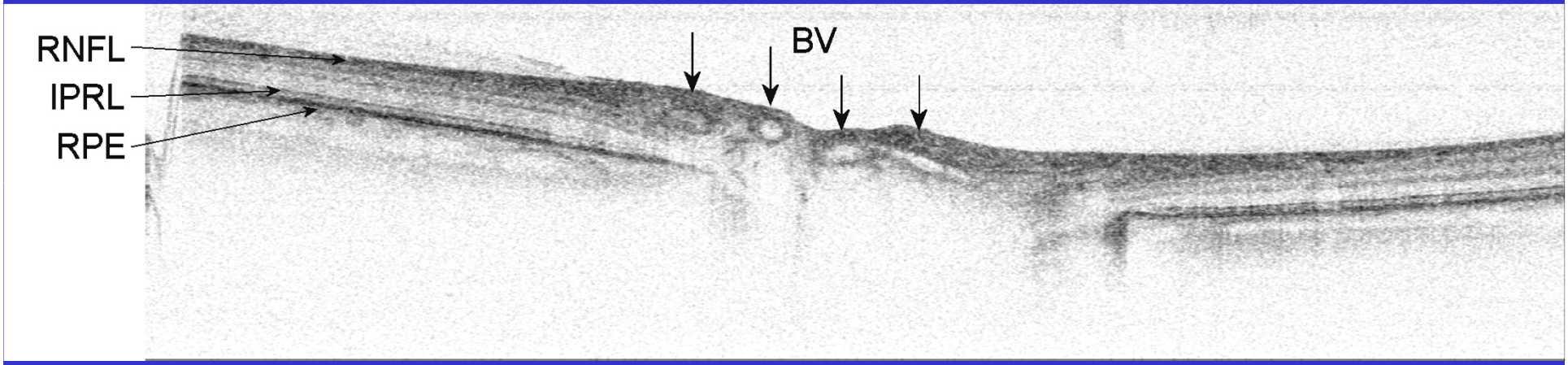

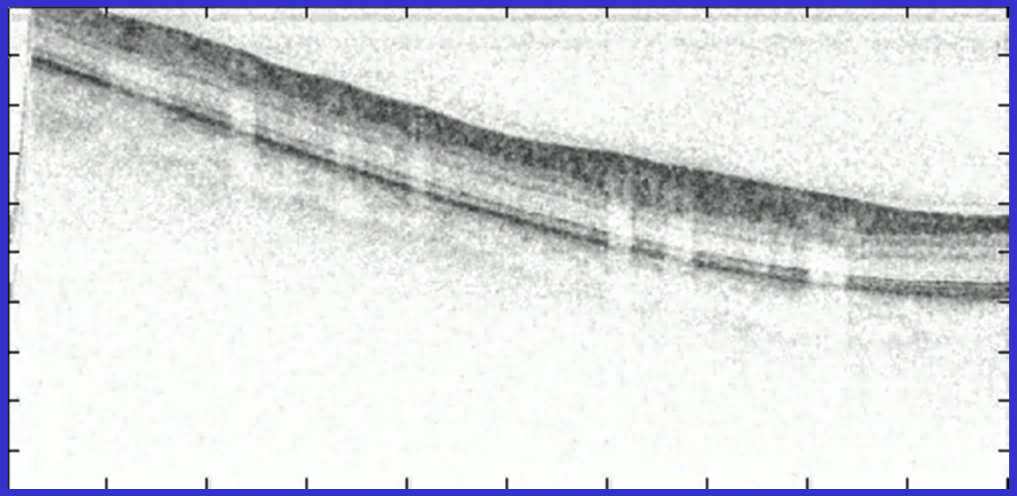

2 x magnified

N. A. Nassif *et al.*, Opt. Express 12, 367-376 (2004)

Optical Coherence Tomography

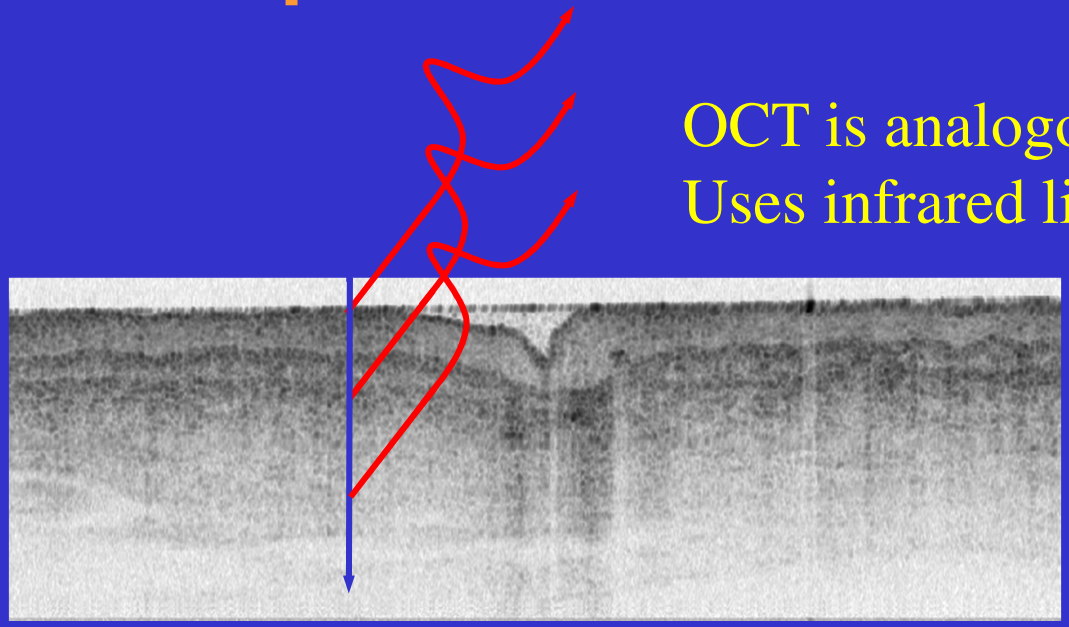

OCT is analogous to ultrasound imaging
Uses infrared light in stead of sound

Speed of sound ~ 1480 m/sec (in water)
Speed of light – 3×10^8 m/sec

Human skin
5 mm wide x 1.6 mm deep
Resolution: 10-30 μm

Interferometry
is used to measure
small time delays
of scattered photons

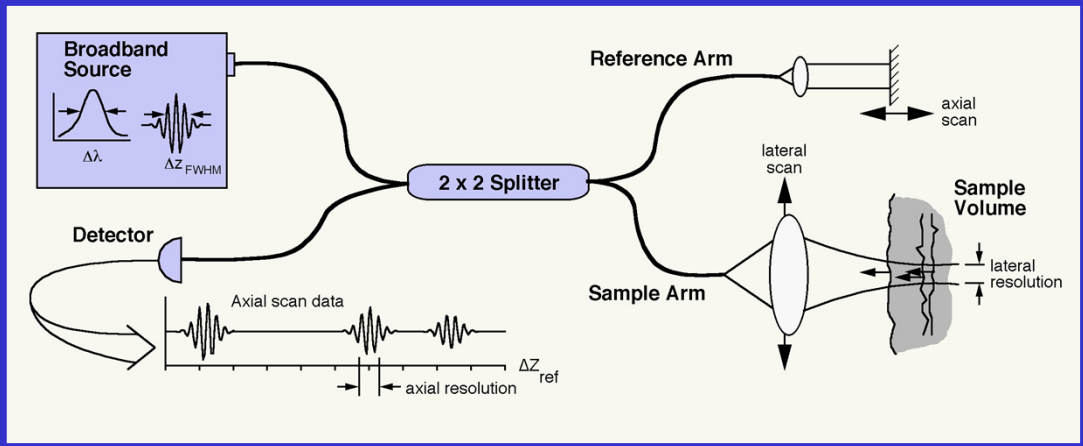

Principle of OCT

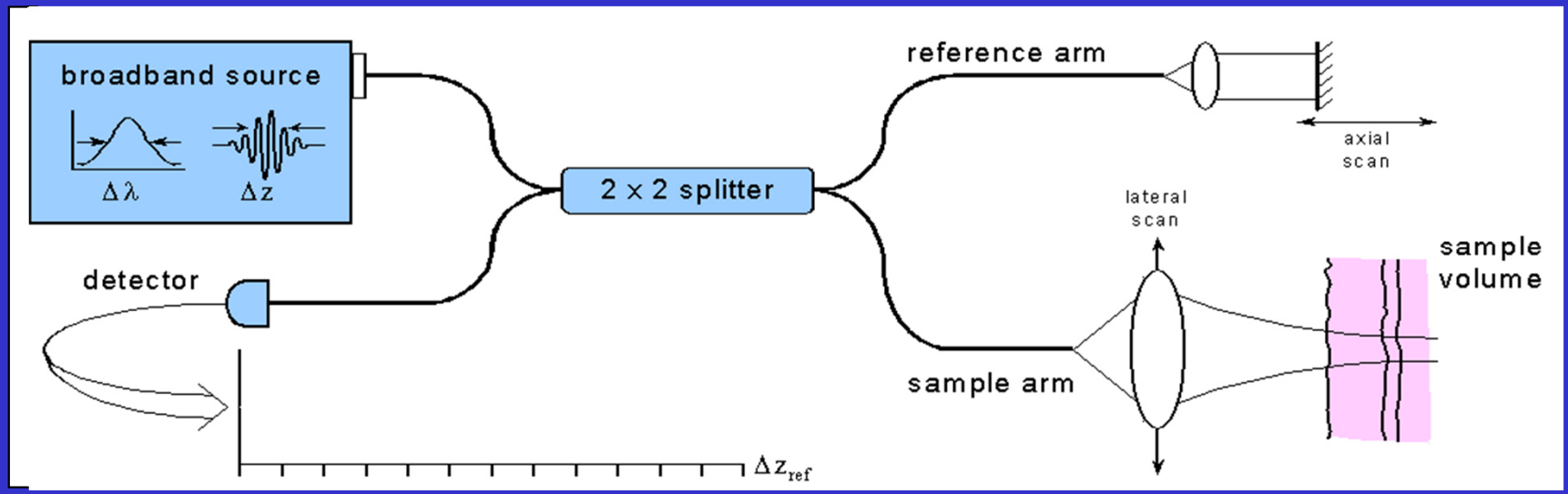

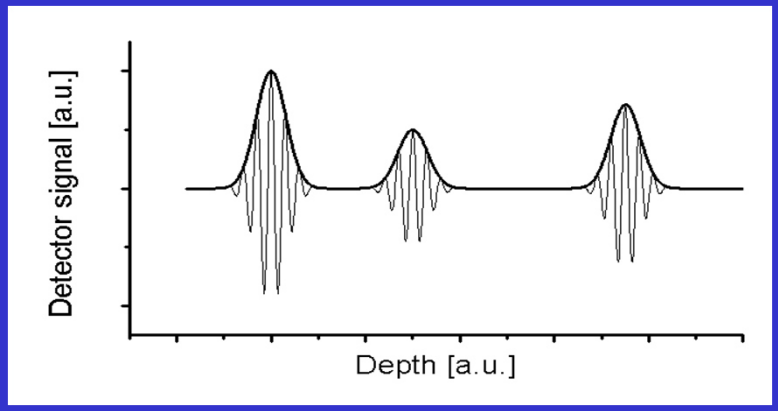

B-Scan

A-line

Michelson Interferometer

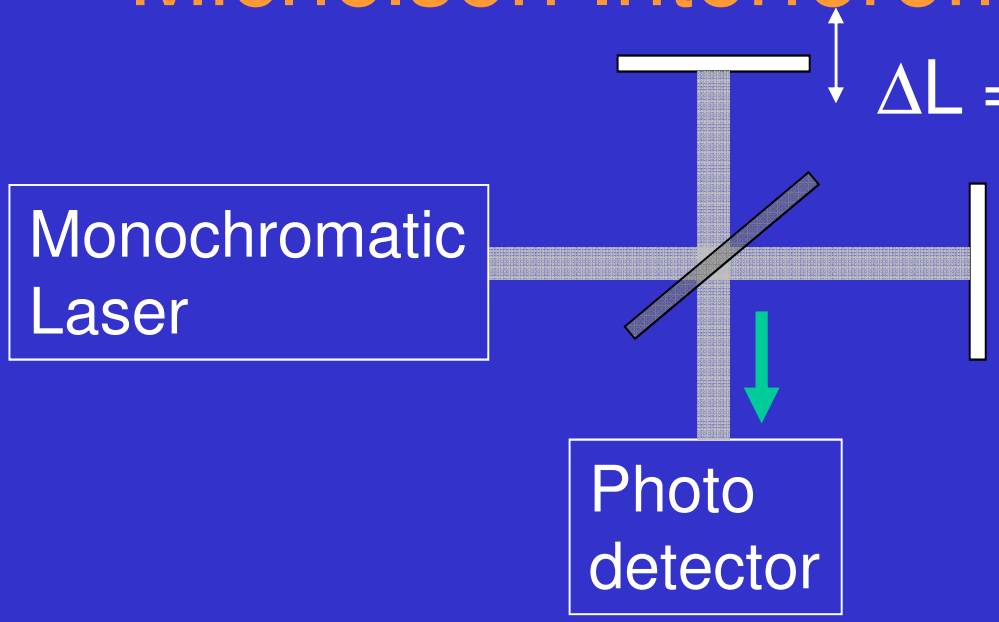

$$\Delta\phi = k\,\Delta L$$

$$I = I_0 \cos^2(\Delta\phi)$$

$$I = I_0 \cos^2(ft)$$

$$f = 2v/\lambda$$

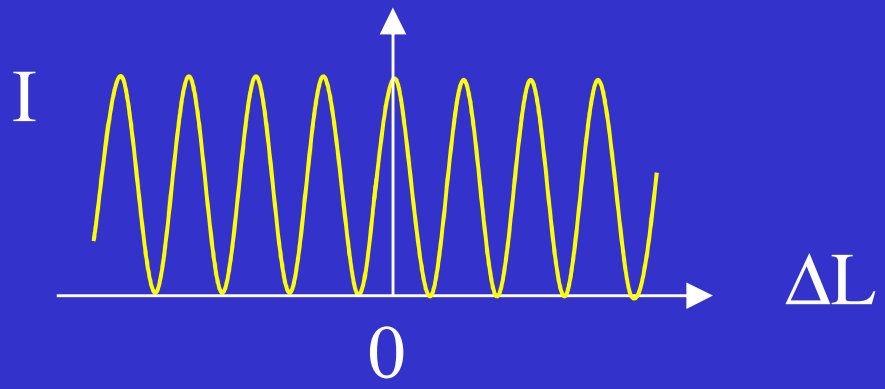

Low-coherence Interferometer

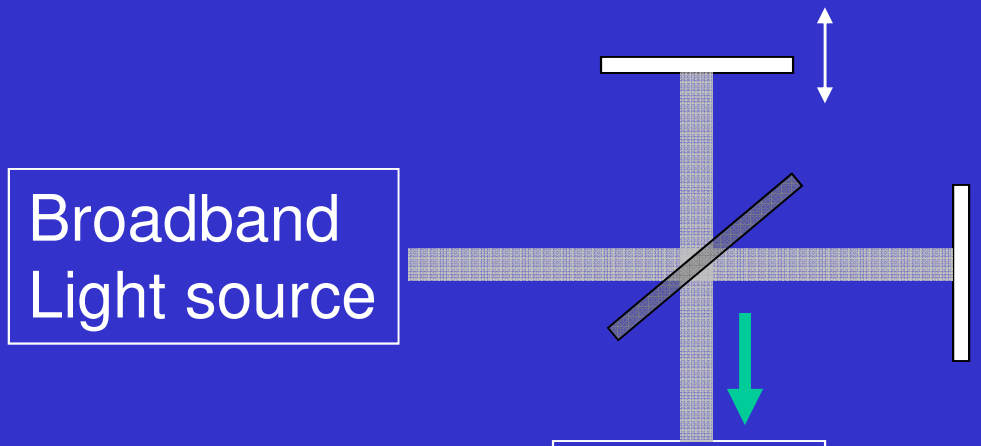

$$I = I_0 \cos^2(\Delta\phi)\ \mathbf{e}_1 \cdot \mathbf{e}_2\ \Gamma(\Delta L)$$

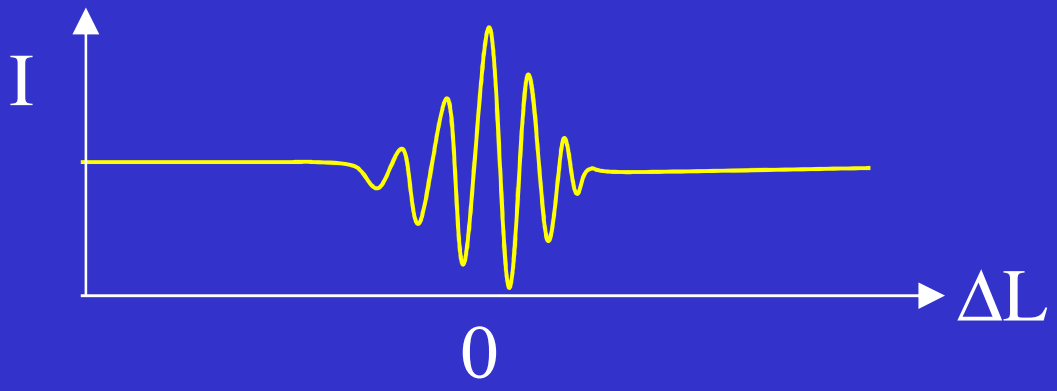

Low Coherence Fringe

$$FWHM = L_c = \frac{2\lambda_0^2 \ln 2}{\pi \Delta\lambda} = \frac{0.44\lambda_0^2}{\Delta\lambda}$$

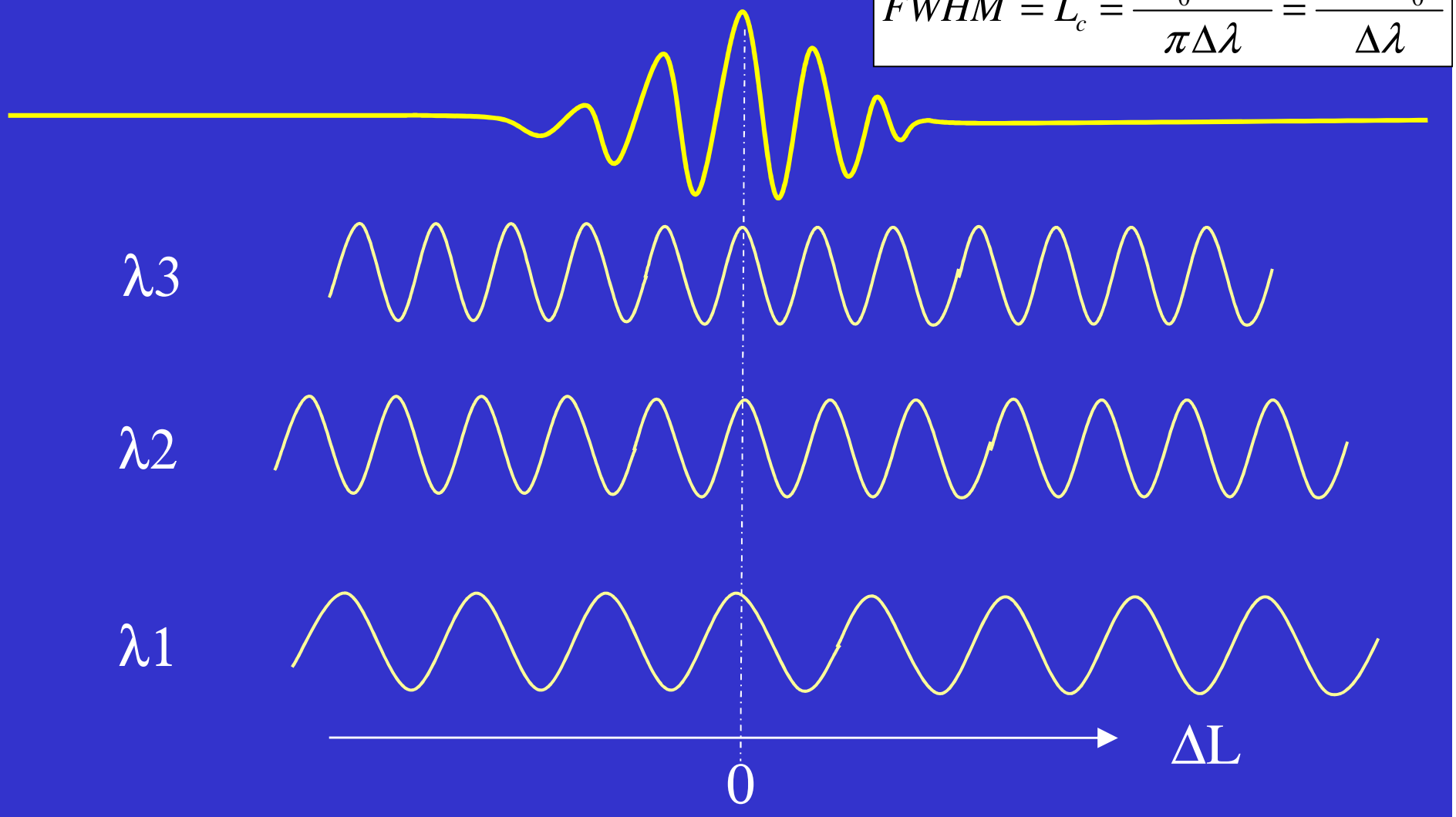

Each wavelength encoded at unique frequency

Frequency of fringe pattern determined by the velocity of the mirror and λ_c

$f = 2v/\lambda_c$

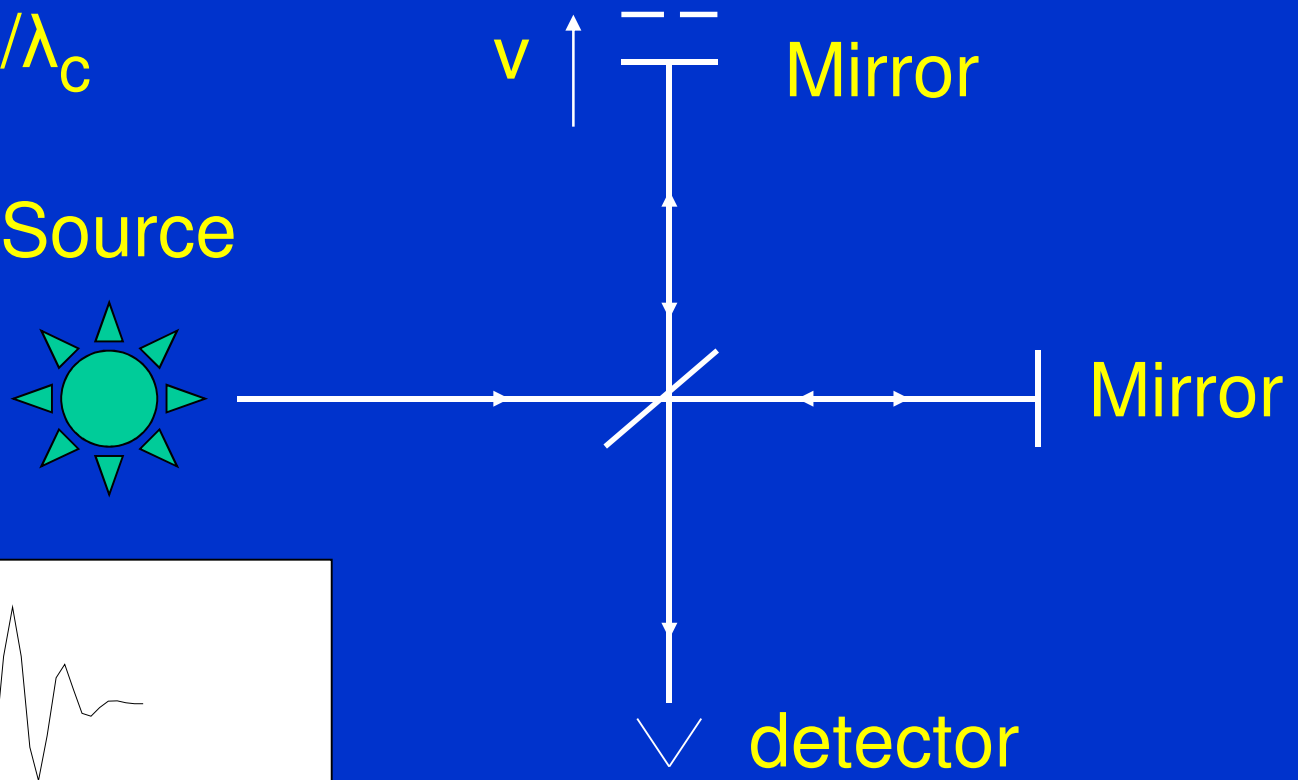

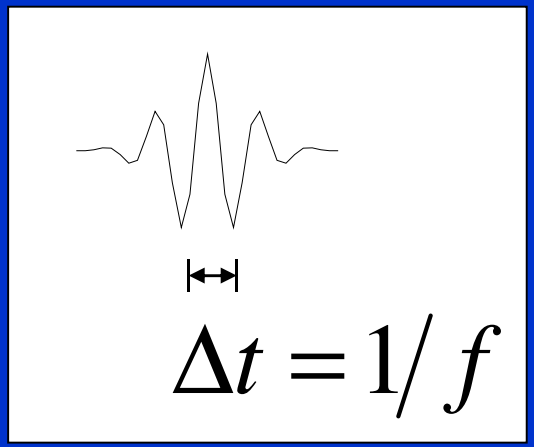

Intensity at the detector

$$E(z) = \int \tilde{e}(k)\exp(-ikz)dk \qquad k = 2\pi/\lambda$$

$$\left\langle \tilde{e}^*(k)\tilde{e}(k')\right\rangle = S(k)\delta(k-k') \quad S(k) \propto \exp\left[-\left(\frac{k-k_0}{\kappa}\right)^2\right] \quad FWHM\ \Delta\lambda = \frac{\kappa\sqrt{\ln 2}\lambda_0^2}{\pi}$$

$$I = \left\langle (E_r + E_s)\times(E_r^* + E_s^*)\right\rangle = \left\langle E_r E_r^*\right\rangle + \left\langle E_s E_s^*\right\rangle + \left\langle E_r E_s^*\right\rangle + \left\langle E_r^* E_s\right\rangle$$

$$\left\langle E_r E_s^*\right\rangle = \left\langle \int \tilde{e}(k)e^{-ikz_r}dk \times \int \tilde{e}^*(k')e^{ik'z_s}dk'\right\rangle = \int S(k)e^{ik(z_s-z_r)}dk$$

$$I(\Delta z) = I_r + I_s + 2\int S(k)\cos(2k\Delta z)dk$$

$$Signal = \int S(k)\cos(2k\Delta z)dk \propto \cos(2k_0\Delta z)\exp[-(\Delta z/\Delta l)^2]$$

$$\Delta l = 1/\kappa$$

$$FWHM \quad L = \Delta l\, 2\sqrt{\ln 2} = \frac{2\ln 2\,\lambda_0^2}{\pi\Delta\lambda} = 0.44\frac{\lambda_0^2}{\Delta\lambda}$$

If the reference arm power doubles, how much does the signal increase

Interference fringe pattern = Gaussian x cosine wave

Cosine wave determined by central wavelength of source

Gaussian

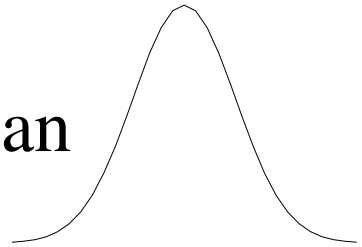

$$Exp[-(\Delta z/\Delta l)^2]$$

$\times$

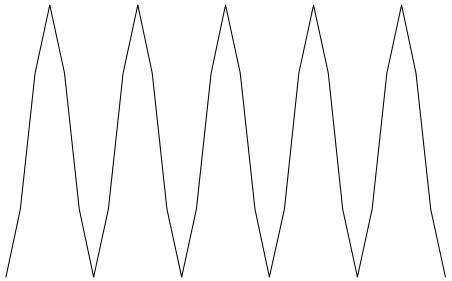

$$\cos(2k_0\Delta z)$$

$$FWHM = L_c = \frac{2\lambda_0^{\,2}\ln 2}{\pi\Delta\lambda} = \frac{0.44\lambda_0^{\,2}}{\Delta\lambda}$$

$$\Delta l = \frac{L_c}{2\sqrt{\ln 2}}$$

$=$

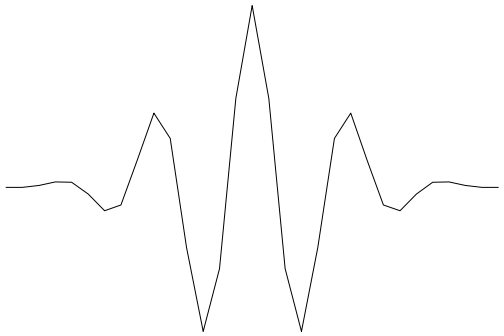

$$\cos(2k_0\Delta z)\times Exp[-(\Delta z/\Delta l)^2]$$

Confocal imaging:

Principle of confocal microscopy

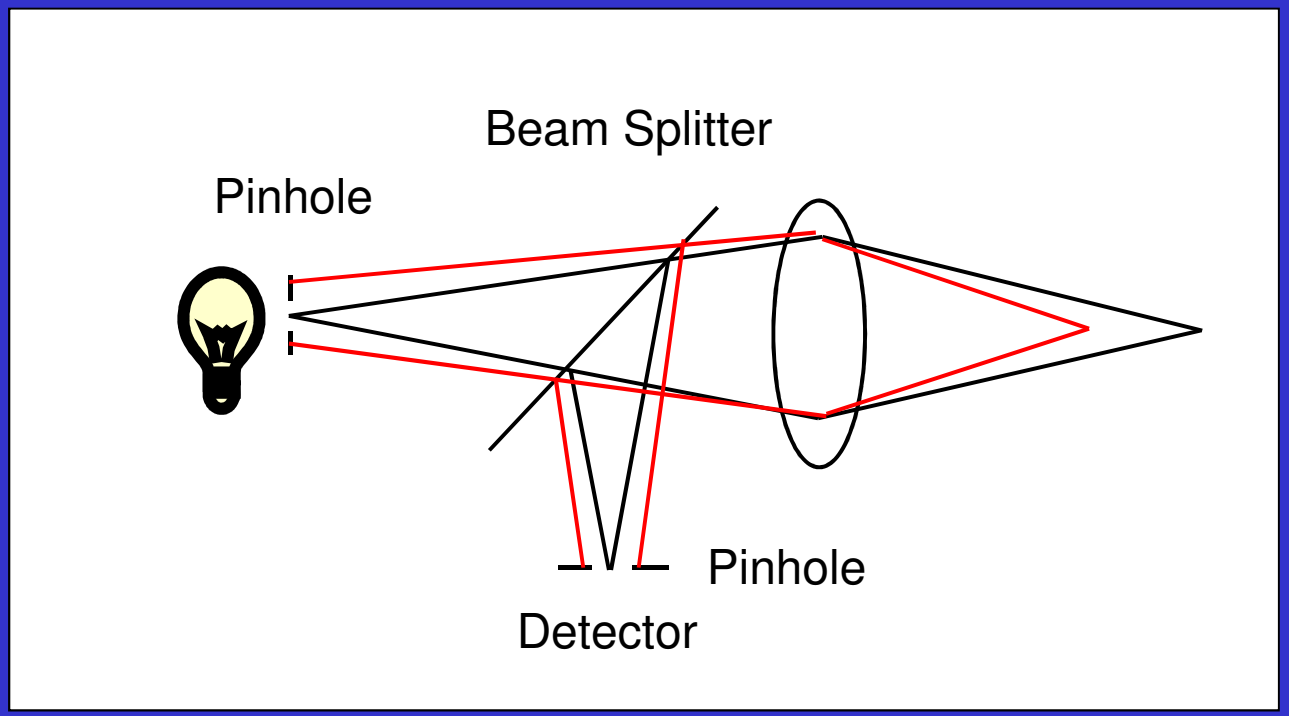

Direct Detection

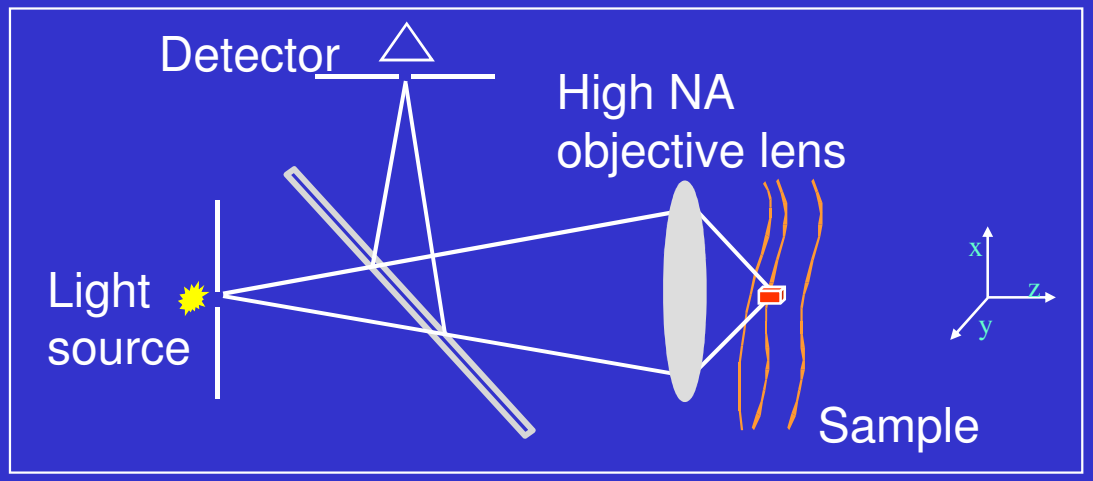

Light source

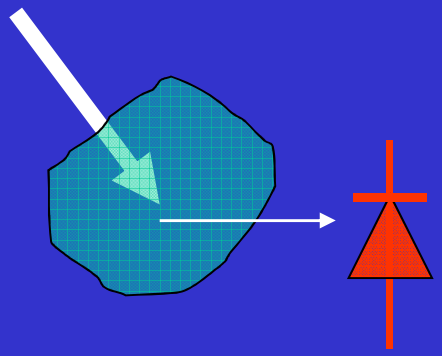

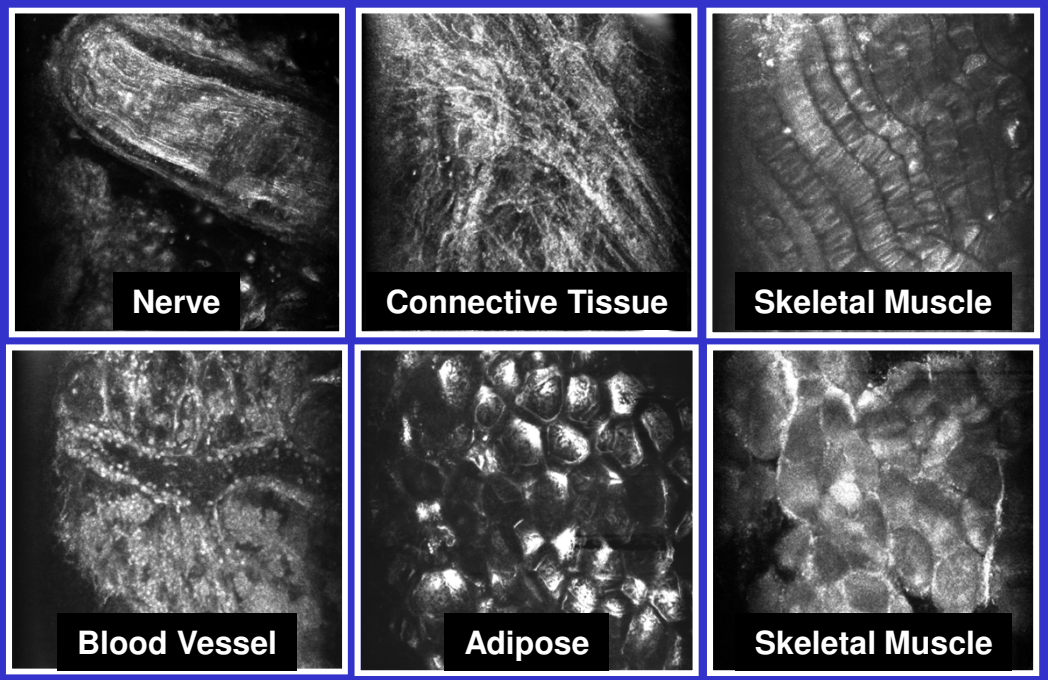

Confocal microscopy creates *en face* cross sectional images

Lateral resolution and depth of focus

$$w_0 = \frac{\lambda f}{\pi w} \qquad z_R = \frac{\pi w_0^2}{\lambda}$$

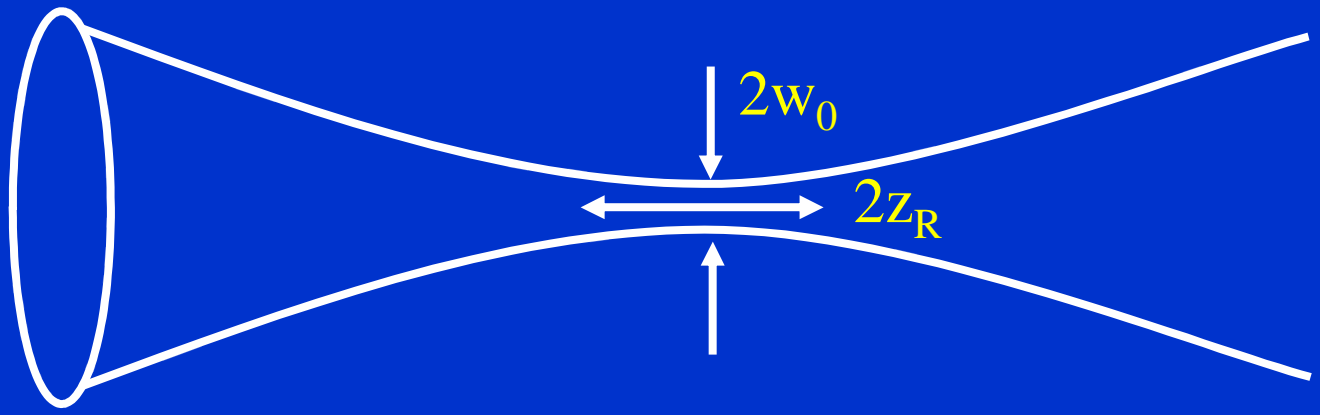

Beam Diameter = 30 μm

Depth of Focus = 1 mm

OCT: Fast scan axis is axial

Confocal: Fast scan axis is lateral ⟹ Better lateral resolution

OCT vs. CM

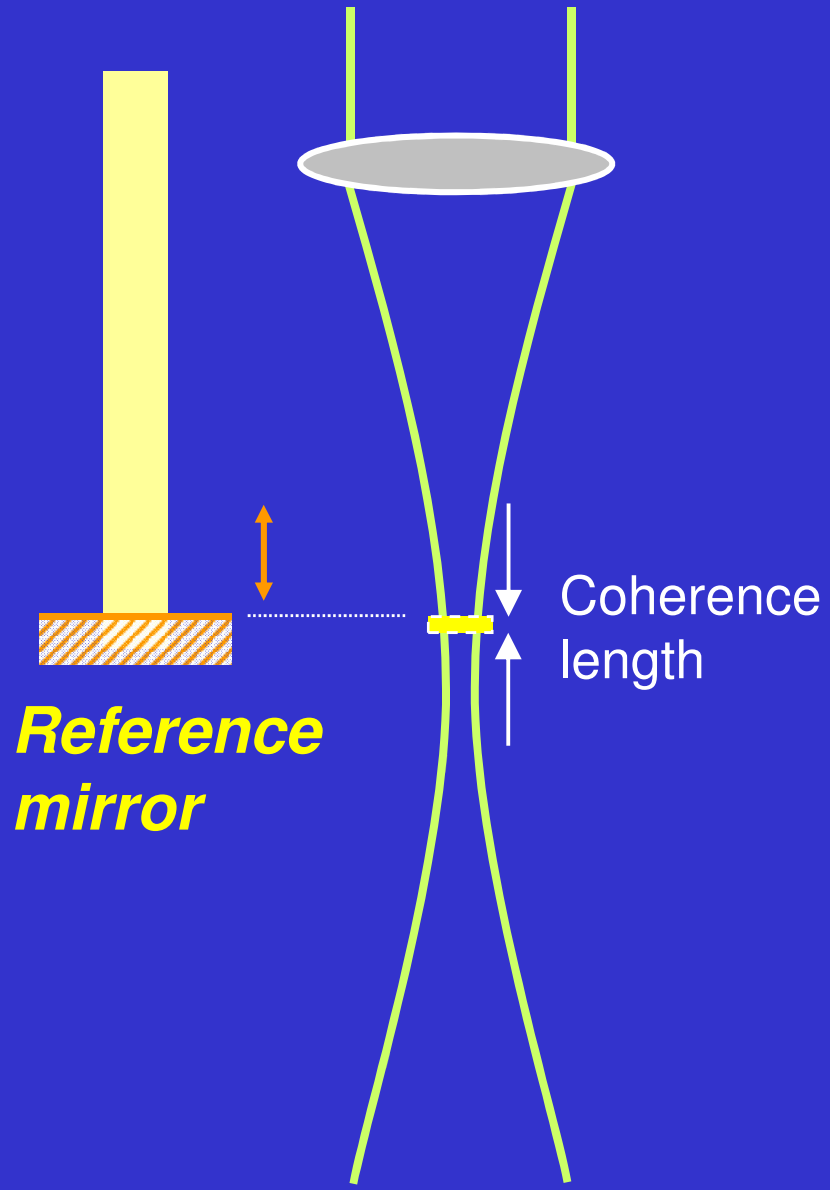
Coherence
length
Reference
mirror

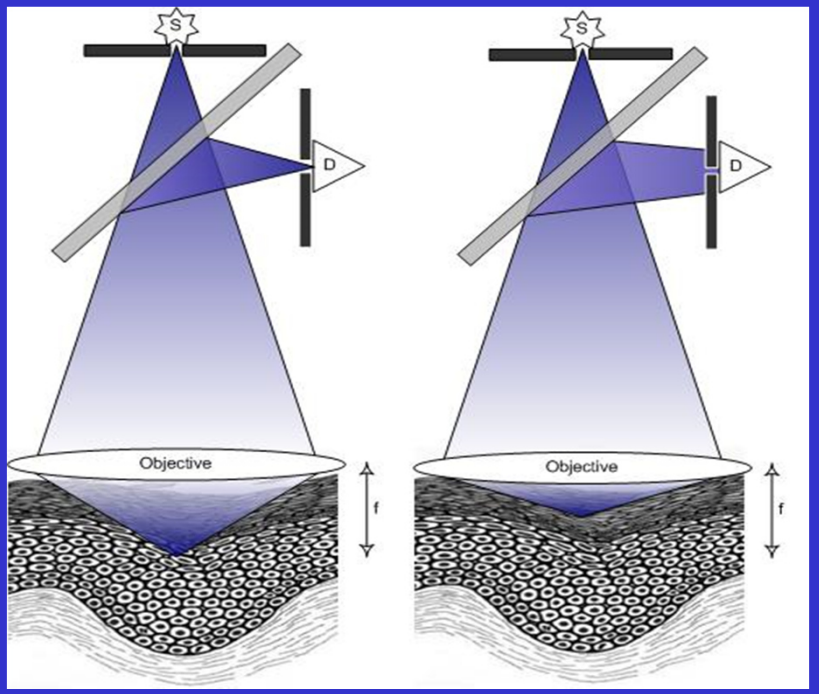
S
D
Objective
f
S
D
Objective
f

Wavelength and attenuation

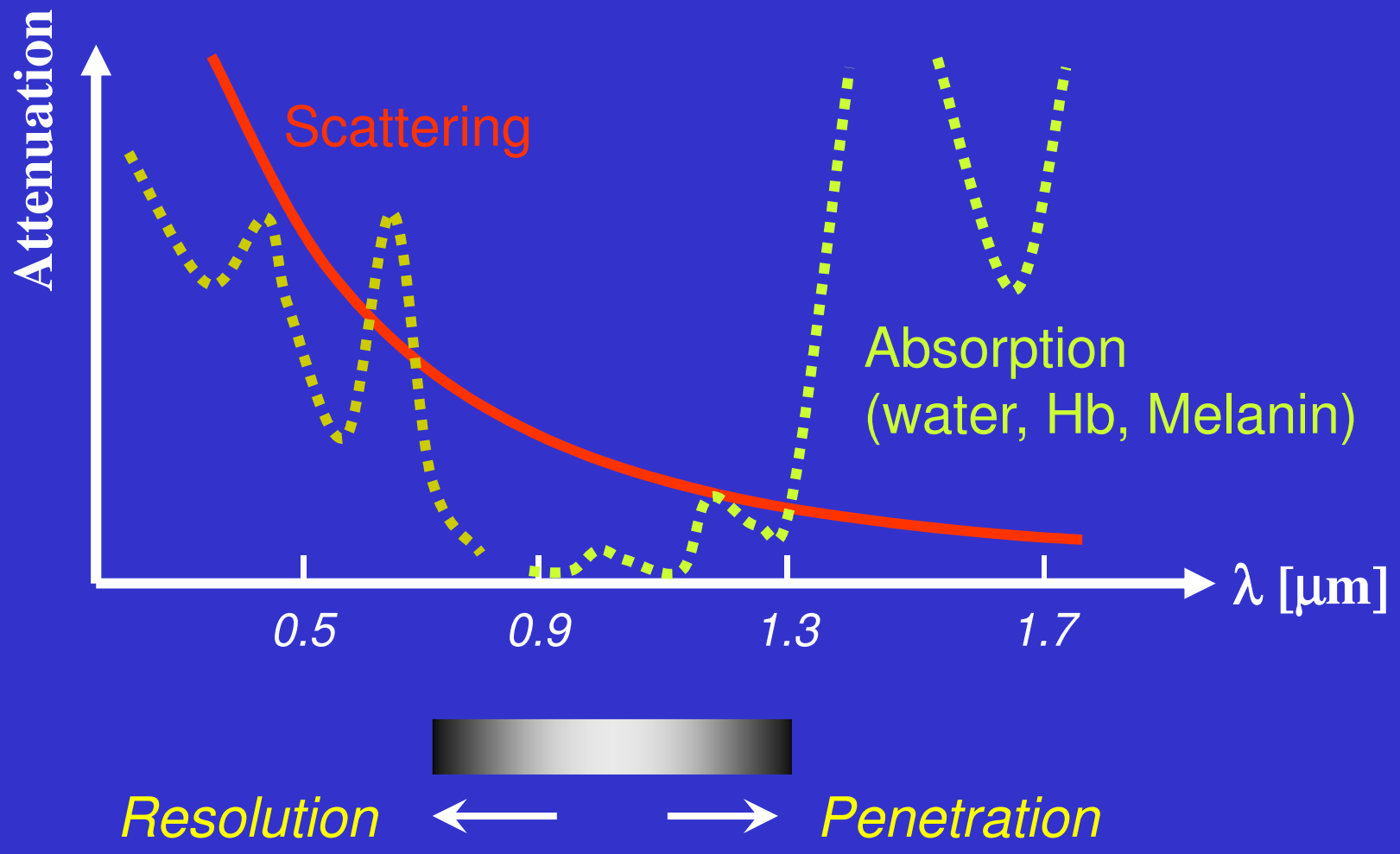

OCT: Summary of technique

- Fringe amplitude proportional to amount of reflected light from a specific depth
- Longitudinal (depth) resolution by coherence gate of the reference arm, determined by the coherence length L_c (~2-10 μm)
- Lateral resolution by focussing optics similar to confocal microscopy (5-30 μm)
- Penetration depth determined by the scattering coefficient of tissue; Signal decays exponential with depth

Noise contributions

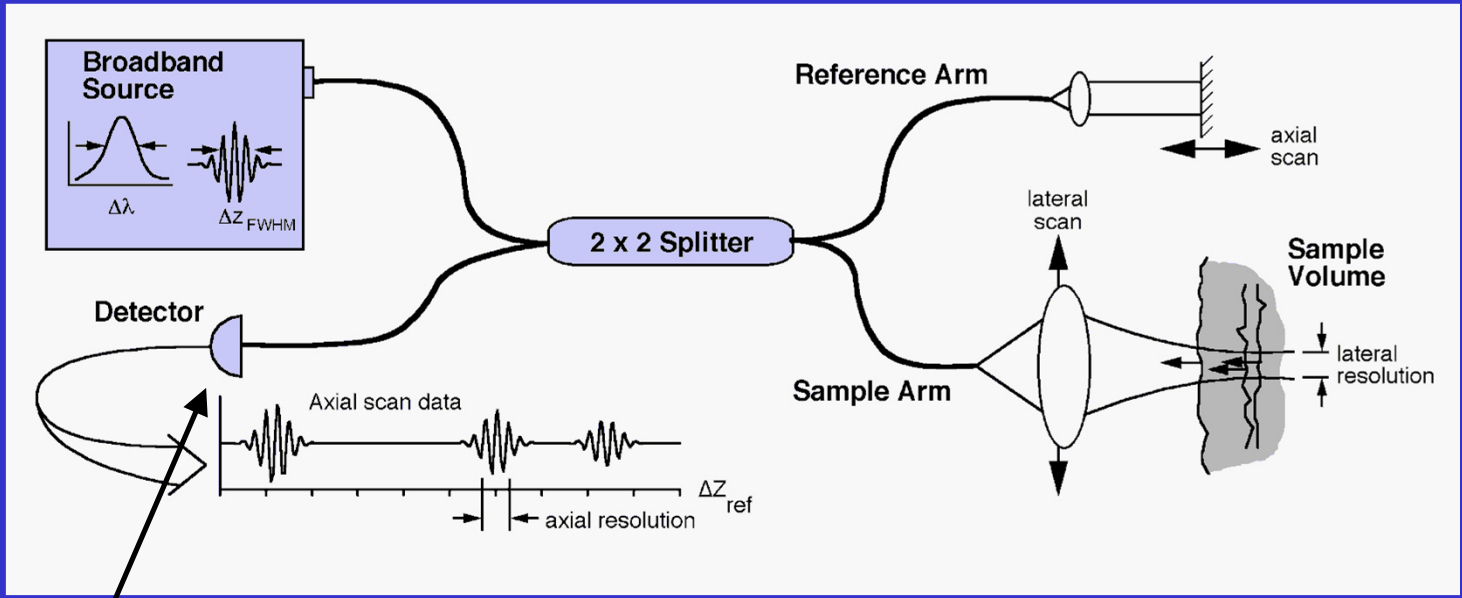

What noise arrives at the detector?
Sample arm power much weaker than reference

=>Noise dominated by the reference arm power

Intensity at the detector

$$I = \left\langle (E_r + E_s) \times (E_r^* + E_s^*) \right\rangle = \underbrace{\left\langle E_r E_r^* \right\rangle}_{I_r} + \underbrace{\left\langle E_s E_s^* \right\rangle}_{I_s} + \underbrace{\left\langle E_r E_s^* \right\rangle + \left\langle E_r^* E_s \right\rangle}_{\text{interference}}$$

$$I(\Delta z) = I_r + I_s + 2\sqrt{I_r I_s}\cos(2k\Delta z)\exp[-(\Delta z / \Delta l)^2]$$

If the reference arm power doubles, how much does the interference increase?

Signal is square of intensity, $S = I(\Delta z)^2$

Structural image of nailfold

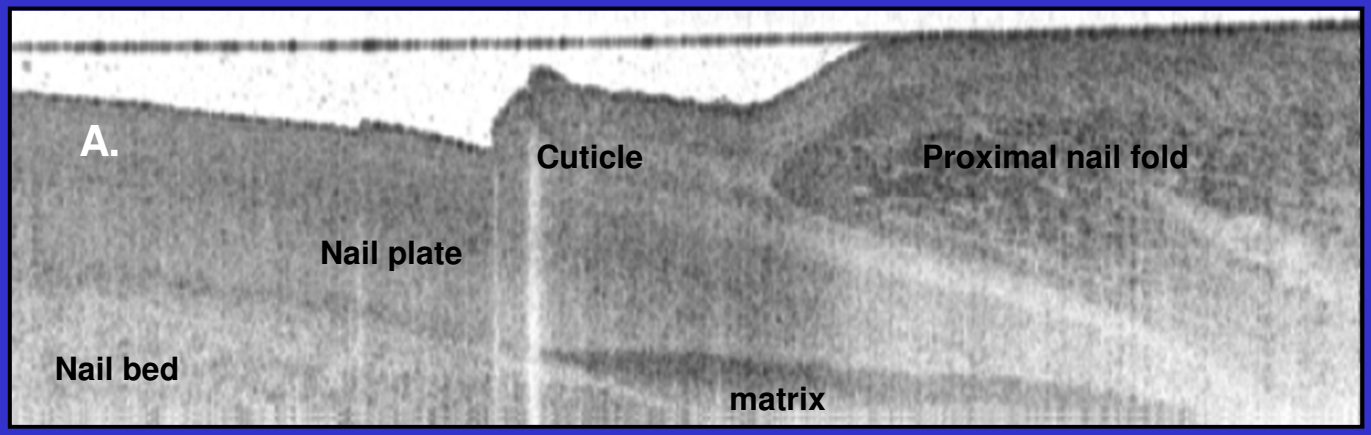

Size: 1.2 mm x 4 mm

Source FWHM = 70 nm
Center wave length = 1310 nm

⇒ Resolution = 8 μm
(n = 1.35)

Park et al., Opt. Exp. 11: 782 (2003)

Transimpedance Amplifier

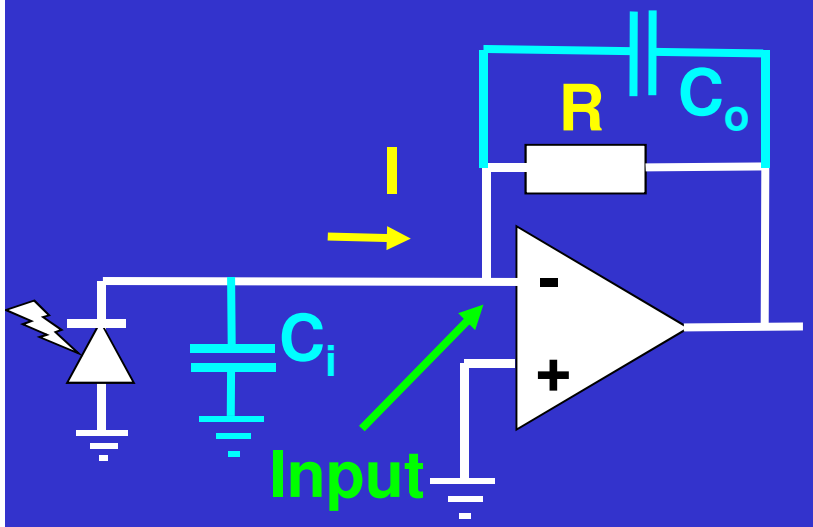

Converts current to voltage

V = I x R **Gain = R**

Output Noise

$$\Delta V_o = \Delta V_i + R \times \Delta I_i$$

Due to C_i , C_o is necessary to stabilize the amplifier to avoid wild oscillations.

This limits the bandwidth of the amplifier to

$$f = 1/(2\pi R C_o) = BW$$

Interestingly,
GxBW = constant
(specified as unity gain bandwidth)

Noise in light detection

Detector noise

Photodetector – Amplifier – Cut off filter

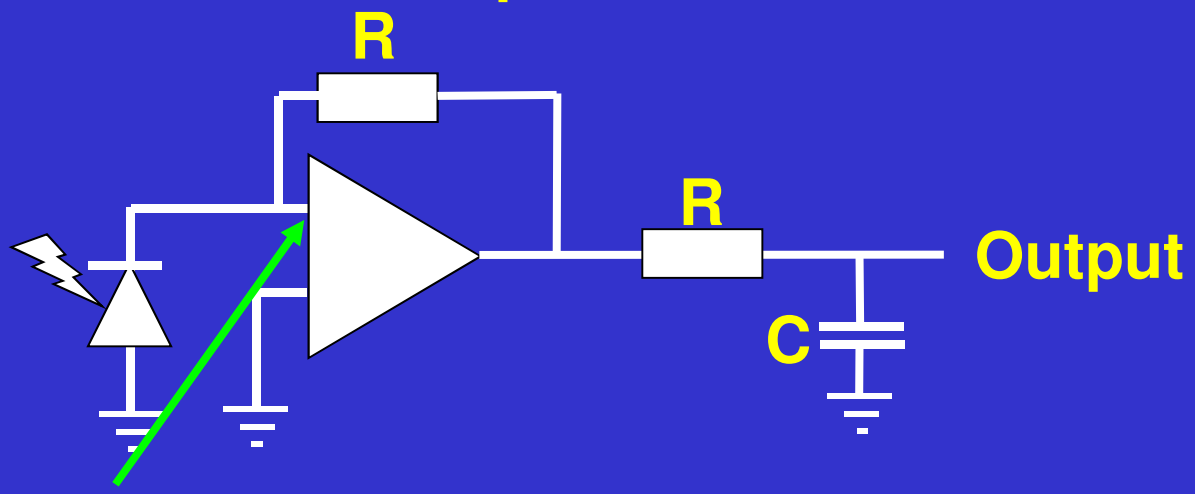

Input Noise
ΔI_i
ΔV_i

Output Noise
$\Delta V_o = \Delta V_i + R \times \Delta I_i$

Detector noise is constant as a function of light intensity

Duality of Light

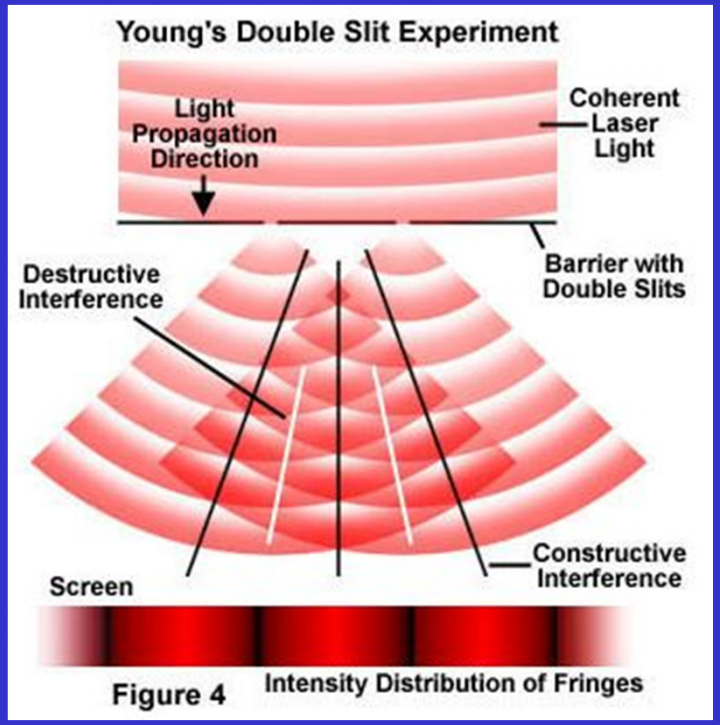

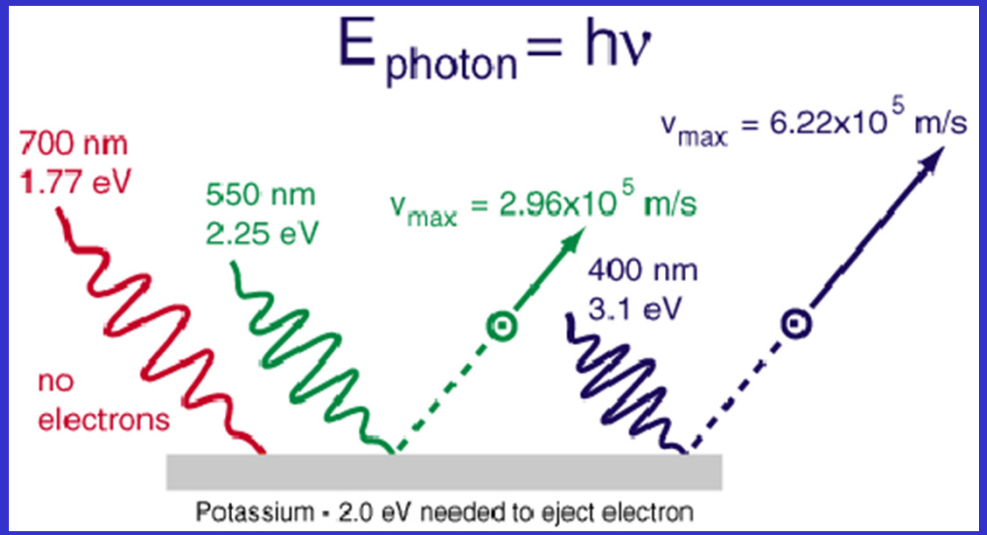

Young 1800
Fresnel, Maxwell

Einstein 1905
Photoelectric effect

E-field

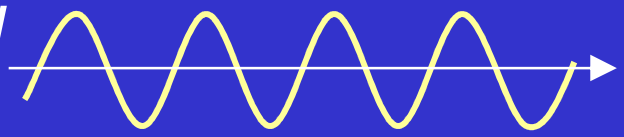

Shot Noise

Photon → electron

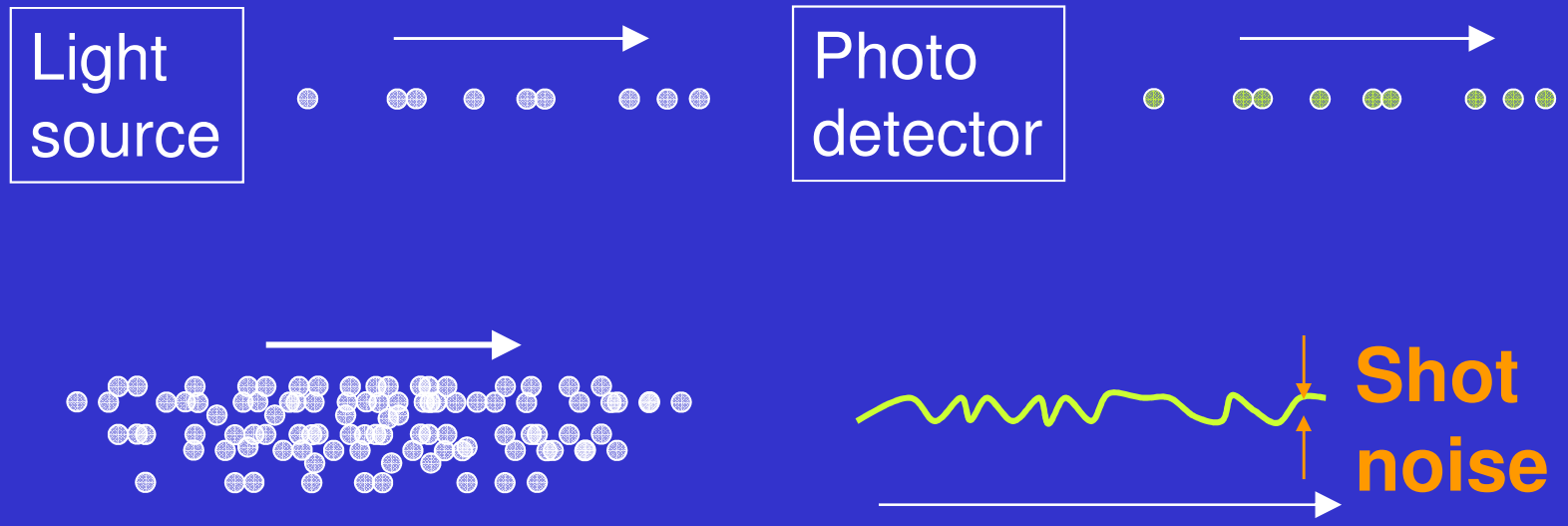

Shot noise current* = $Sqrt(2q\ i\ BW)$

*Further reading: A. Yariv, Optical Electronics

Shot noise

Stream of photons

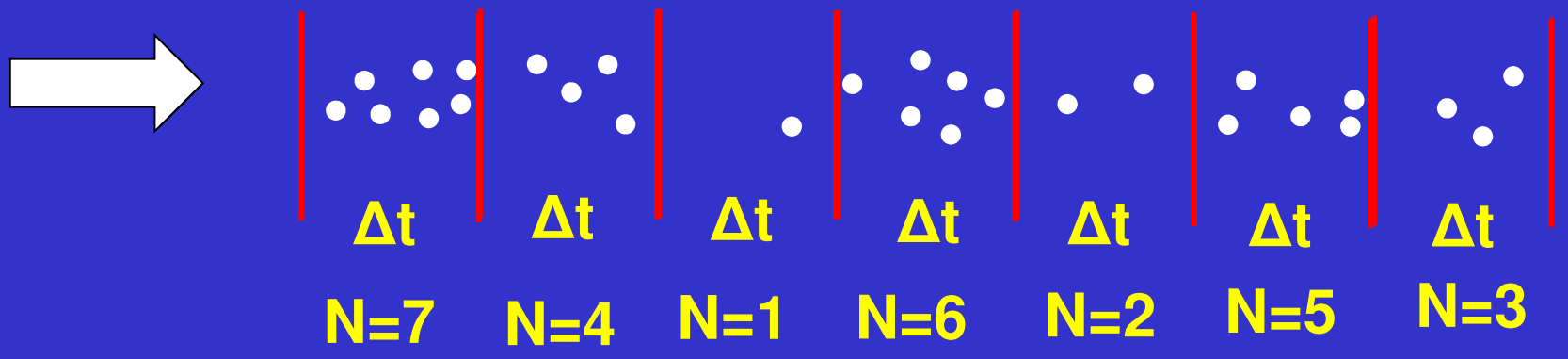

In each time interval the number of detected photons will fluctuate. Mean is 4

Noise is proportional to $\Delta N^2 = N$ **i.e.,**

$$\left\langle \left(I - \langle I \rangle \right)^2 \right\rangle \propto \langle I \rangle$$

In this case = 4

Frequency distribution of shot noise

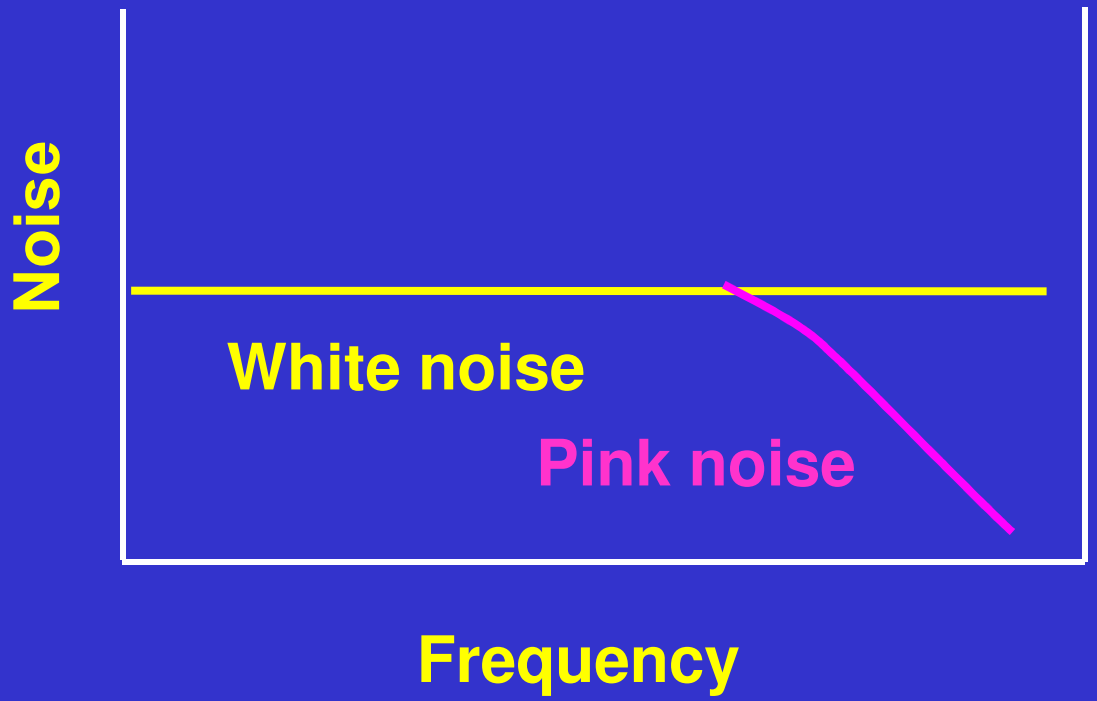

Shot noise is white noise
Noise is equal at all frequencies

Noise of a thermal light source

Bose-Einstein Distribution:

$$P_{\omega}(n) = \frac{1}{\bar{n}+1}\left(\frac{\bar{n}}{\bar{n}+1}\right)^{n}$$

$$(\Delta n)^2 = \bar{n} + \bar{n}^2$$

(single mode of the radiation field)

$$(\Delta n)^2 = \bar{n} + \frac{\bar{n}^2}{N_m}$$

Shot noise

BE noise or Relative Intensity Noise (RIN)

For N_m thermal modes, with

$$\frac{N_m}{V} = \frac{\omega^2}{\pi^2 c^3}\partial\omega = \frac{8\pi\Delta\lambda}{\lambda^4}$$

Note that shot noise dominates for large Nm

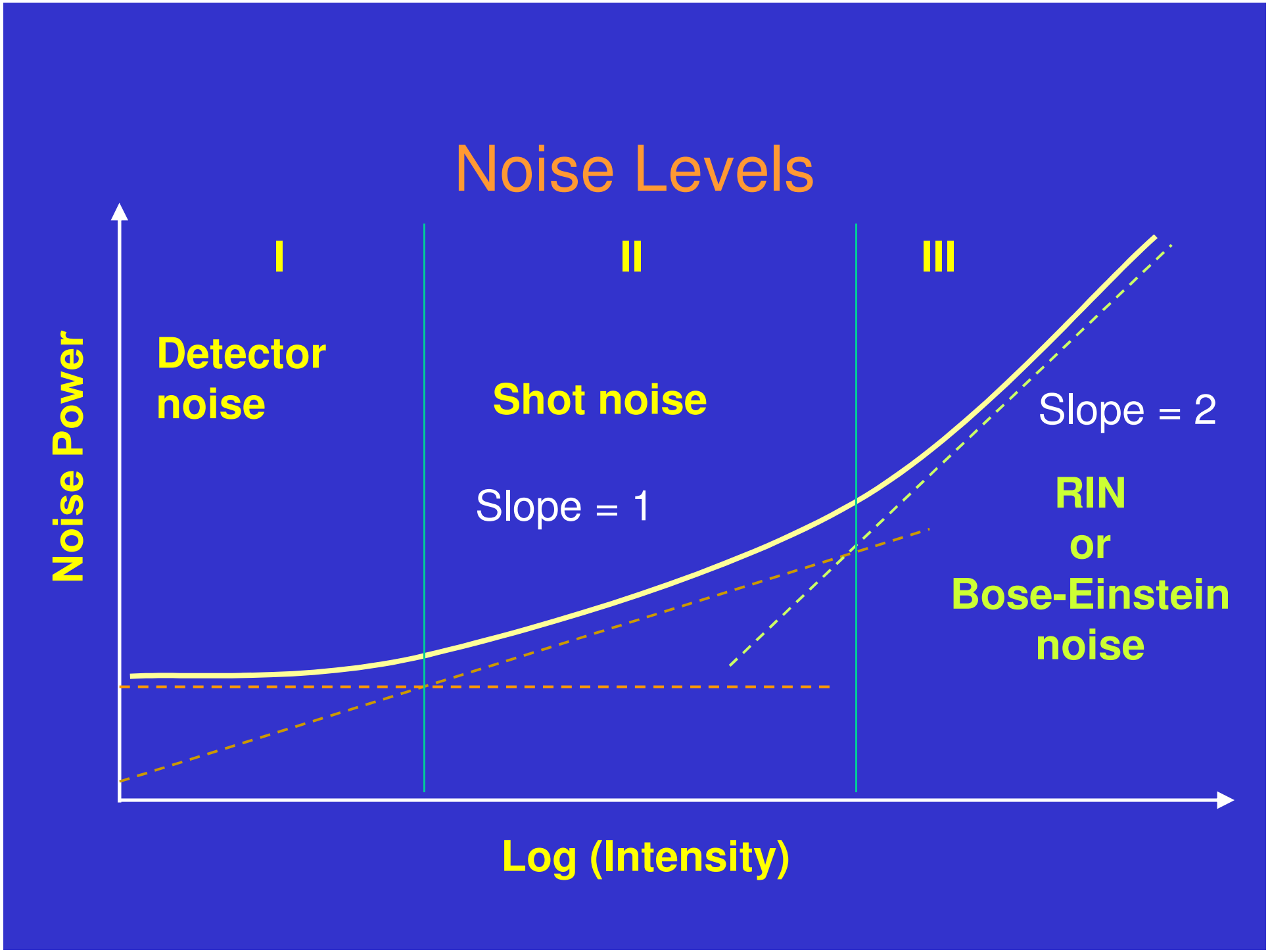
Noise Levels
I
II
III
Detector noise
Shot noise
Slope = 1
Slope = 2
RIN or Bose-Einstein noise
Noise Power
Log (Intensity)

Signal and noise power

$$I_{peak} = 2\cos(k_0 z)\sqrt{P_{ref} P_{sample}}\,, S = \left\langle I_{peak}^2 \right\rangle = 2P_{ref} P_{sample}$$

$$S_{signal} = 2\eta^2 e^2 P_{ref} P_{sample} / E_v^2 \quad [A^2]$$

$$N_{noise}(f) = \frac{4kT}{R_{fb}} + \frac{2\eta e^2 P_{ref}}{E_v} + 2\left(\frac{\eta e P_{ref}}{E_v}\right)^2 \tau_{coh} \quad [A^2 / Hz]$$

(Reference arm only)

$$\frac{S_{signal}}{N_{noise}} = \frac{\eta P_{sample}}{E_v\, BW}$$

$$SNR \propto \frac{P_{sample} \times resolution}{speed \times depth\, range}$$

η = detector efficiency (80–100 %)
BW = band width = $4v\Delta\lambda/\lambda_o^2$
E_v= photon energy (1.5×10^{-19} J)

SNR = 115 dB = 10 Log (3.3×10^{11}) for P = 5 mW

BW = 100 kHz for v = 250 x 1.4 mm, Δλ = 50 nm, λ = 840 nm

Why is this interesting or important?

Background

Over the past 15 years, optical coherence tomography (OCT) has undergone a rapid development from inception to a versatile method for non-invasive high-resolution optical imaging.

The potential diagnostic applications having the highest impact, however, require screening or surveillance of large tissue volumes at high speed. OCT needs to operate in the shot noise limit for optimal performance

Time Domain and Spectral Domain OCT configurations

Fujimoto (1991)

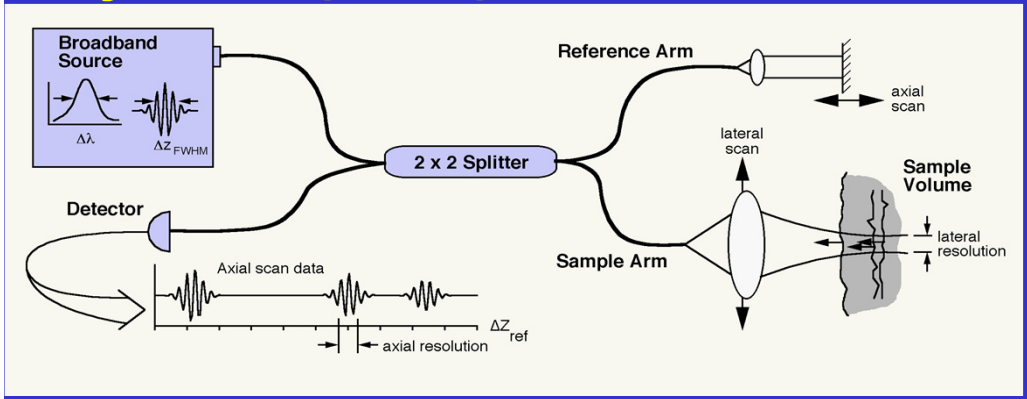

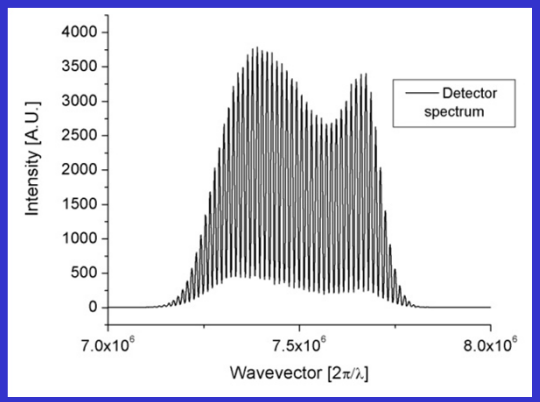

Huang, D., Swanson, E.A., Lin, C.P., Schuman, J.S., Stinson, W.G., Chang, W., Hee, M.R., Flotte, T., Gregory, K., Puliafito, C.A., and Fujimoto, J.G., Optical coherence tomography. Science, 1991. 254(5035): p. 1178-81.

Fercher (1995)

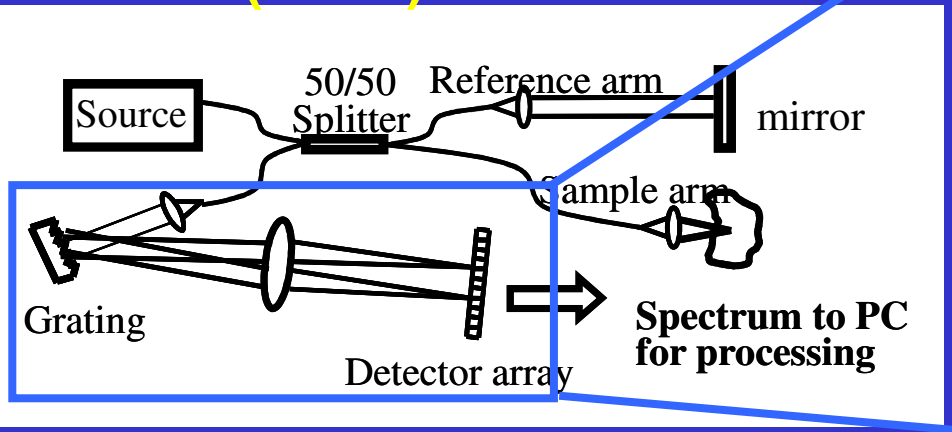

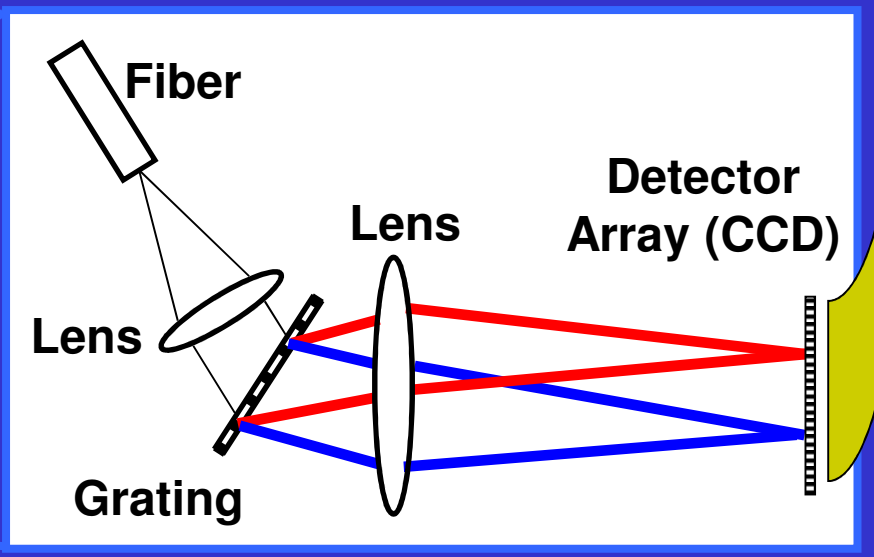

A. F. Fercher, C. K. Hitzenberger, G. Kamp, and S. Y. El-Zaiat, "Measurements of intraocular distances by backscattering spectral interferometry," Opt. Comm. 117, 43-48 (1995).

SD-OCT

$$I(k) = I_r(k) + 2\sqrt{I_s(k) I_r(k)} \sum_n \alpha_n \cos(k\, z_n) + I_s(k)$$

FFT

$$\left| FT^{-1}[I(k)] \right|^2 = \Gamma^2(z) \otimes \left\{ \delta(0) + \sum_n \alpha_n^2 \delta(z - z_n) + \sum_n \alpha_n^2 \delta(z + z_n) + O\left[I_s^2 / I_r^2 \right] \right\}$$

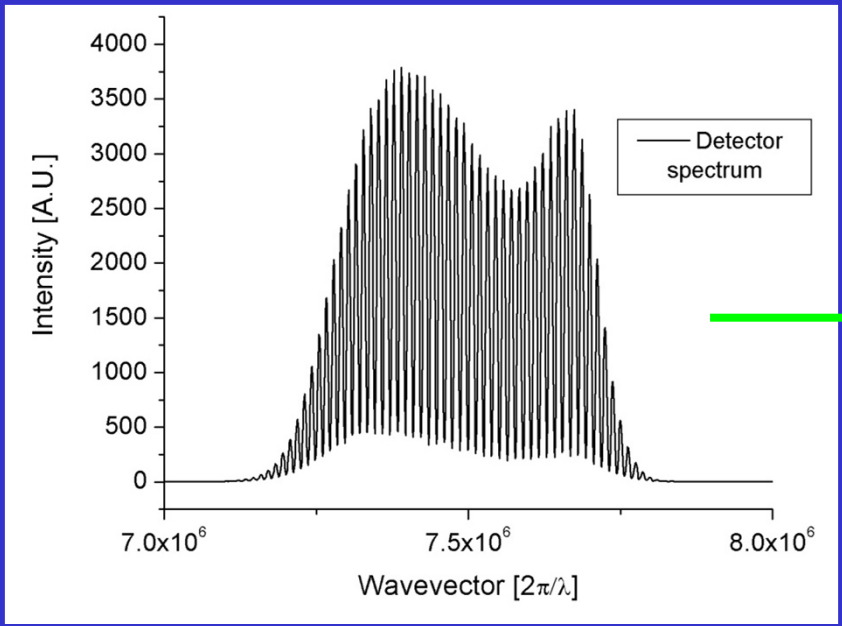

FFT

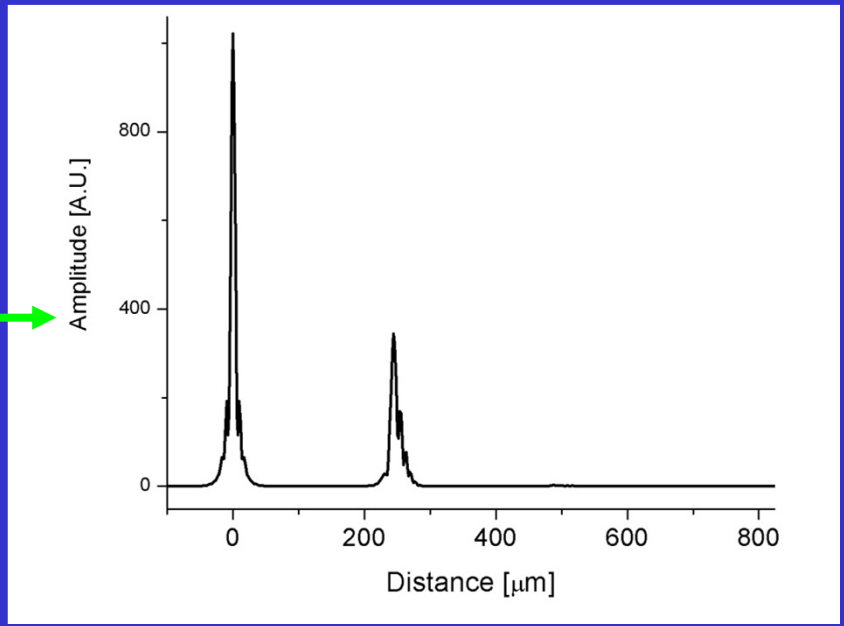

N. A. Nassif *et al.*, Opt. Express 12, 367-376 (2004)

Spectral Domain OCT

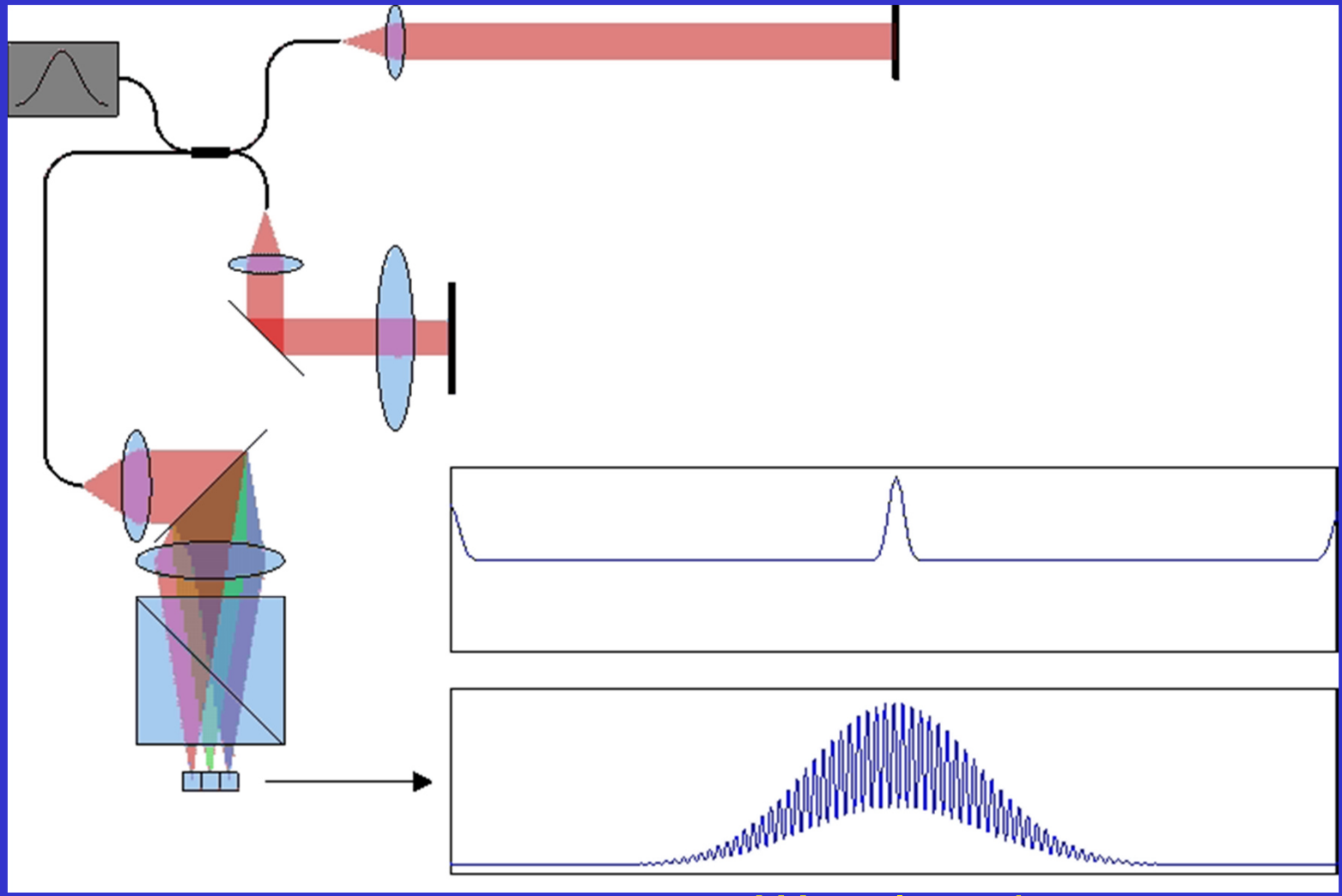

Signal to Noise SD-OCT

$$S_{SD} = \frac{\eta^2 e^2 P_{ref} P_{sample} \tau_i^{\,2}}{E_v^{\,2}} \quad [e^2]$$

$$\sigma^2_{noise} = \sigma^2_{r+d} + \frac{\eta e^2 P_{ref} \tau_i}{E_v} + \left(\frac{\eta e P_{ref}}{E_v}\right)^2 \tau_i \tau_{coh} \quad [e^2]$$

Shot Noise

RIN

$$SNR_{SD} = \frac{\eta P_{sample} \tau_i}{E_v}$$

(Shot Noise dominated)

N. Nassif *et al.* Optics Letters 29 (5), 480 (2004)

Sensitivity advantage of SD-OCT

First recognition:

- **1998 Gerd Hausler's group, Erlangen, Germany**
- **1999 T. Mitsui**
- **Torun (Poland) and Vienna (Austria) groups (2002)**

2003: Leitgeb (OE), de Boer (OL), Choma (OE)

2 to 3 orders better sensitivity

P. Andretzky, M. W. Lindner, J. M. Hermann, A. Schultz, M. Konzog, F. Kiesewetter, and G. Hausler, "Optical coherence tomography by spectral radar: dynamic range estimation and in vivo measurements of skin," Proc. SPIE 3567, 78-87 (1998).

T. Mitsui "Dynamic range of optical reflectometry with spectral interferometry" Jap. Journal of Applied Physics 38 (10) 6133 (1999)

Theoretical comparison of SNR, TD versus SD

$$SNR_{TD} = \frac{\eta P_{sample}}{E_\nu BW}, \quad SNR_{SD} = \frac{\eta P_{sample} \tau_i}{E_\nu}$$

η = Detector QE
E_ν= Photon energy
τ_i = Integration time

Source: Δλ = 50 nm, λ = 830 nm, 250 A-lines/sec, 1.4 mm range

➡ TD: BW = 100kHz SD: τ_i= 10μs

Same SNR for 250 depth profiles in TD
and 100,000 depth profiles in SD
Speed increase by a factor of 400 with same SNR!

- SNR is independent of source spectral width !
- SD-OCT sensitive to a single photon !

R. Leitgeb et al, Opt. Express 11, 889-894 (2003)

J. F. de Boer *et al*, Opt. Lett. 28, 2067-2069 (2003)

Direct experimental comparison

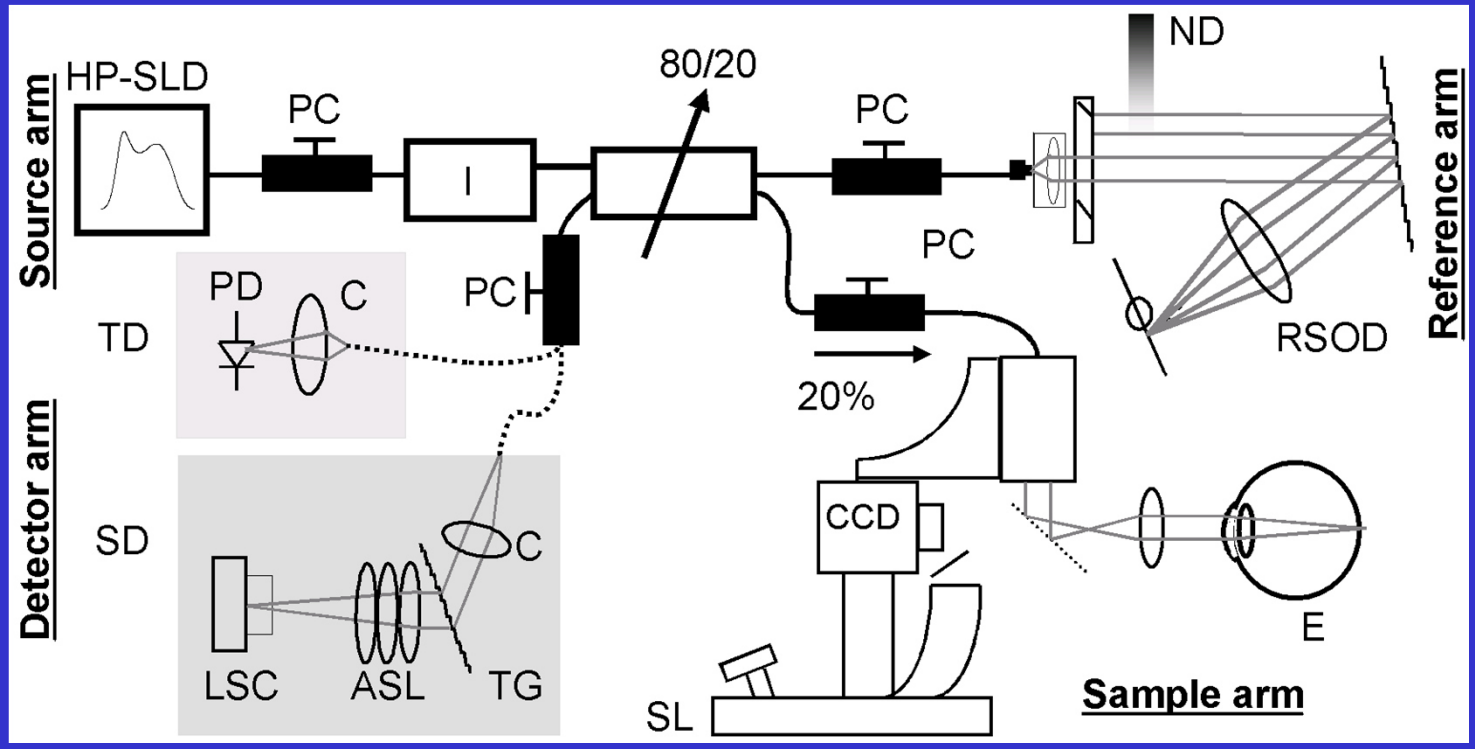

P_{sample} = 1.27 nW

Spectrometer: CCD line scan camera (Basler) 2048 pixels

Max line speed: 29.3 kHz, well depth 177,000 e, 10 bit resolution

Designed spectral resolution 0.075 nm (effective 0.139 nm)

Axial scan range of 2.35 mm in air

QE spectrometer = 0.28

N. Nassif *et al.* Optics Letters 29 (5), 480 (2004)

Experimental verification of sensitivity

Experimental SNR
TD = 44.3 dB
SD = 50 dB

Theoretical prediction
TD = 46.7 dB
(QE=0.85, BW = 100kHz
SD = 51.9 dB
(QE = 0.28, τ_i = 100 μs)

SNR benefit =
5.7 + 16 = 21.7 dB

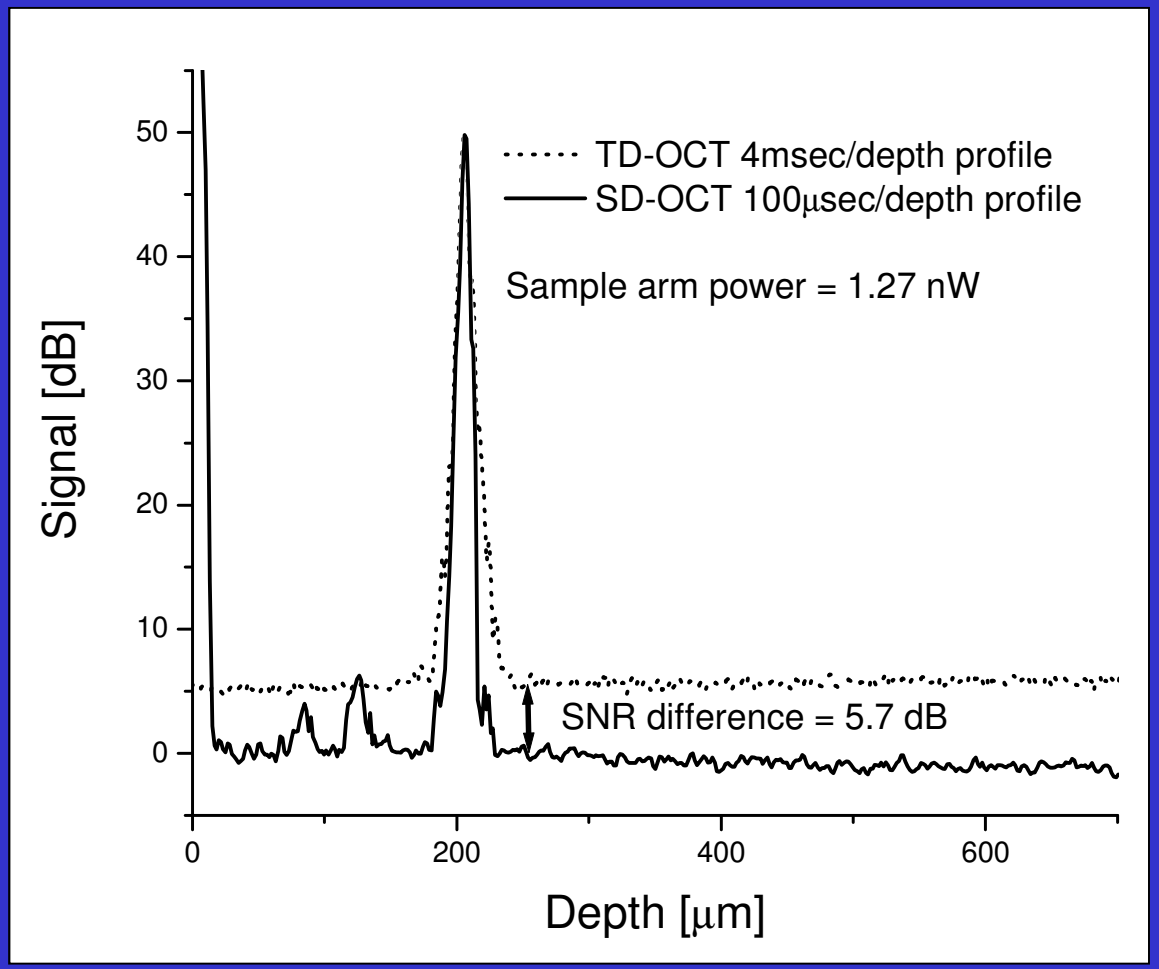

Demonstrated SNR improvement of 21.7 dB (factor of 150)

N. Nassif *et al.* Optics Letters 29 (5), 480 (2004)

Sensitivity advantage of hybrid OCT

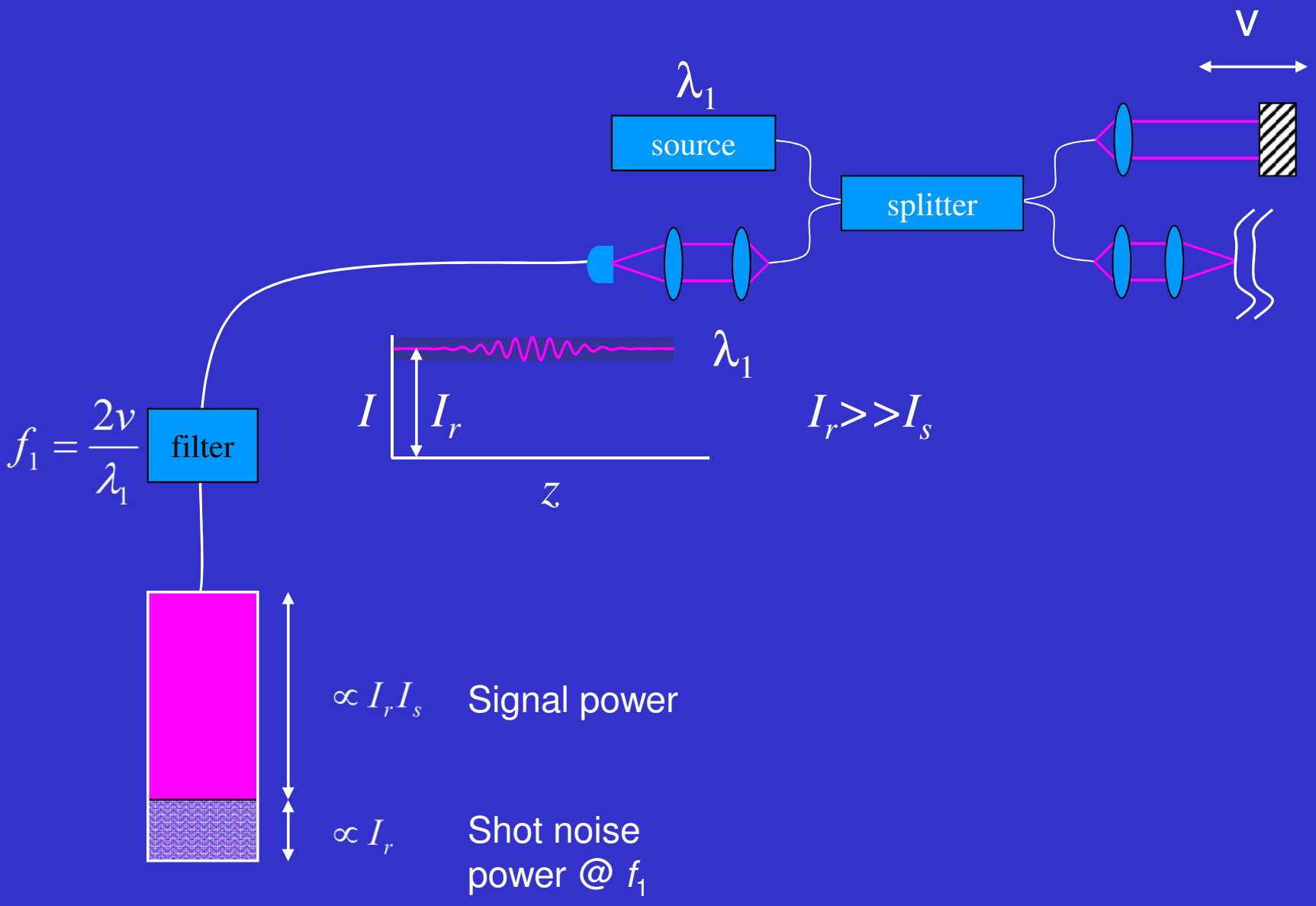

Sensitivity advantage of hybrid OCT

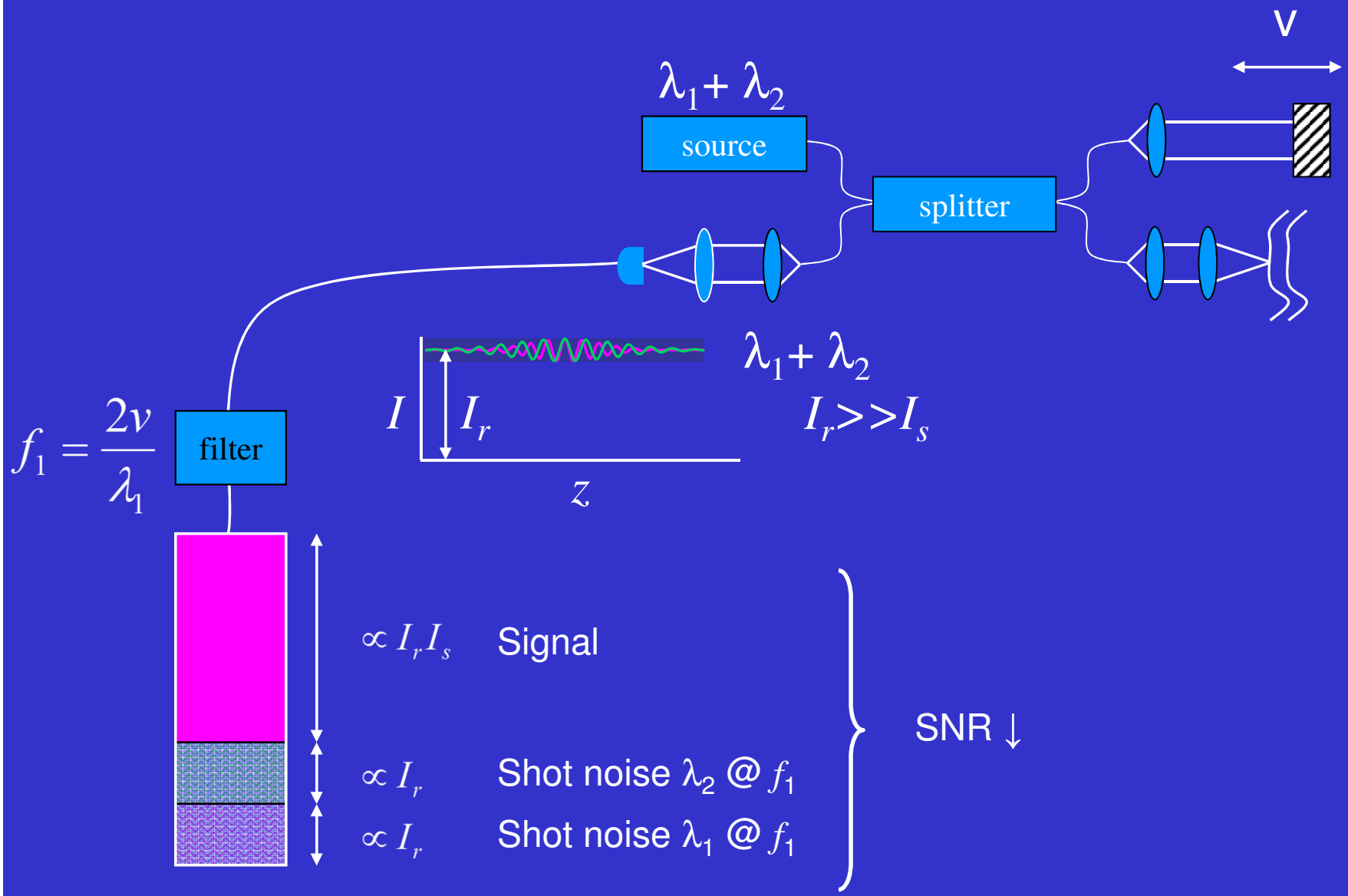

Sensitivity advantage of hybrid OCT

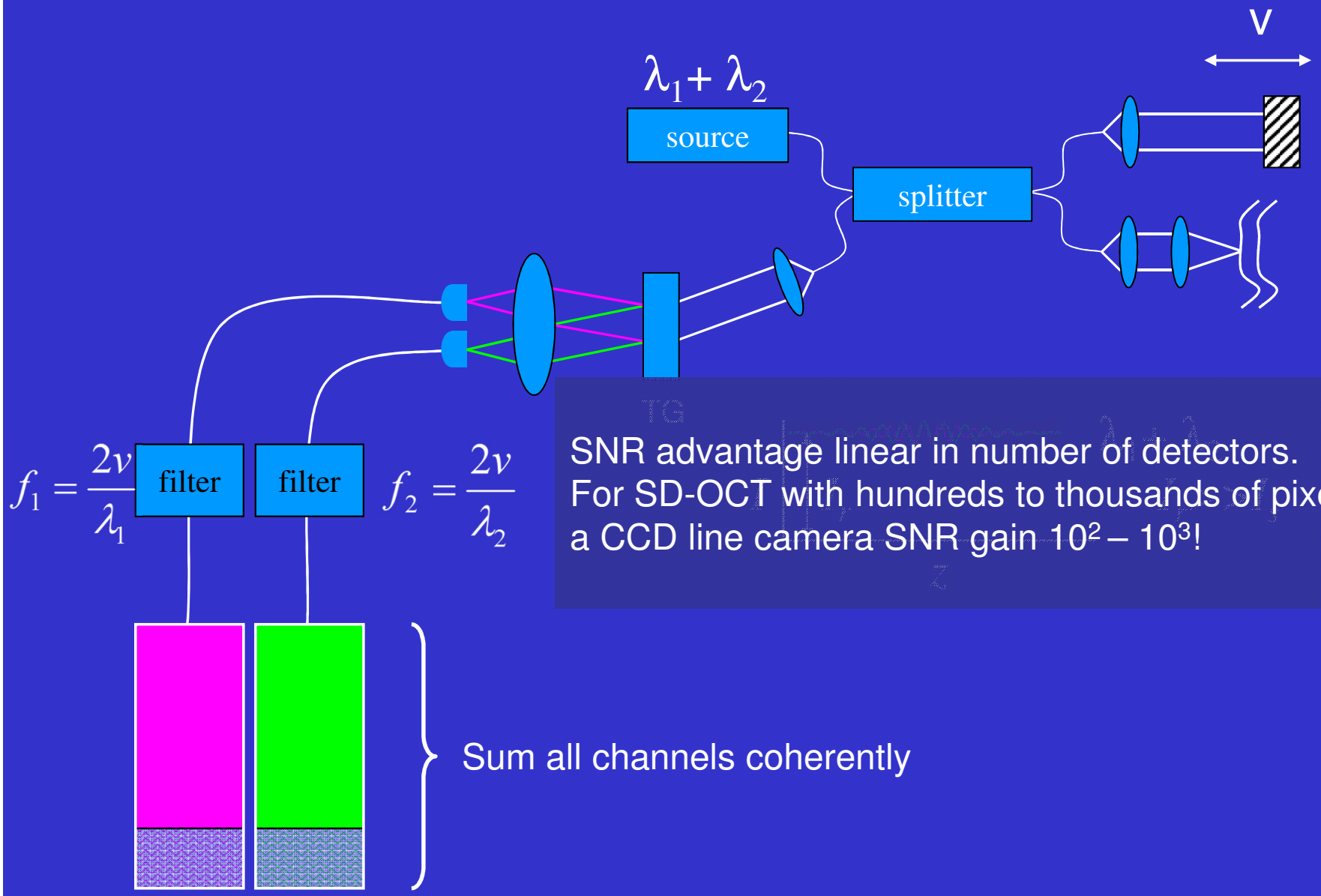

SNR advantage linear in number of detectors.
For SD-OCT with hundreds to thousands of pixels on a CCD line camera SNR gain 10^2 – 10^3!

The human eye

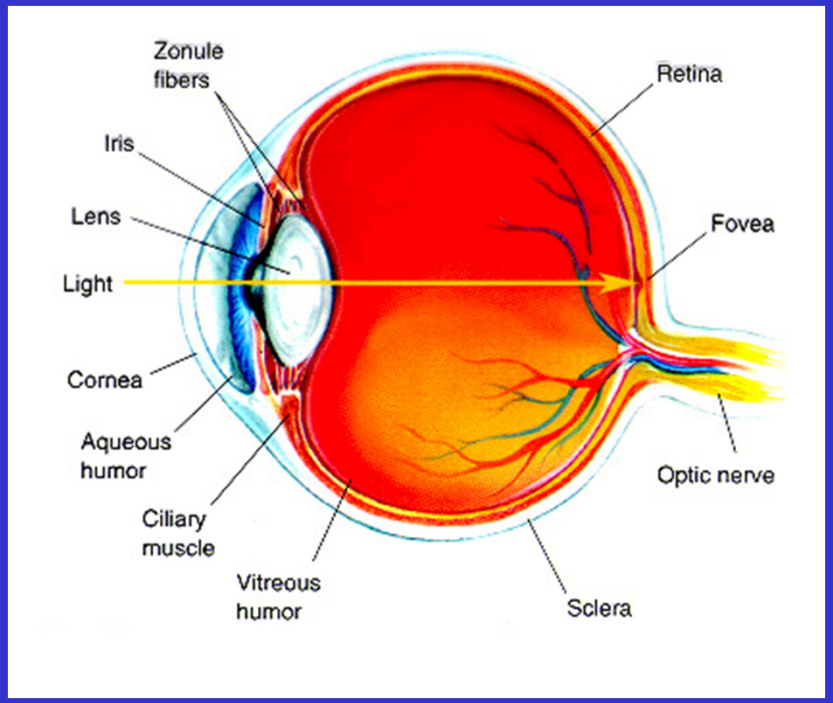

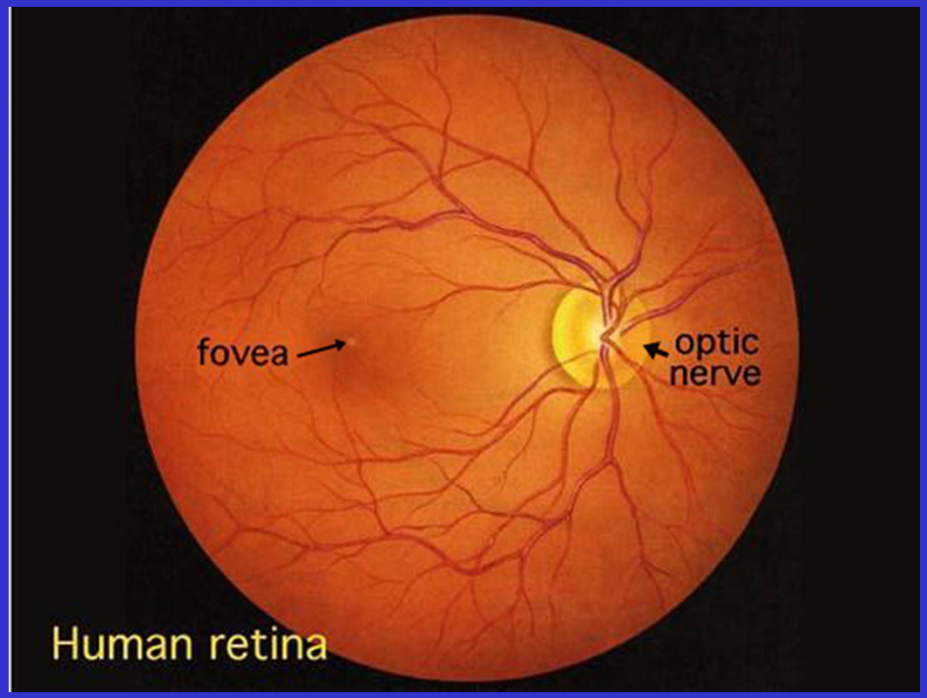

OCT in ophthalmology: Fercher and Fujimoto groups (early 1990's)
High resolution OCT: Fujimoto, Drexler (late 1990's)

First video rate images of the human retina (2003-2004)

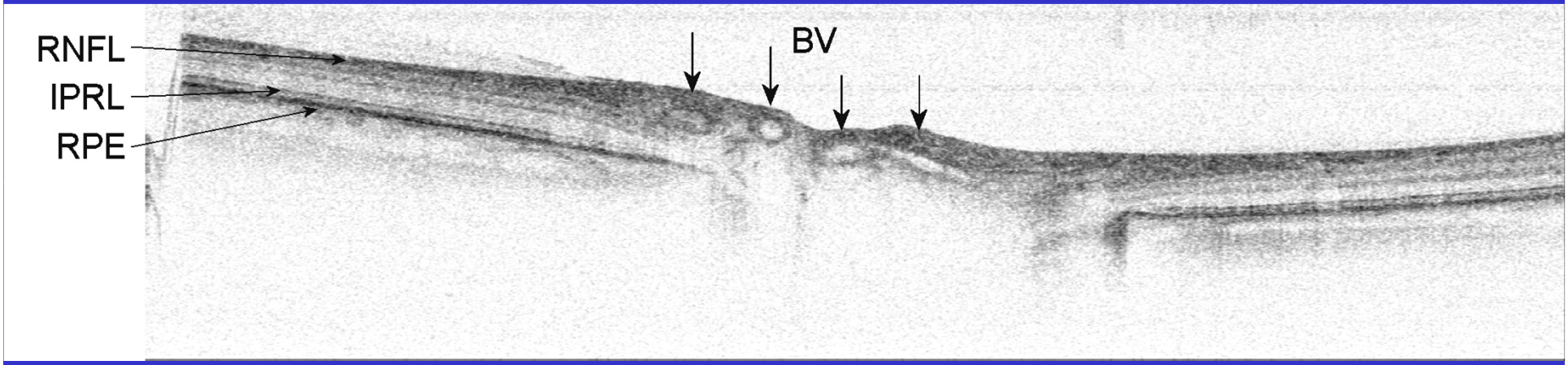

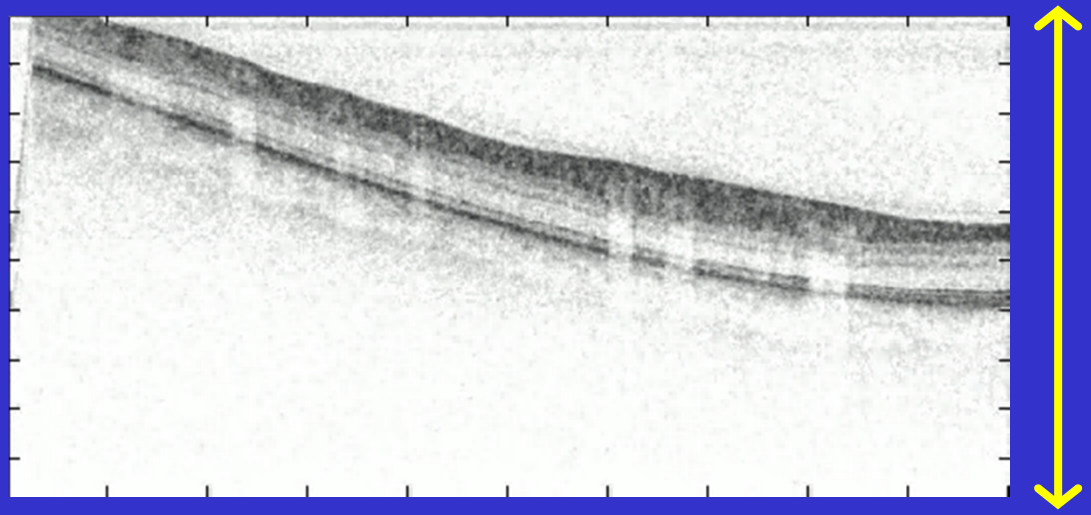

2 x magnified

N. A. Nassif *et al.*, Opt. Express 12, 367-376 (2004)

Depth-dependent sensitivity decrease

Before Zero-padding

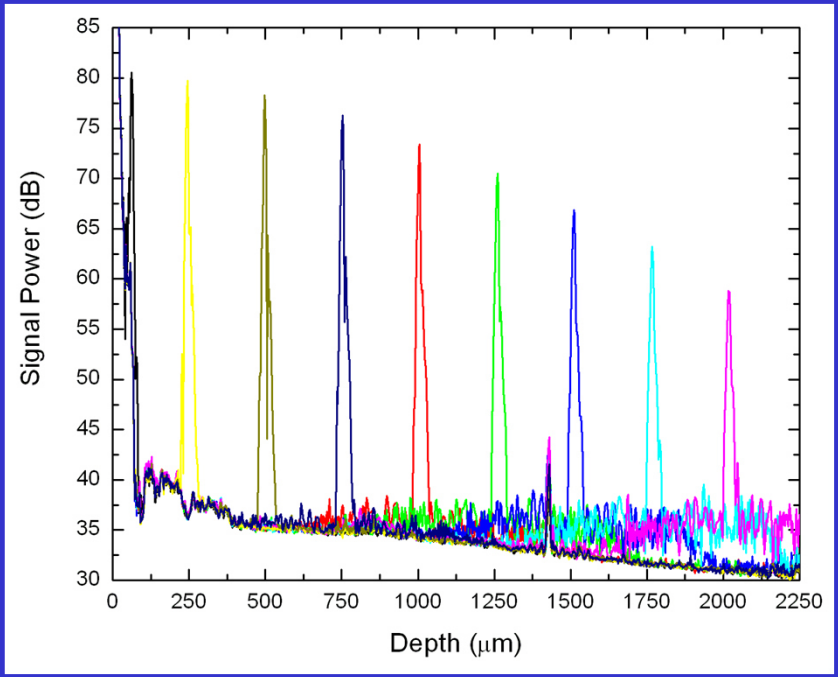

After Zero-Padding

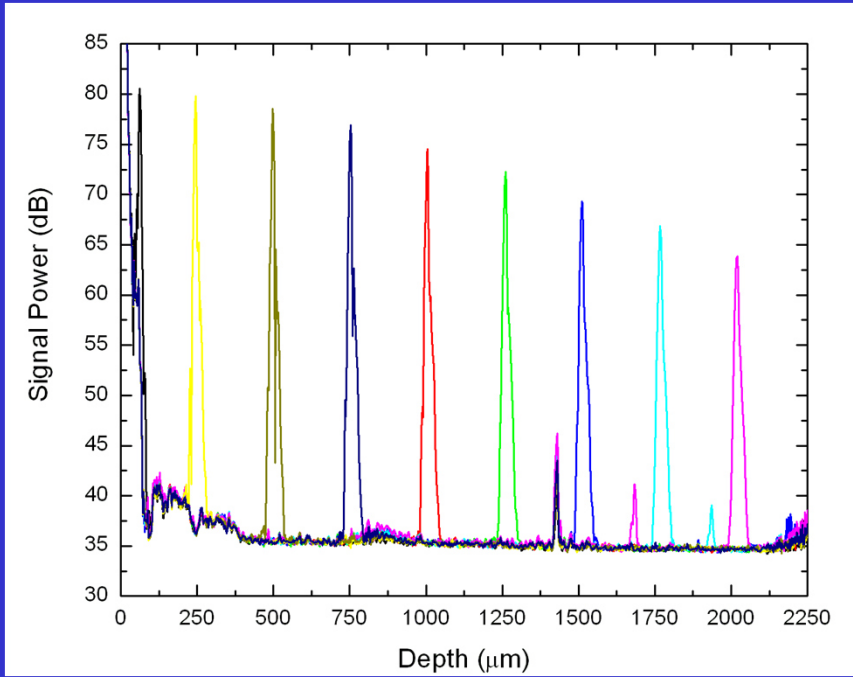

C. Dorrer, *et al.* J. Opt. Soc. Am. B 17, 1795-1802 (2000)

N. A. Nassif *et al.*, Opt. Express 12, 367-376 (2004)

Depth-dependent sensitivity decrease

S. H. Yun *et al.* Opt. Express 2003: **11**, 3598-3604.

$$R(z) = \frac{\sin^2(\pi z/2d)}{(\pi z/2d)^2} \exp\left[-\frac{\pi^2\omega^2}{8\ln 2}\left(\frac{z}{d}\right)^2\right]$$

R. Leitgeb *et al.* Opt. Express 2003:**11**, 889-894.

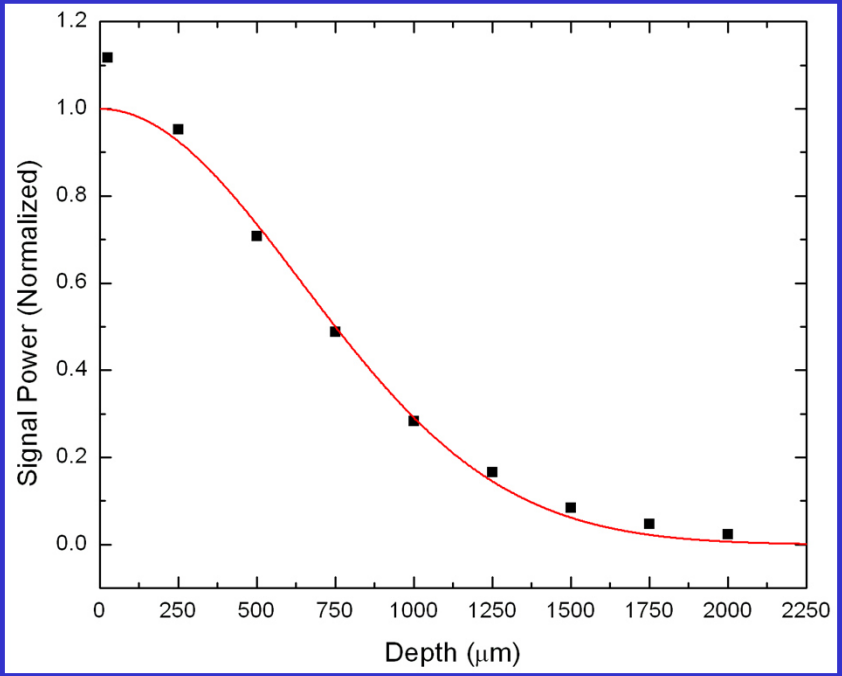

OFDI Principle

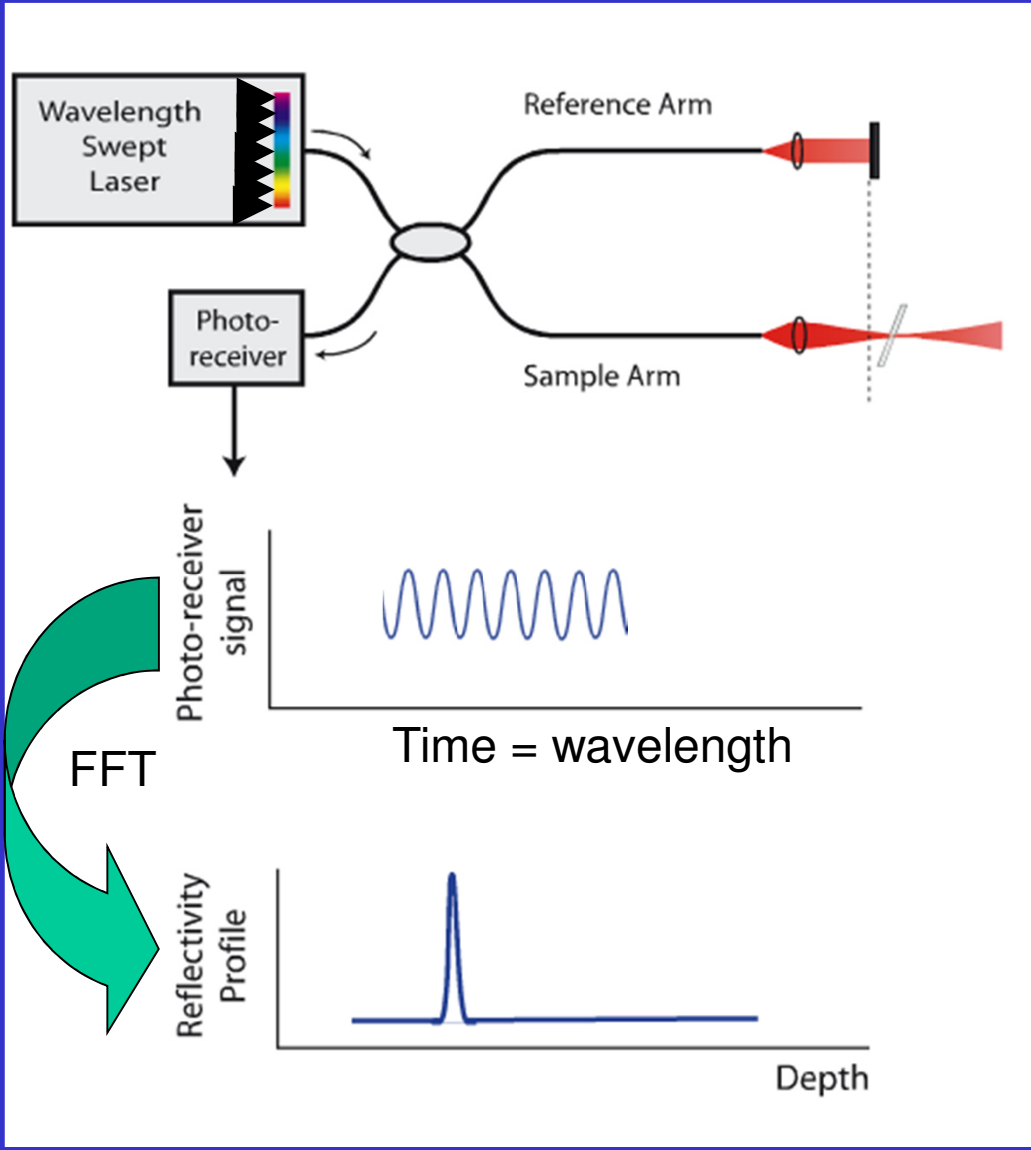

Equivalent with SD-OCT:

Wavelength resolved interference recorded as a function of time

Sensitivity advantage

Fist high speed OFDI system:
S.H. Yun *et al*,
Opt. Express **11**, 2953-2963 (2003).

OFDI system configuration

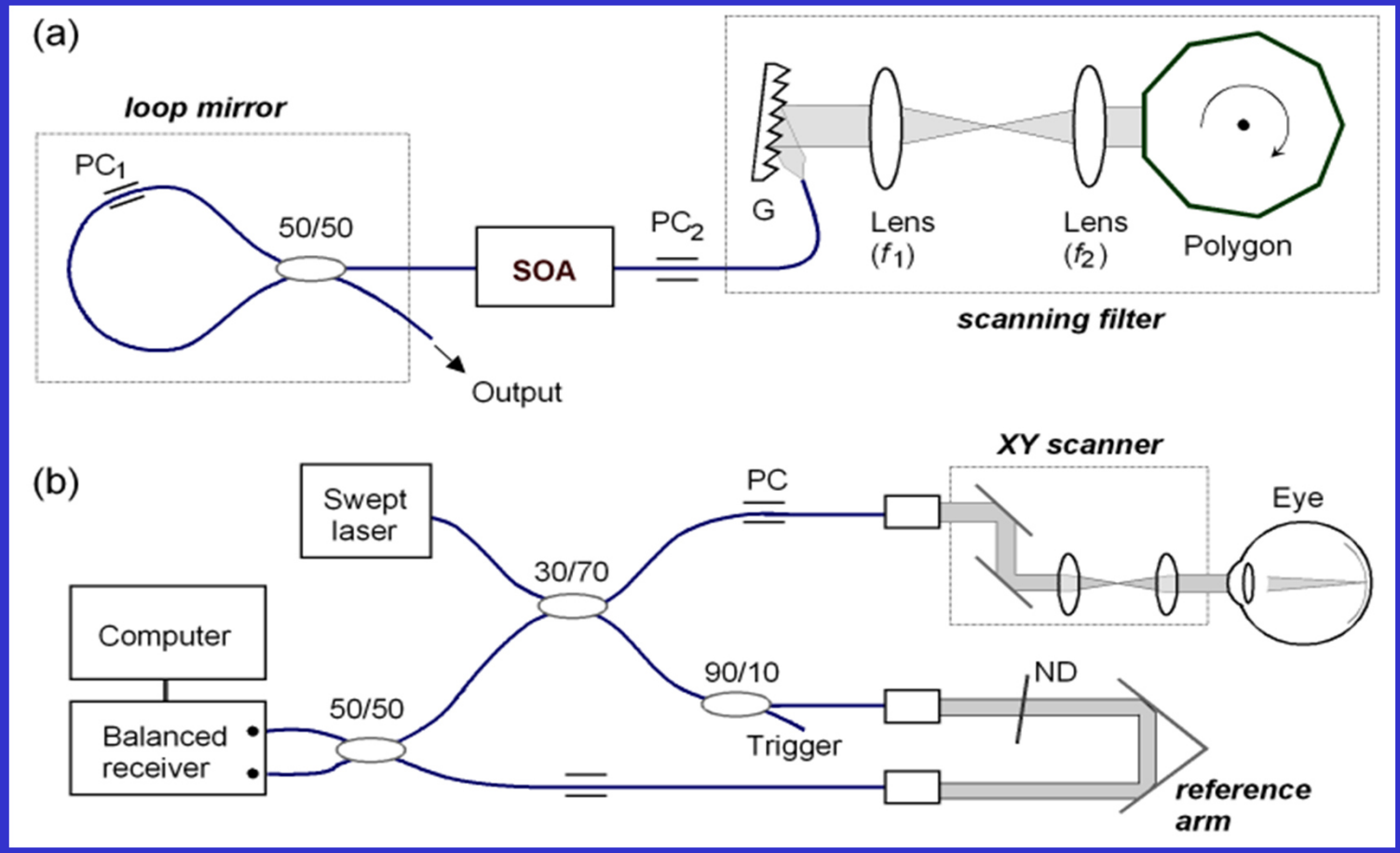

Short cavity

Fist high speed OFDI system:
S.H. Yun *et al*, Opt. Express **11**, 2953-2963 (2003).

FDML laser (long cavity)

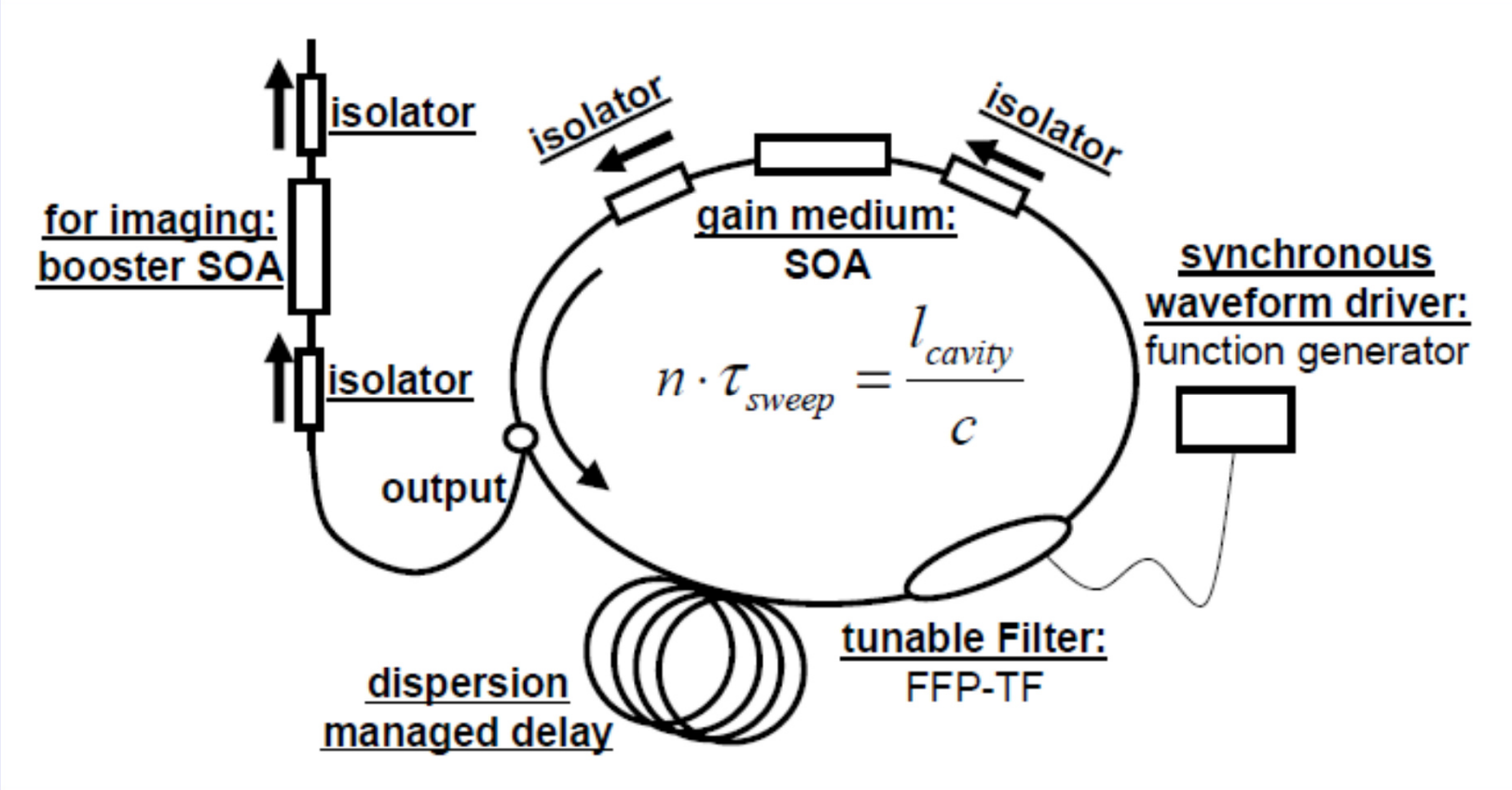

Long cavity, resonant with wavelength filter
Up to 290 KHz sweep rate

Huber et al, Optics Express 14, 8 (2006)

OCT scanning catheters

- Side-looking vs. front-looking
- Proximal actuated vs. distal actuated
- Various sizes

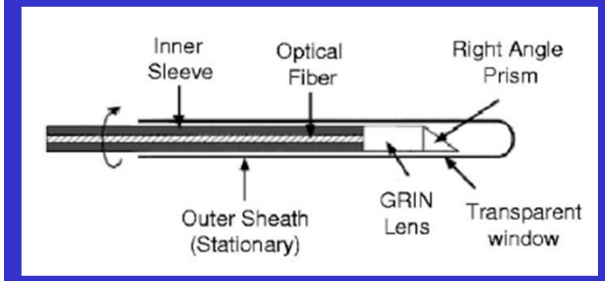

Side-looking, proximal actuation

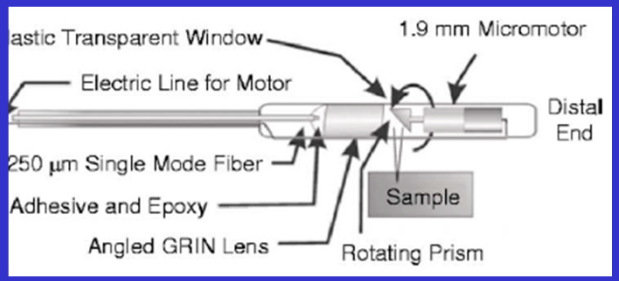

Side-looking, distal actuation

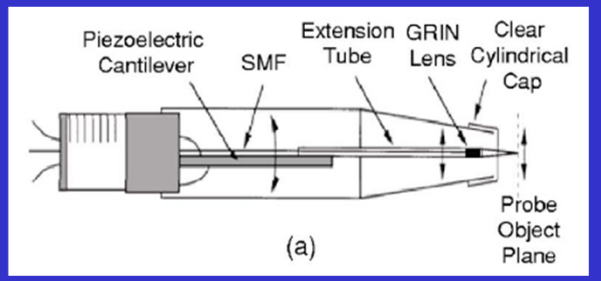

Front-looking, distal actuation

Source: Yaqoob, Z. et. al. J Biomed Opt, 2006

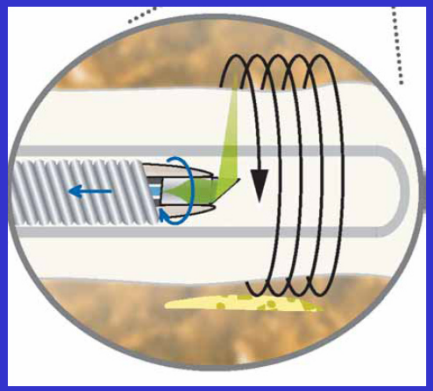

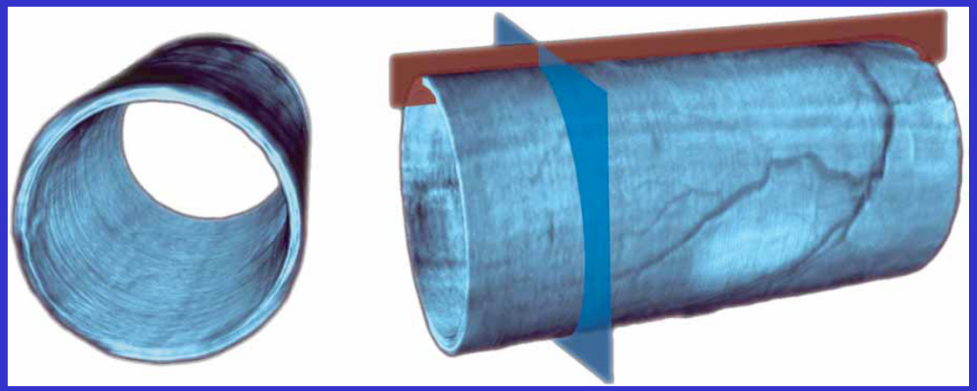

Imaging of tubular organ (esophagus) *Yun, S. H. et. al., Nat. Med., 2006*

In vivo high speed OFDI

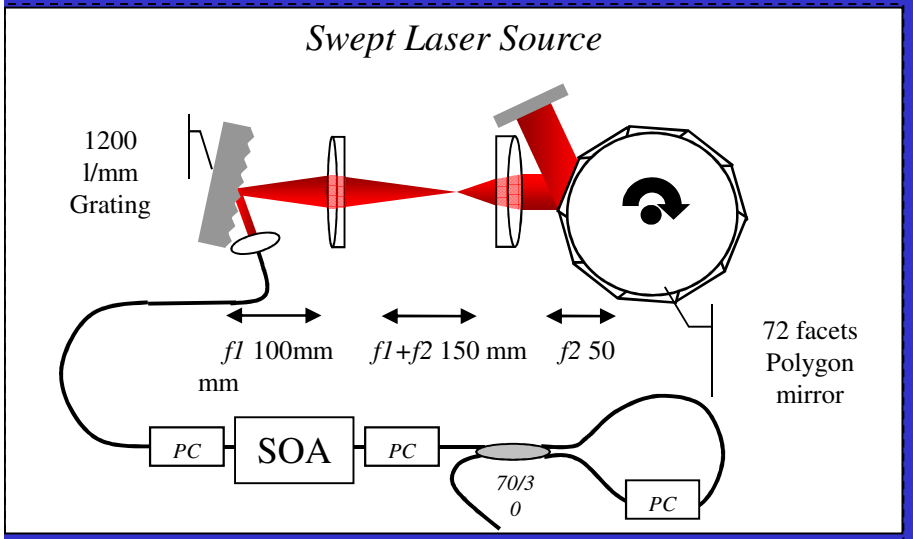

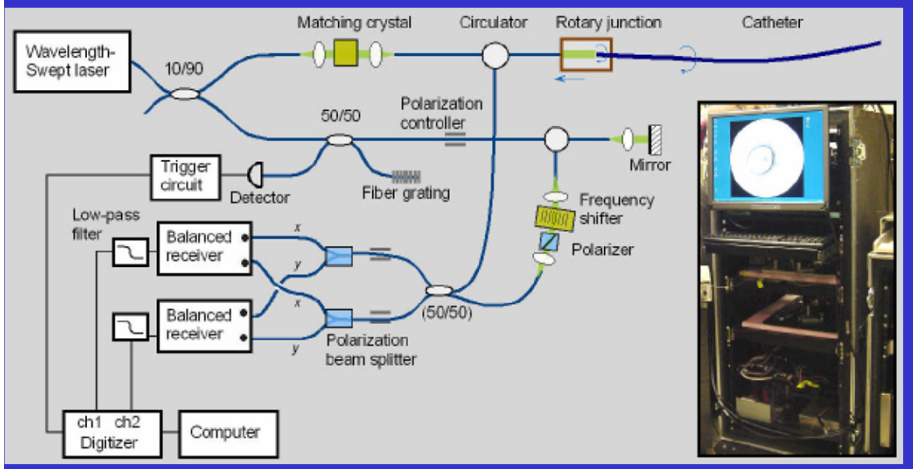

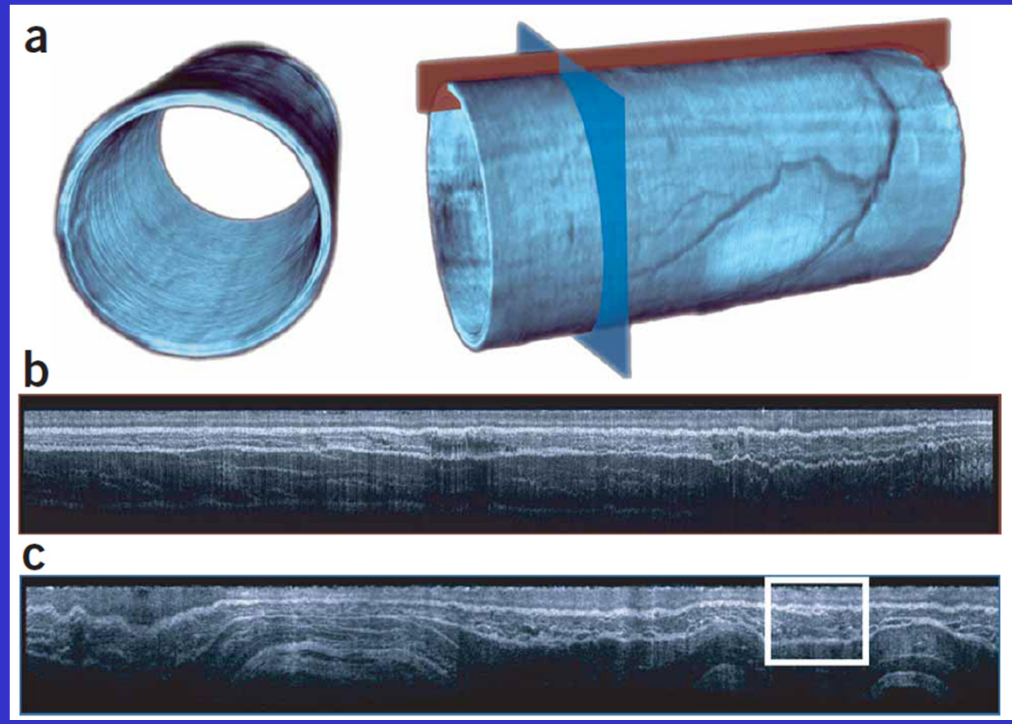

In vivo swine esophagus

63kHz A-line rate, 7.3 mm in air
5.8 min for 4.5 cm, 21 M A-lines
Yun et al. Nature Medicine 12, 12 (2006)

Swept source: OFDI @1310nm

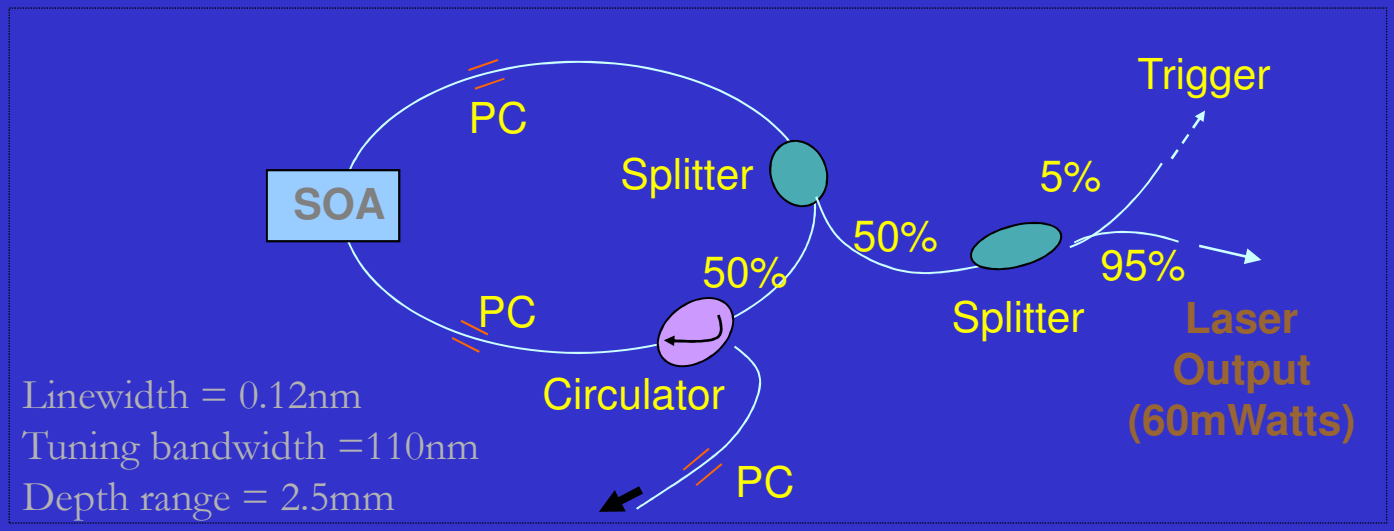

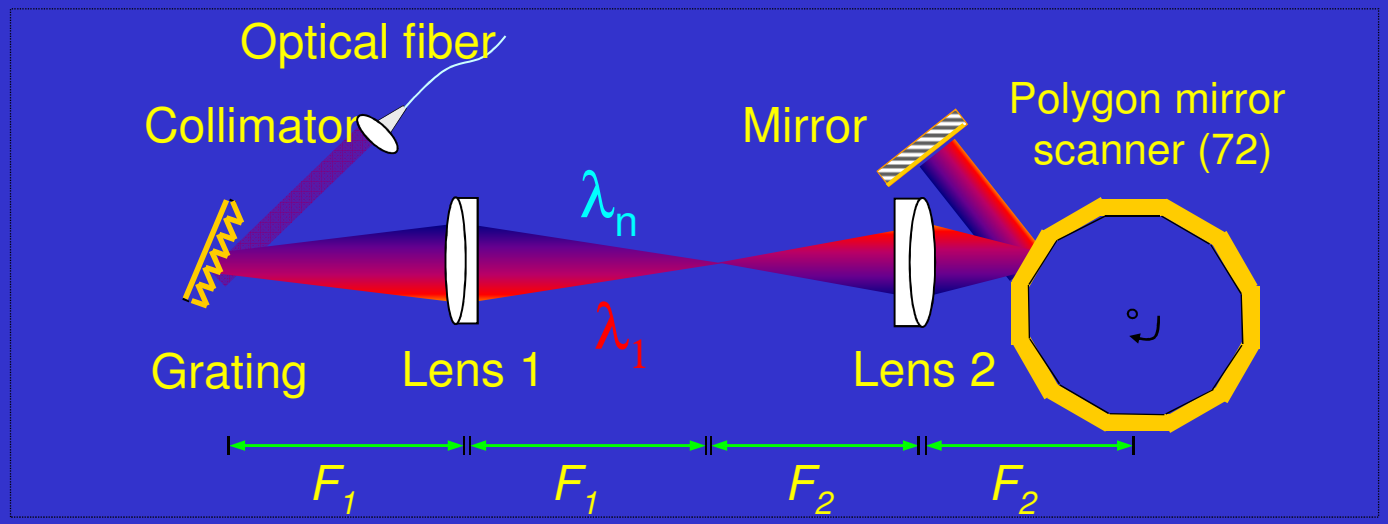

Swept source: OFDI @1310nm

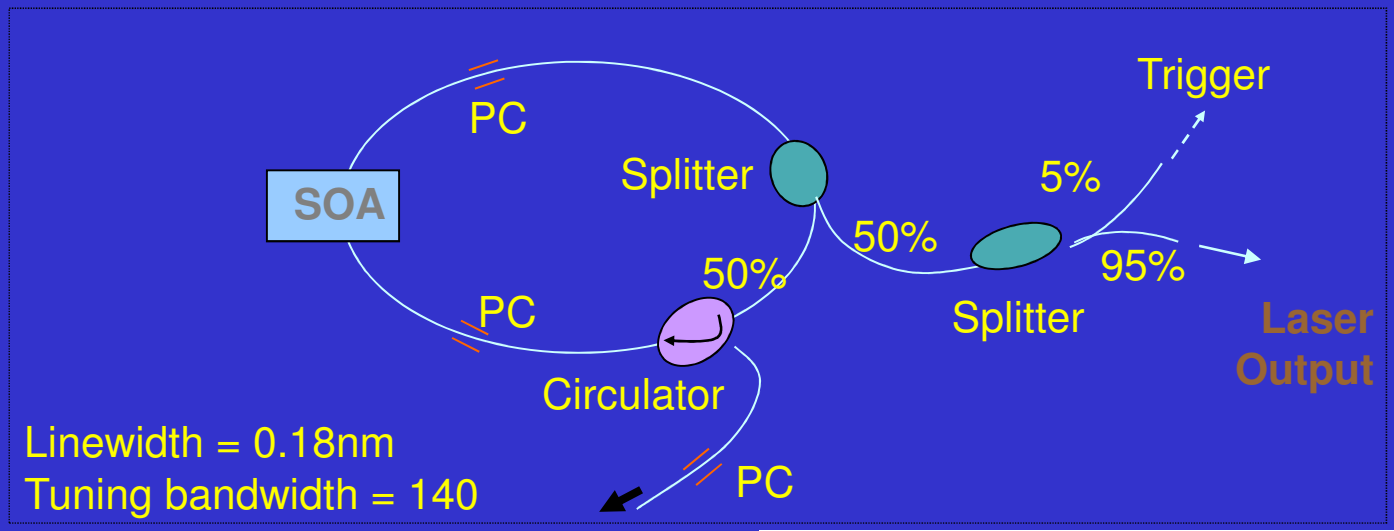

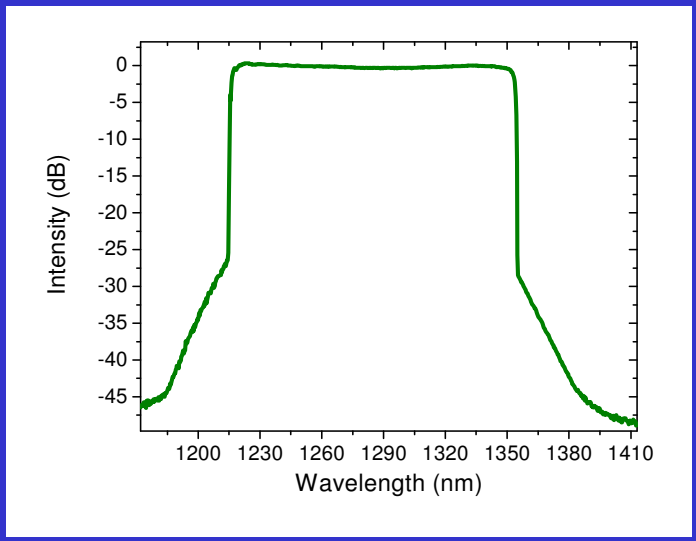

Measured spectrum of the OFDI source using OSA (resolution~7μm in tissue)

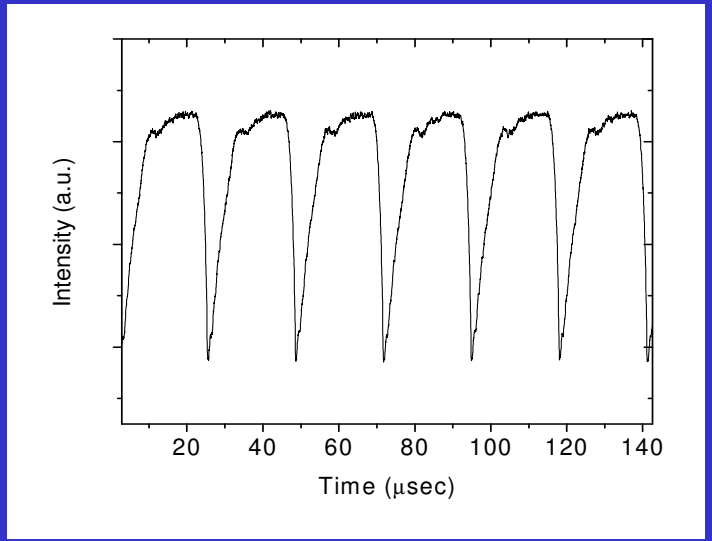

Time response showing six wavelength sweeps (speed 43 KHz)

Volumetric rendering

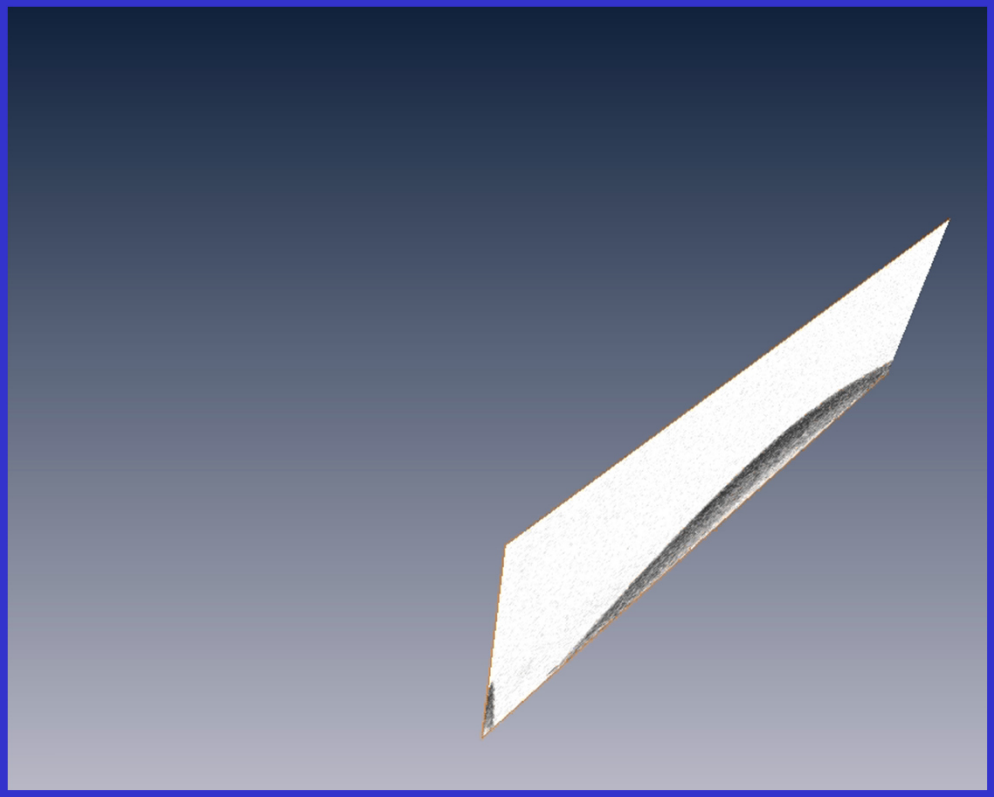

Three dimensional tomography of the anterior segment of the human eye. Acquisition time: 1.4 sec
Volume :13.4x12x4.1mm^3 (490x120x840) pixels

High resolution doppler OCT

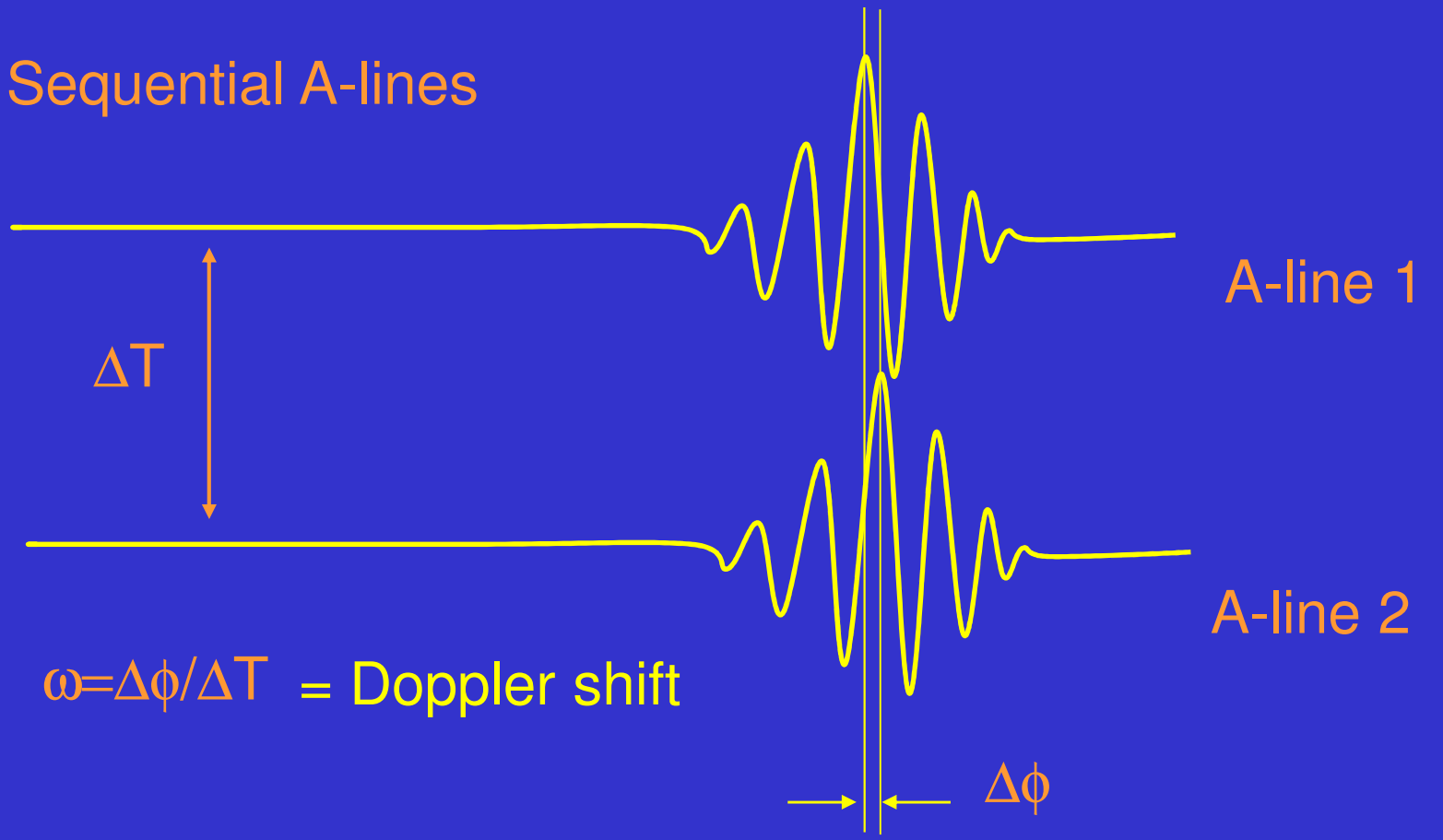

Zhao et al. Optics Letters 25, 2 (2000)

Phase stability: TD versus SD-OCT

Phase Noise of Interferometer:

Time Domain

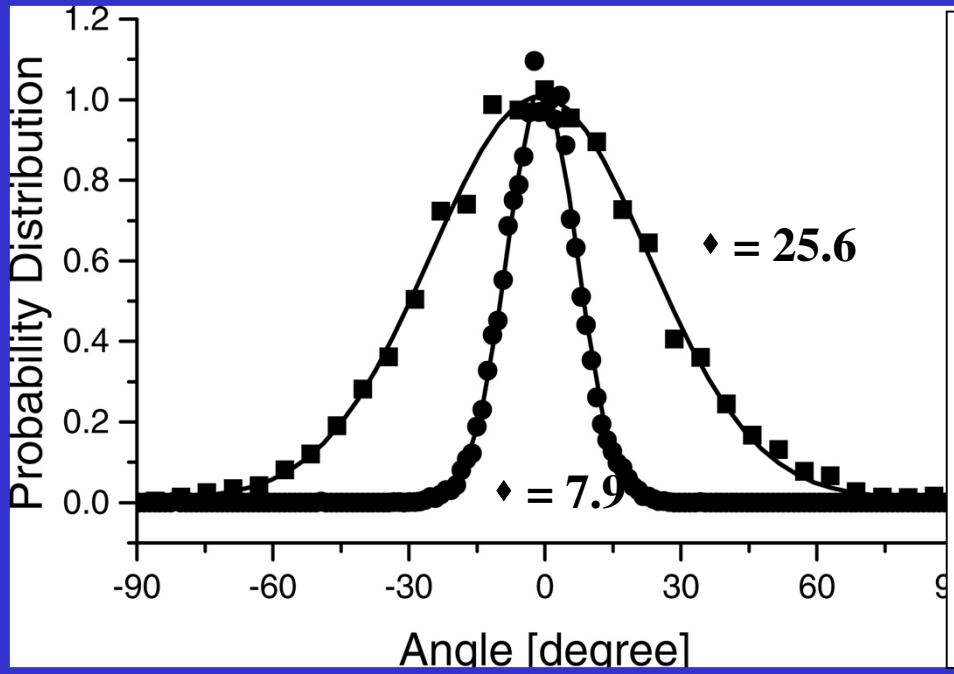

Spectral Domain

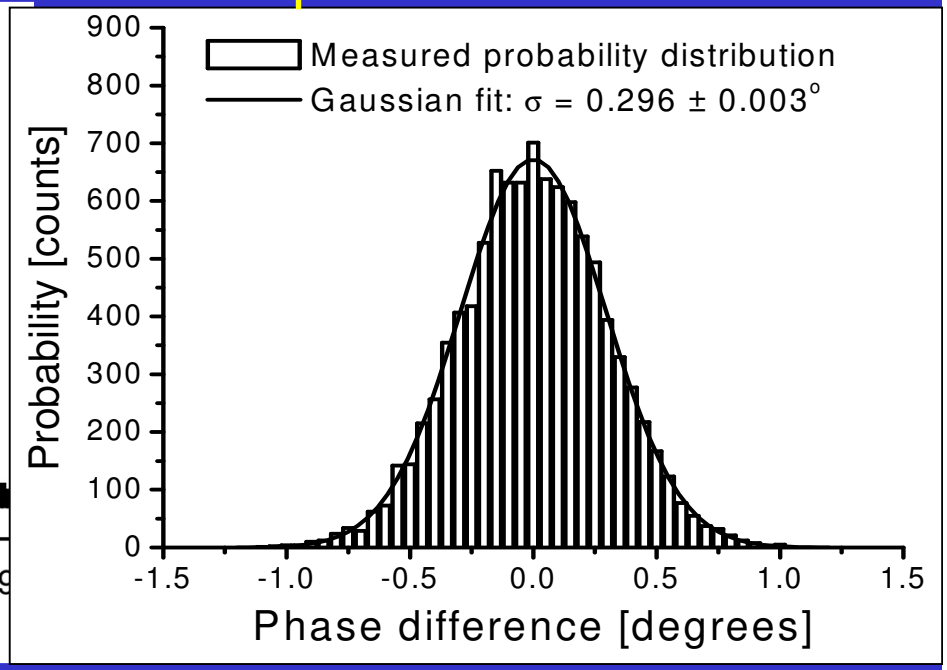

STD is 7.9 (PM) and 25.6 degrees (No PM)
Doppler shift STD ± 22 Hz
Max Dopler shift 500 Hz
Dynamic range: 23

de Boer et al Appl Optics 40 (31) 5787 (2001)

STD is 0.296 degrees (=3.5 nm).
Doppler shift STD ± 25 Hz
Max Doppler shift 15 kHz
Dynamic range: 600

White et al. Opt Express 11(25) 3490 (2003)

In vivo retinal flow imaging

RNFL →

RPE →

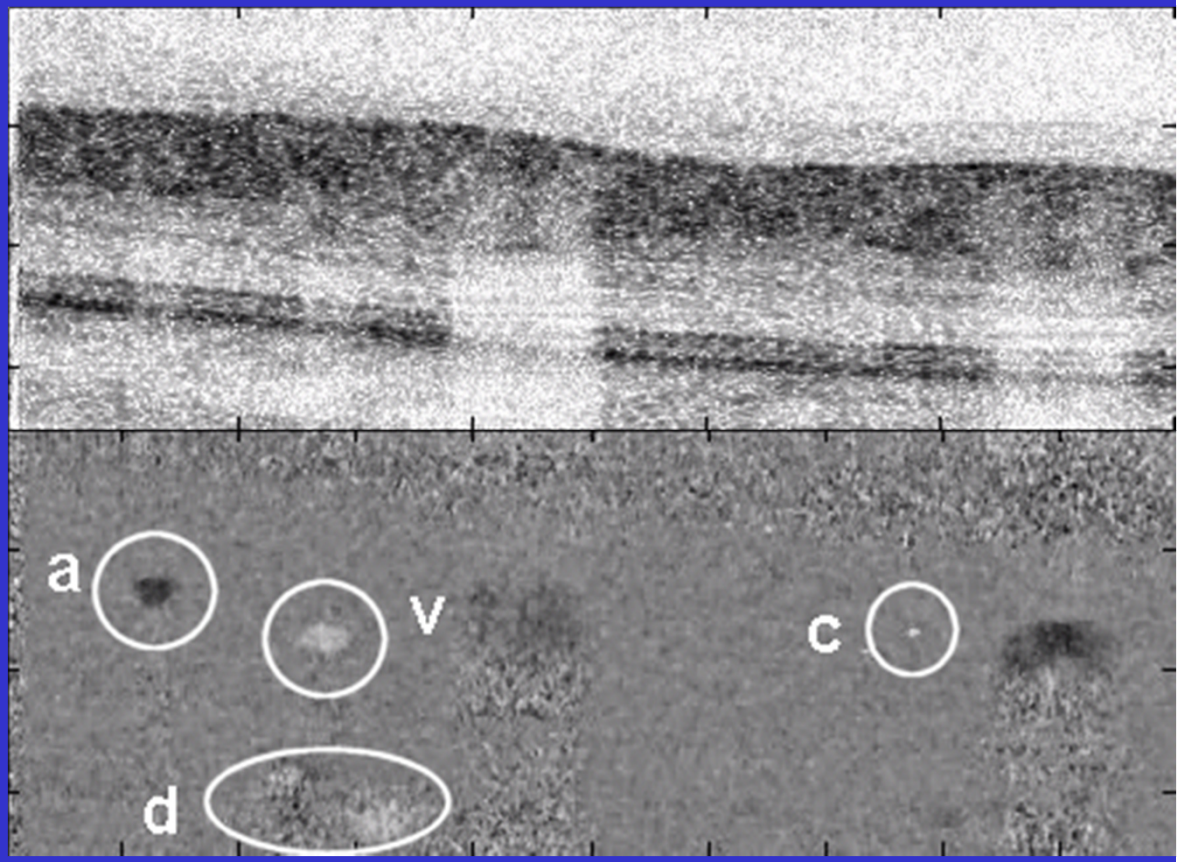

a: artery
v: vein
c: capillary
d: choroidal vessel

$\Delta\phi = +0.8\pi$ (+12 kHz) = black
$\Delta\phi = 0$ = gray
$\Delta\phi = -0.8\pi$ (-12 kHz) = white

1.6 mm x 0.58 mm

B. R. White et al. Opt. Express 11 (25), 3490-3497 (2003)

Retinal Blood Flow Pulsation

2

1.15 mm X 608 µm

circle diameter
112 µm; 128 µm

vessel diameter
60 µm ; 70 µm

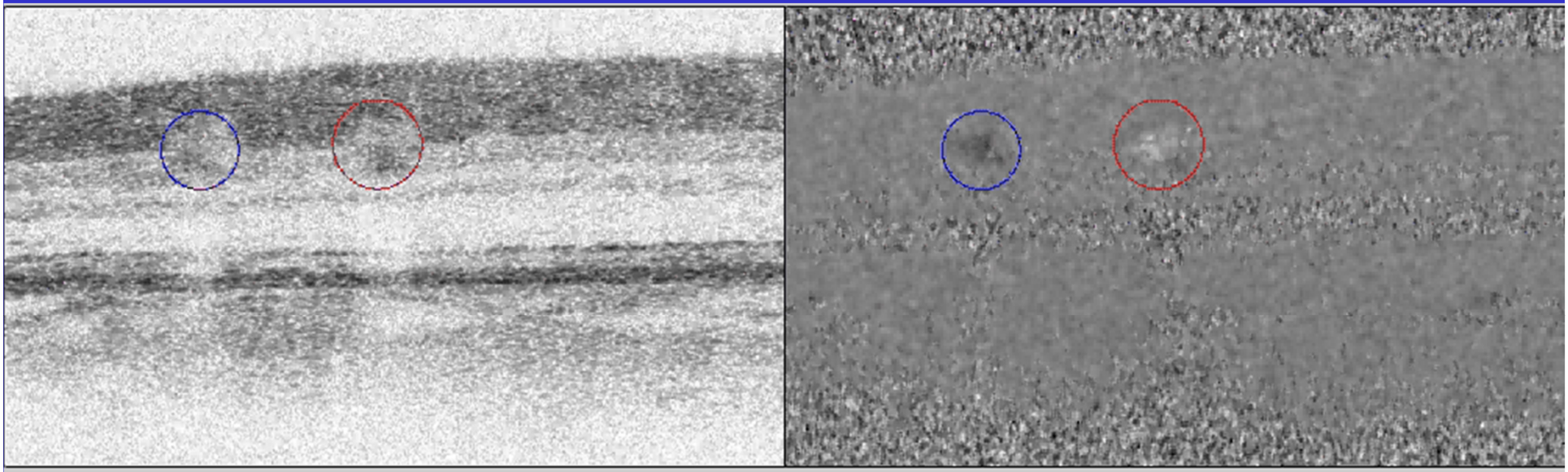

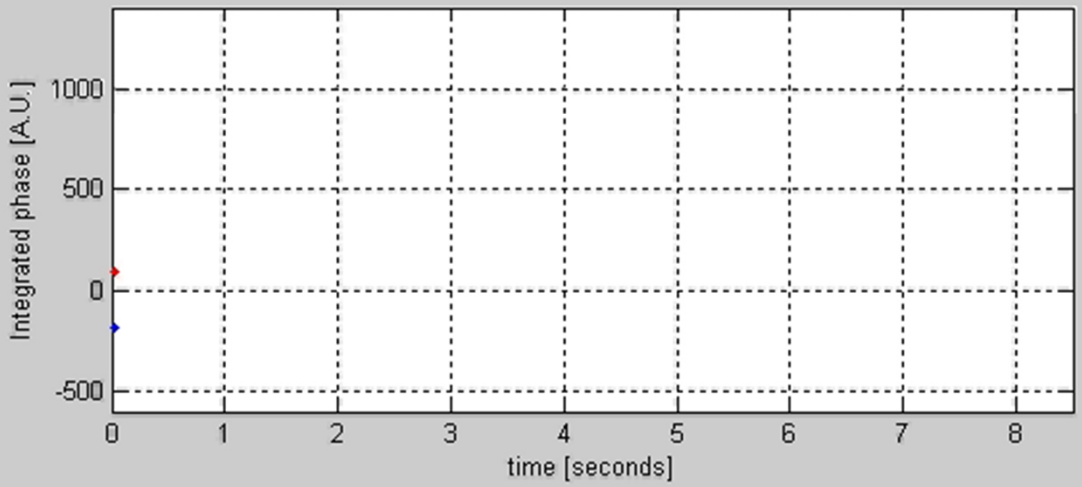

Light polarization

Light is a transverse wave,
oscillation perpendicular to propagation direction

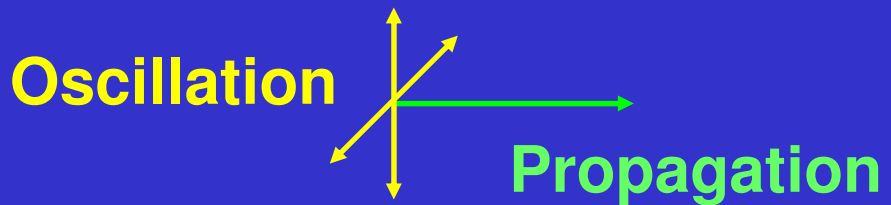

Sound is a longitudinal wave,
oscillation parallel to propagation direction

Oscillation **Propagation**

Use of polarization in imaging

Reject multiple scattered light (Transmission)
→ Multiple scattered light has random polarization
Reject single scattered light (Reflection)
→ Probe deeper into tissue

Polarization is changed by tissue in a predictable manner → Birefringence

Birefringent biological structures:
Collagen, Muscle, Nerves, Tendon, Cartilage

Number of variables to characterize polarization properties of light

Purely polarized light: 3
Amplitude E_x, Amplitude E_y,
Phase relation a between E_x and E_y

Partially polarized light: Add degree of polarization P

Degree of Polarization

Unpolarized light: No correlation between orthogonal wave components (Sunlight)

Hor. Comp E field.

Vert. Comp E field

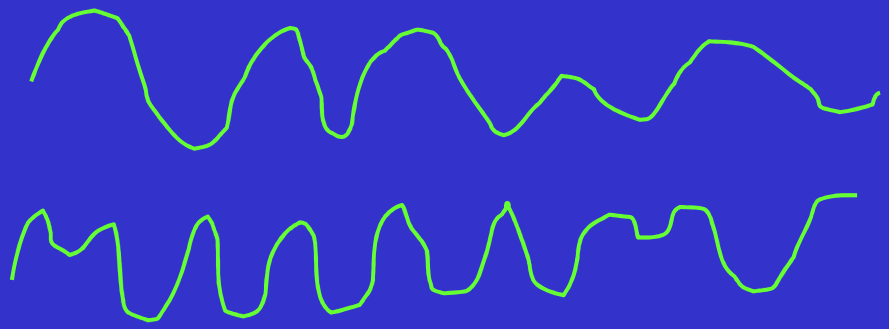

No Correlation: Unpolarized light

Hor. Comp E field.

Vert. Comp E field

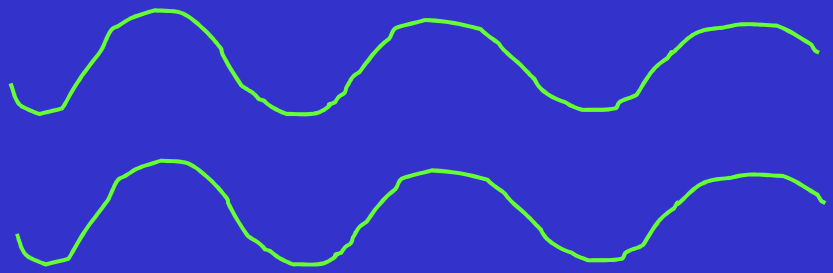

Correlation: Polarized light

Scattering and Coherence

Processes that can change the degree of polarization involve transfer of phase

- Inelastic scattering
- Raman scattering
- Fluorescence

Elastic scattering preserves coherence

How about second harmonic generation?

Birefringence

Birefringence:

Different refractive index along fast and slow axis

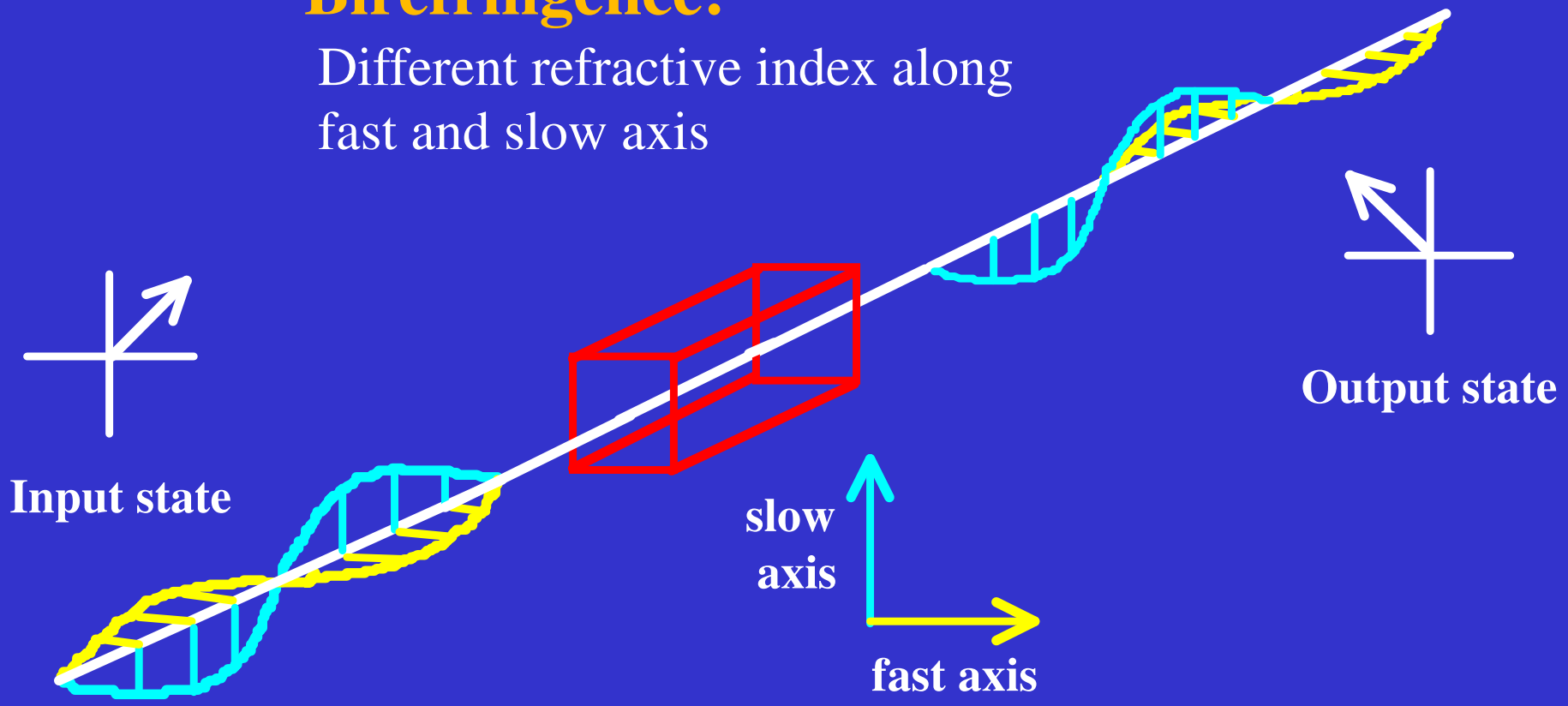

Optical Birefringence of fibrous structures

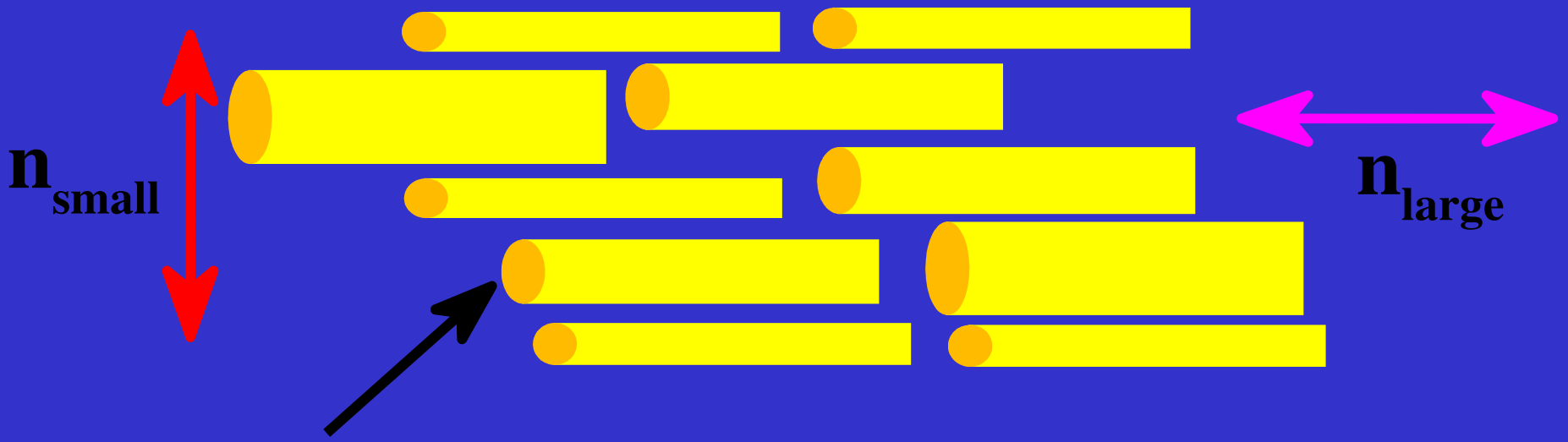

Birefringence = $\Delta n = n_{large} - n_{small}$

Measure birefringence by use of polarized light.
Birefringence will change the polarization state of the light and create a phase difference.

Polarization States

Definition of the Stokes parameters

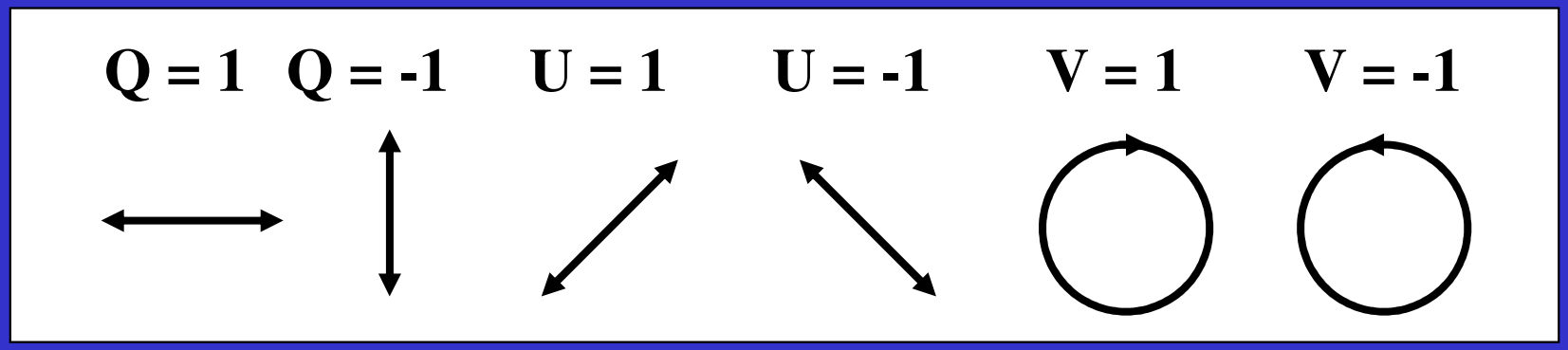

Degree of polarization P $= (Q^2 + U^2 + V^2)^{1/2}/I$

Three parameters:
E-Field along x and y axis and relative phase

Four independent measurements needed to determine Stokes parameters

Stokes Vectors and Poincaré Sphere

Stokes Vector

$$\begin{vmatrix} I \\ Q \\ U \\ V \end{vmatrix}$$

Intensity

Pol. { Linear component ↔ ↕
Linear component ↗ ↘
L, R circular component

- **Degree of polarization:**

  $P = (Q^2 + U^2 + V^2)^{1/2} / I$

- **Birefringence modeled as rotation around an axis in the Q-U plane.**

Poincaré Sphere

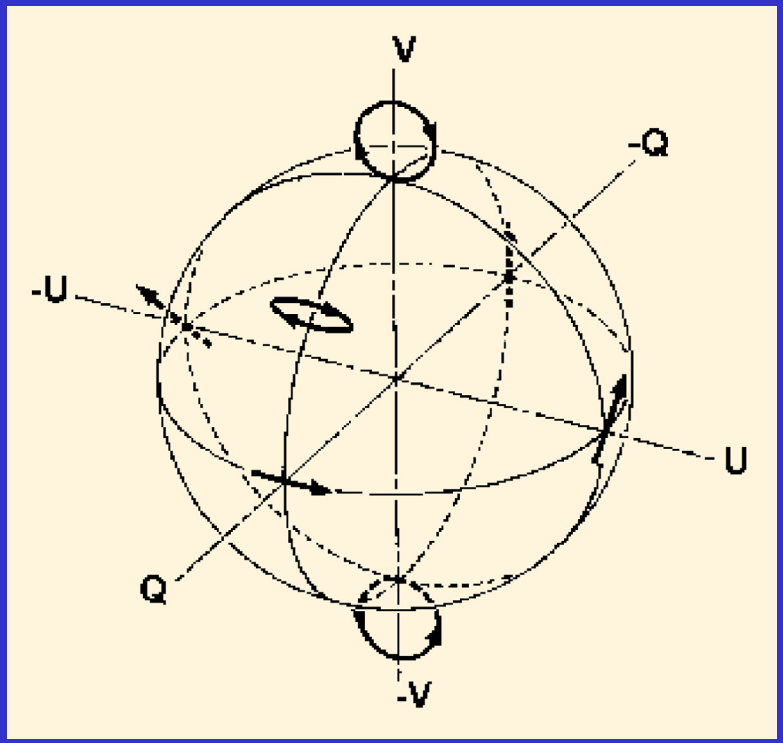

Determination of OpticAxis

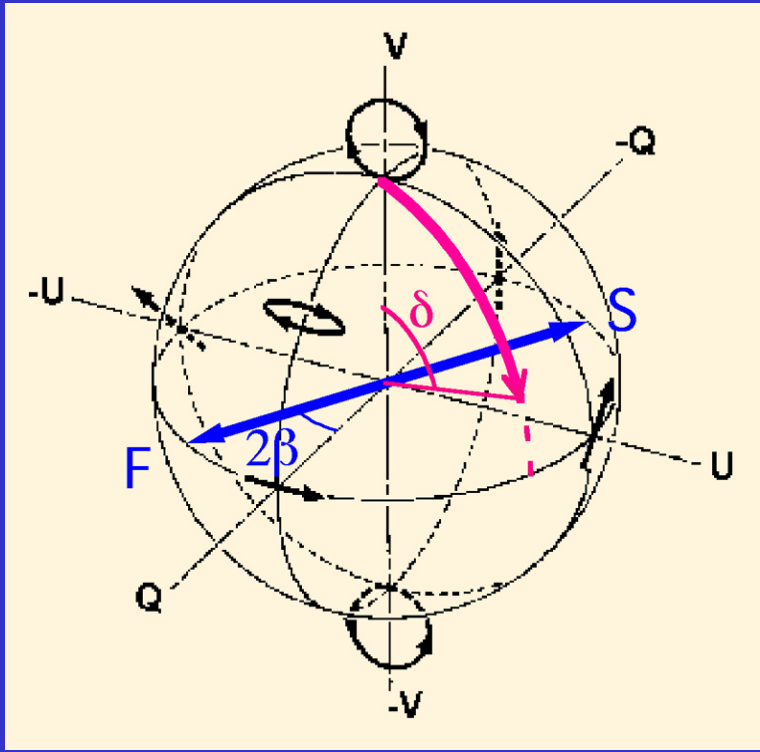

β = optic axis angle

δ = retadance

$$\begin{vmatrix} I \\ Q \\ U \\ V \end{vmatrix} = \begin{vmatrix} 1 \\ 0 \\ 0 \\ 1 \end{vmatrix}$$

Circular input polarization

$$\begin{vmatrix} I' \\ Q' \\ U' \\ V' \end{vmatrix} = \begin{vmatrix} 1 \\ -\sin 2\beta \sin \delta \\ \cos 2\beta \sin \delta \\ \cos \delta \end{vmatrix}$$

Polarization after linear retarder

Polarization-Sensitive OCT

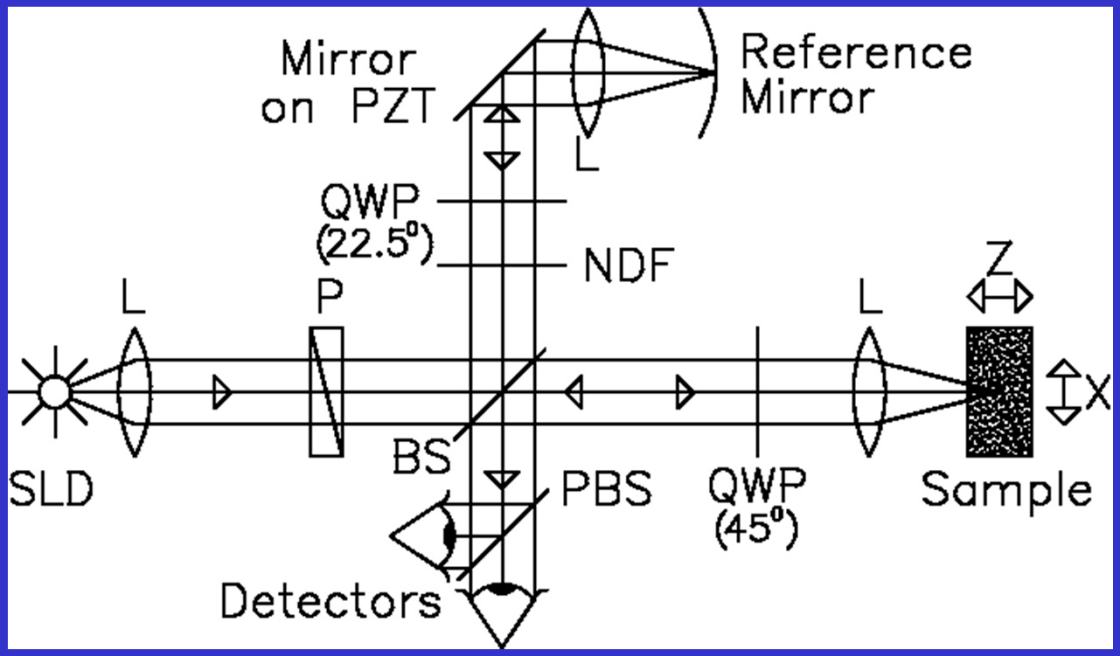

Polarization diversity: $|\mathbf{E}x \bullet Ex|^2 + |\mathbf{E}y \bullet Ey|^2$

Polarization detection: (Ex, Ey)

De Boer et al, Opt Lett 1997

Birefringence Analysis

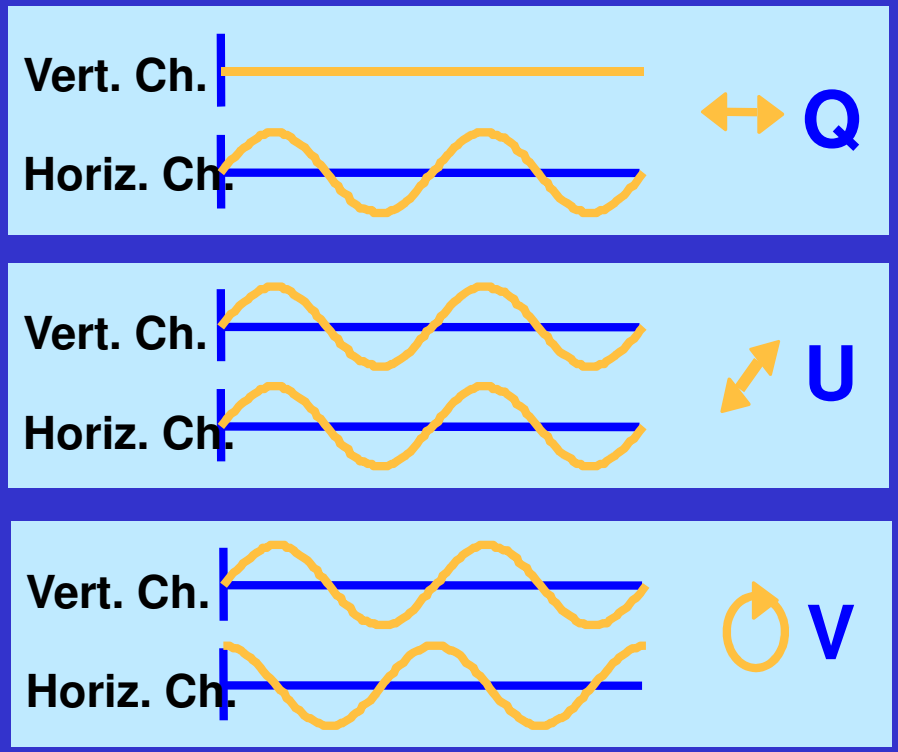

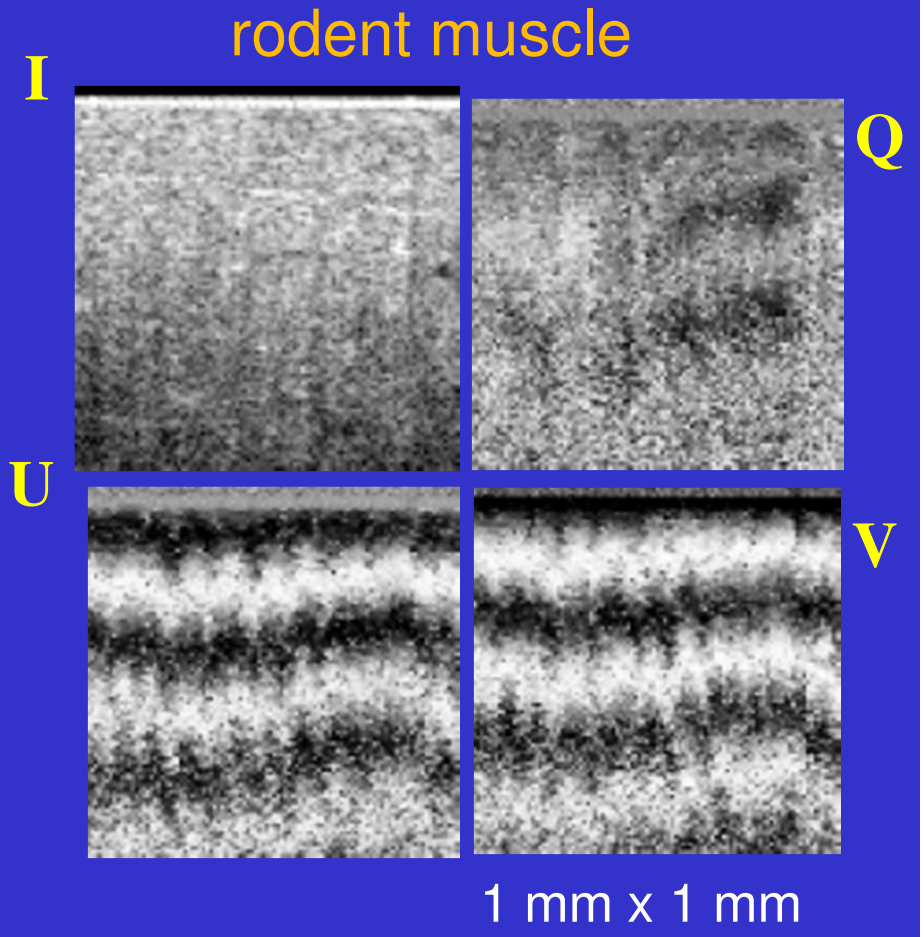

De Boer et al, Opt. Lett. 1999

Fiber-based PSOCT System

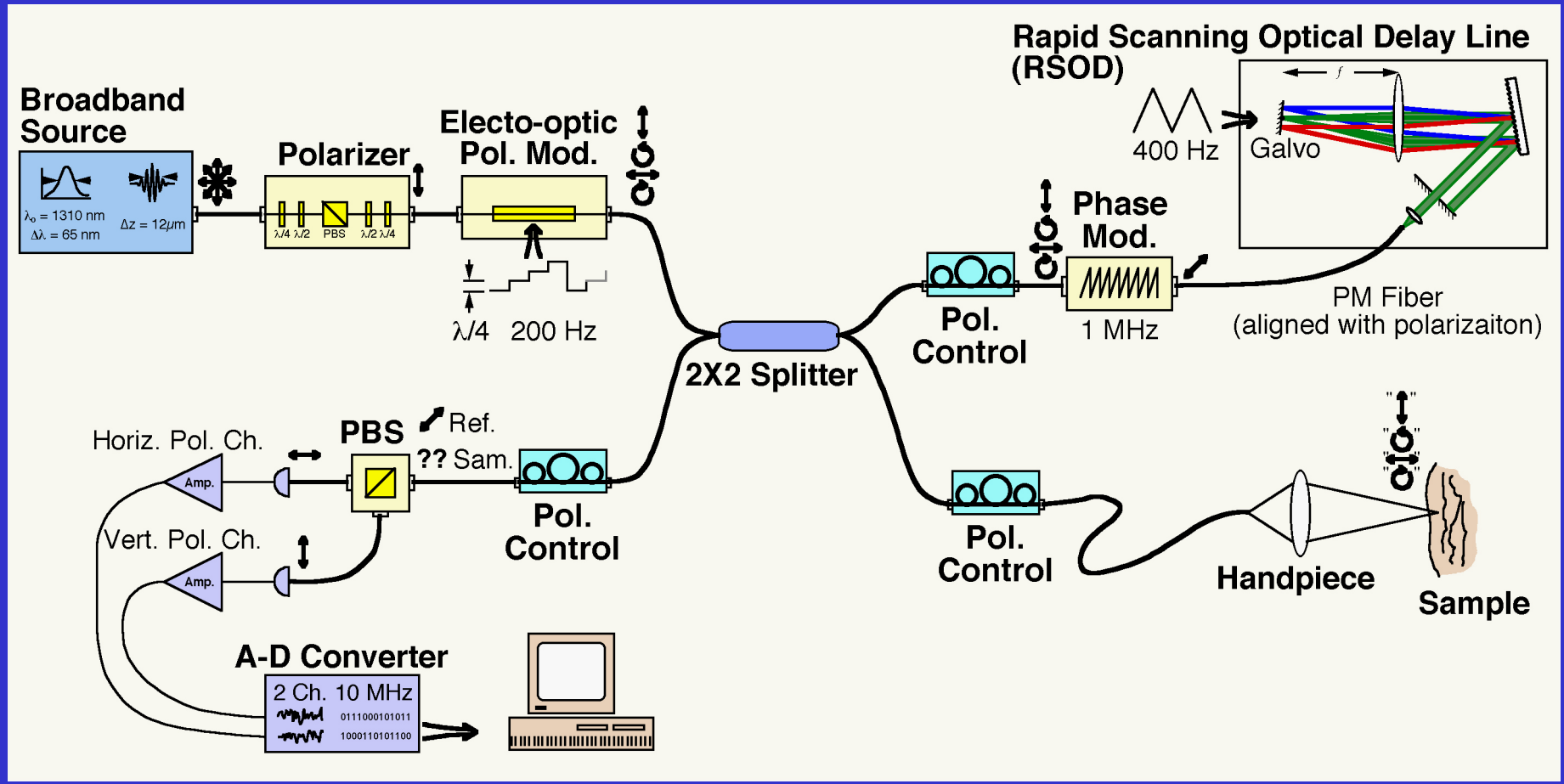

C. E. Saxer *et al*,. Opt. Lett. 25: 1355, 2000.

Fiber-based PS-OCT

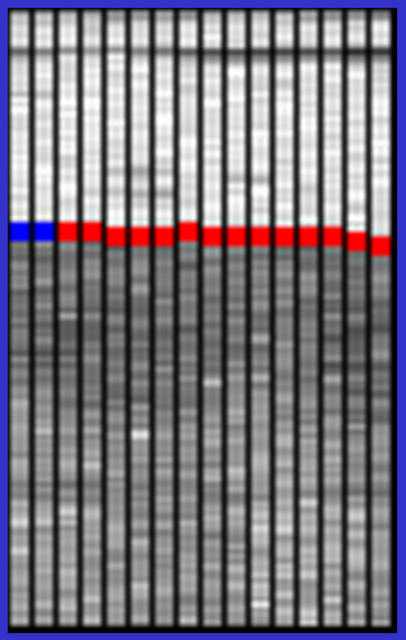

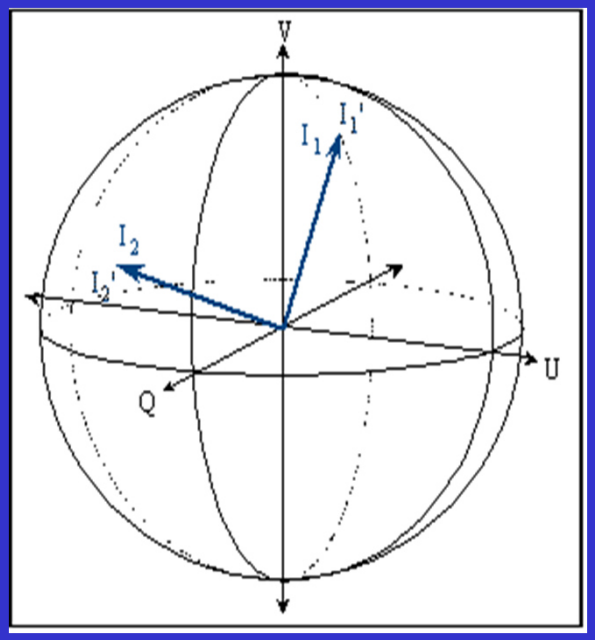

The sample polarization properties can be determined by alternating between incident polarization states orthogonal in a Poincaré sphere representation, and using the polarization states reflected back from the surface and from some depth.

de Boer et al., Opt. Lett. 24: 300 (1999), Saxer et al., Opt. Lett. 25: 1355 (2000),
Park et al., J. Biomed. Opt. 6: 474 (2001), Park et al., Opt. Exp. 11: 782 (2003)

Vector-based methods

- Simple method
  - Assumption: no diattenuation.

  Advantage:
  - computationally efficient.
  - Implemented in real-time systems and used in clinical studies

  - Disadvantages: phase wrapping at 180°

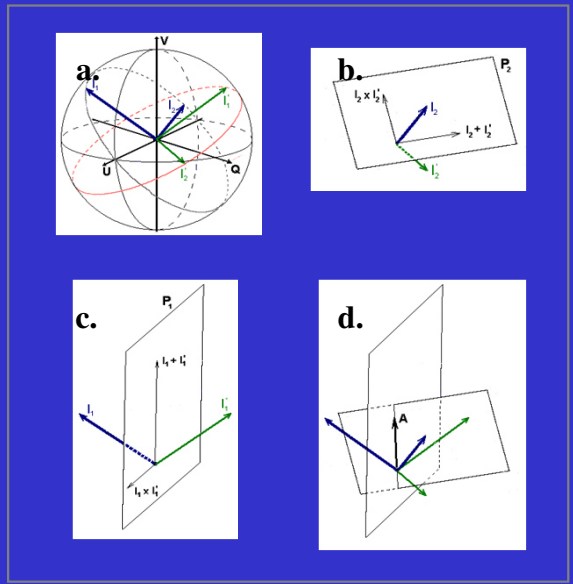

de Boer et al., Opt. Lett. 24: 300 (1999), Saxer et al., Opt. Lett. 25: 1355 (2000),
Park et al., J. Biomed. Opt. 6: 474 (2001), Park et al., Opt. Exp. 11: 782 (2003)

Jones matrix

$$\vec{E} = \begin{bmatrix} H \\ V \end{bmatrix}$$

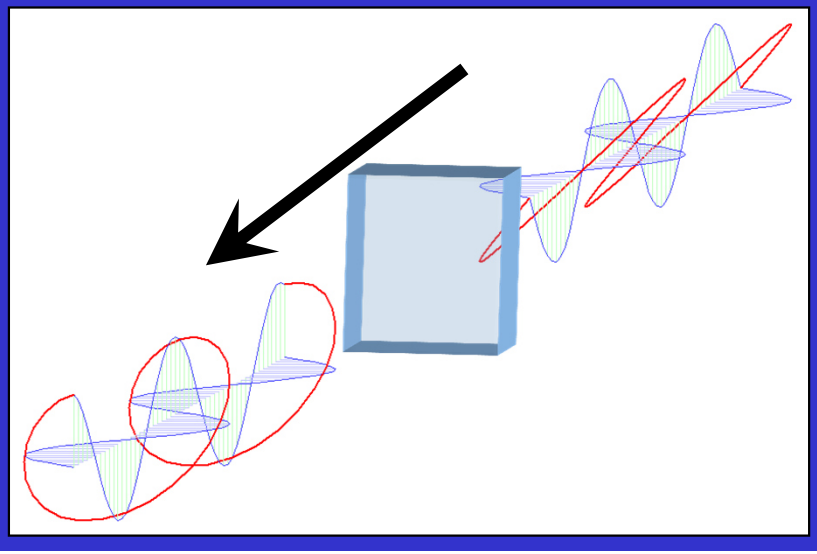

$$\vec{E'} = \begin{bmatrix} H' \\ V' \end{bmatrix}$$

$$\vec{E'} = \begin{bmatrix} H' \\ V' \end{bmatrix} = e^{i\phi} \begin{bmatrix} J_{11} & J_{21} \\ J_{12} & J_{22} \end{bmatrix} \begin{bmatrix} H \\ V \end{bmatrix} = \mathbf{J}\vec{E}$$

- A Jones matrix is composed of 4 complex numbers, however, an arbitrary phase factor reduces a Jones matrix to 7 independent variables.
- The relation between an incident and transmitted polarization state yields 3 independent equations (a_H, a_V, $\Delta\delta$).
- Assuming diattenuation and birefringence axis are identical, number of independent parameters in J is reduced to 5 (Jiao, Wang)

Jones matrices

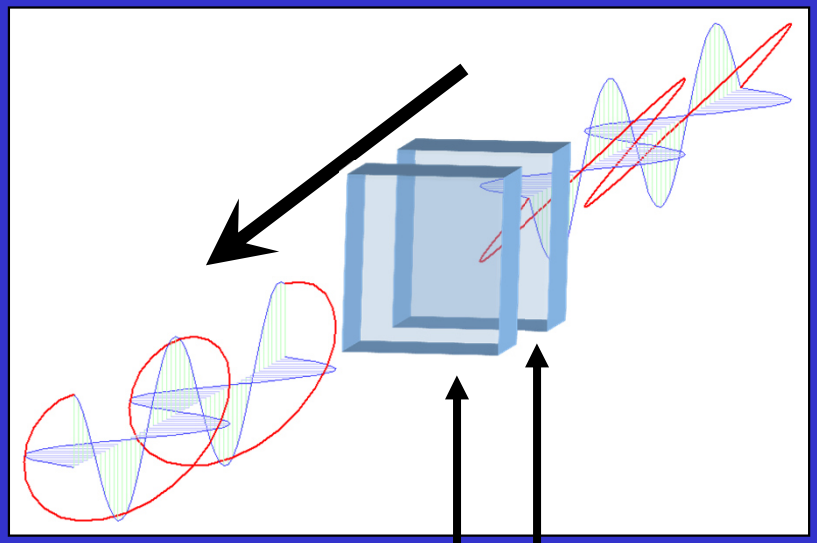

$$\vec{E'} = e^{i\phi}\mathbf{J}_2\mathbf{J}_1\vec{E}$$

- Transmission through multiple optical elements can be expressed mathematically by the product of Jones matrices

Jones matrix solution

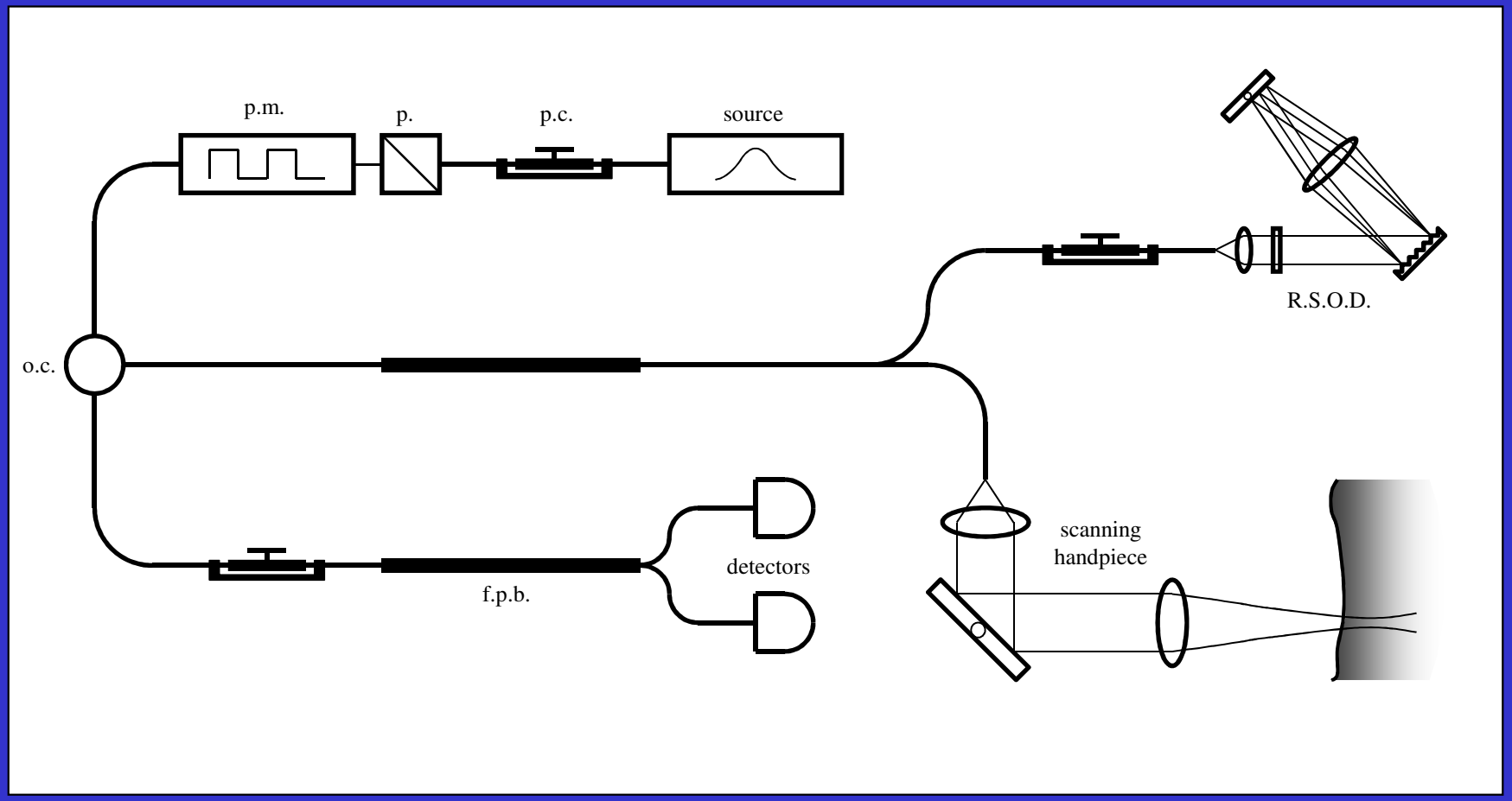

B.H. Park, et al., "Optic axis determination accuracy for fiber-based polarization-sensitive optical coherence tomography," Optics Letters 30(19): *in press* (2005).
B.H. Park, et al., "Jones matrix analysis for a polarization-sensitive optical coherence tomography system using fiber-optic components," Optics Letters 29(21): 2512-4 (2004).

Jones matrix solution

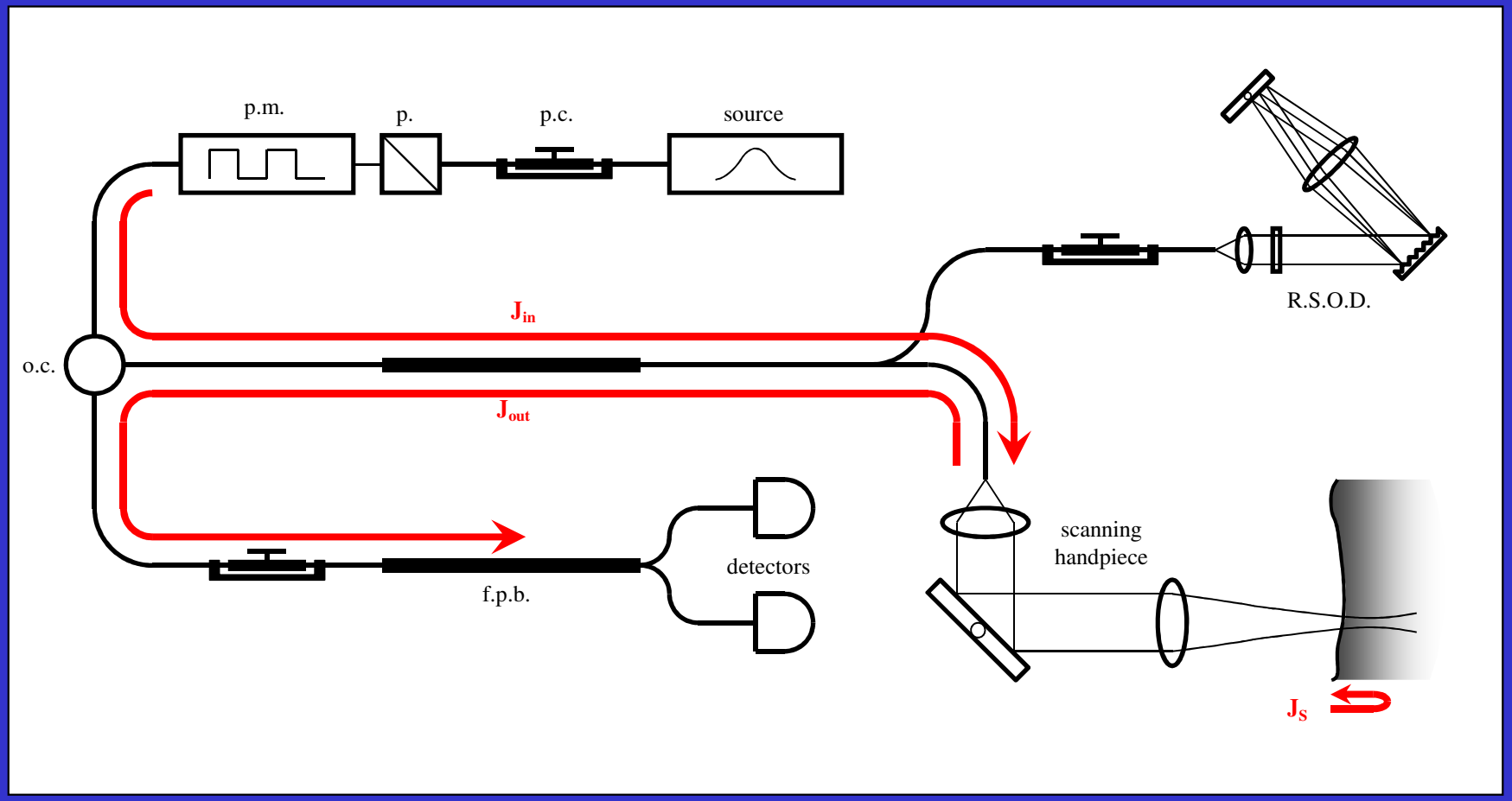

B.H. Park, et al., "Optic axis determination accuracy for fiber-based polarization-sensitive optical coherence tomography," Optics Letters 30(19): *in press* (2005).
B.H. Park, et al., "Jones matrix analysis for a polarization-sensitive optical coherence tomography system using fiber-optic components," Optics Letters 29(21): 2512-4 (2004).

Jones matrix solution

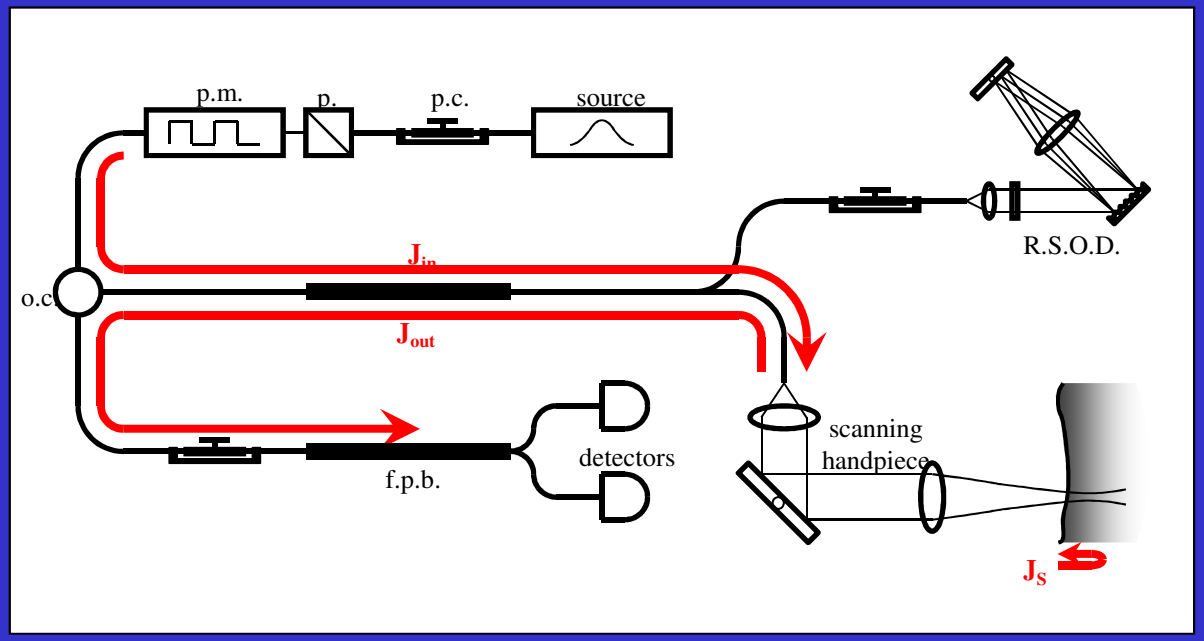

$$\mathbf{J}_{\text{in}}, \mathbf{J}_{\text{out}} \in \mathrm{SU}(2)$$

$$\vec{E} = e^{i\psi}\mathbf{J}_{\text{out}}\mathbf{J}_{\text{in}}\vec{E}_{in}$$

$$\vec{E'} = e^{i\psi'}\mathbf{J}_{\text{out}}\mathbf{J}_{\text{S}}\mathbf{J}_{\text{in}}\vec{E}_{in}$$

$$\vec{E'} = e^{i\psi'}\mathbf{J}_{\text{out}}\mathbf{J}_{\text{S}}\mathbf{J}_{\text{in}}\left(e^{-i\psi}\mathbf{J}_{\text{in}}^{-1}\mathbf{J}_{\text{out}}^{-1}\vec{E}\right) = e^{i\Delta\psi}\mathbf{J}_{\text{out}}\mathbf{J}_{\text{S}}\mathbf{J}_{\text{out}}^{-1}\vec{E}$$

$$\begin{bmatrix} H' \\ V' \end{bmatrix} = e^{i\Delta\psi}\underbrace{\mathbf{J}_{\text{out}}\mathbf{J}_{\text{S}}\mathbf{J}_{\text{out}}^{-1}}_{\mathbf{J}_{\text{T}}}\begin{bmatrix} H \\ V \end{bmatrix}$$

B.H. Park, et al., "Optic axis determination accuracy for fiber-based polarization-sensitive optical coherence tomography," Optics Letters 30(19): *in press* (2005).

B.H. Park, et al., "Jones matrix analysis for a polarization-sensitive optical coherence tomography system using fiber-optic components," Optics Letters 29(21): 2512-4 (2004).

Jones matrix solution

- The measurable Jones matrix, $\mathbf{J}_T$, is a combination of the sample and system fiber contributions, and is given by

$$\mathbf{J}_T = \mathbf{J}_{out}\mathbf{J}_S\mathbf{J}_{out}^{-1} \qquad \text{where} \quad \mathbf{J}_{out} \in SU(2)$$

- The sample Jones matrix, $\mathbf{J}_S$, can be decomposed into a central diagonal matrix, $\mathbf{J}_C=[P_1 e^{ih/2},0;0,P_2 e^{-ih/2}]$, that contains the amounts of diattenuation and birefringence, surrounded by a rotation, $\mathbf{J}_{OA}$, defined by the sample optic axis

$$\mathbf{J}_S = \mathbf{J}_{OA}\mathbf{J}_C\mathbf{J}_{OA}^{-1} \qquad \text{where} \quad \mathbf{J}_{OA} \in SU(2)$$

- By substitution and the closure property of the SU(2) group,

$$\mathbf{J}_T = \mathbf{J}_{out}\left(\mathbf{J}_{OA}\mathbf{J}_C\mathbf{J}_{OA}^{-1}\right)\mathbf{J}_{out}^{-1} = \mathbf{J}_U\mathbf{J}_C\mathbf{J}_U^{-1} \qquad \text{where } \mathbf{J}_U = \mathbf{J}_{out}\mathbf{J}_{OA} \in SU(2)$$

B.H. Park, et al., "Jones matrix analysis for a polarization-sensitive optical coherence tomography system using fiber-optic components," Optics Letters 29(21): 2512-4 (2004).
B.H. Park, et al., "Optic axis determination accuracy for fiber-based polarization-sensitive optical coherence tomography," Optics Letters 30(19): in press (2005).

Jones matrix solution

- With two sets of measurable incident and transmitted polarization states, $\mathbf{J}_T$ can be determined as follows

$$\begin{bmatrix} H' \\ V' \end{bmatrix} = e^{i\Delta\psi} \underbrace{\mathbf{J}_{out}\mathbf{J}_S\mathbf{J}_{out}^{-1}}_{\mathbf{J}_T} \begin{bmatrix} H \\ V \end{bmatrix} \quad \Rightarrow \quad \begin{bmatrix} H_1' \\ V_1' \end{bmatrix} = e^{i\Delta\psi_1}\mathbf{J}_T \begin{bmatrix} H_1 \\ V_1 \end{bmatrix} \text{ and } \begin{bmatrix} H_2' \\ V_2' \end{bmatrix} = e^{i\Delta\psi_2}\mathbf{J}_T \begin{bmatrix} H_2 \\ V_2 \end{bmatrix}$$

$$\begin{bmatrix} H_1' & H_2' \\ V_1' & V_2' \end{bmatrix} = e^{i\Delta\psi_1}\mathbf{J}_T \begin{bmatrix} H_1 & e^{i\alpha}H_2 \\ V_1 & e^{i\alpha}V_2 \end{bmatrix} \quad \Rightarrow \quad \mathbf{J}_T = e^{-i\Delta\psi_1} \begin{bmatrix} H_1' & H_2' \\ V_1' & V_2' \end{bmatrix} \begin{bmatrix} H_1 & e^{i\alpha}H_2 \\ V_1 & e^{i\alpha}V_2 \end{bmatrix}^{-1}$$

- An expression for $\mathbf{J}_C$ can then be derived:

$$\mathbf{J}_T = \underbrace{\begin{bmatrix} e^{i\phi} & 0 \\ 0 & e^{-i\phi} \end{bmatrix}\begin{bmatrix} \cos\theta & -\sin\theta \\ \sin\theta & \cos\theta \end{bmatrix}}_{\mathbf{J}_U} \underbrace{\begin{bmatrix} P_1e^{i\eta/2} & 0 \\ 0 & P_2e^{-i\eta/2} \end{bmatrix}}_{\mathbf{J}_C} \underbrace{\begin{bmatrix} \cos\theta & \sin\theta \\ -\sin\theta & \cos\theta \end{bmatrix}\begin{bmatrix} e^{-i\phi} & 0 \\ 0 & e^{i\phi} \end{bmatrix}}_{\mathbf{J}_U^{-1}}$$

$$e^{i\Delta\psi_1}\underbrace{\begin{bmatrix} P_1e^{i\eta/2} & 0 \\ 0 & P_2e^{-i\eta/2} \end{bmatrix}}_{\mathbf{J}_C} = \underbrace{\begin{bmatrix} \cos\theta & \sin\theta \\ -\sin\theta & \cos\theta \end{bmatrix}\begin{bmatrix} e^{-i\phi} & 0 \\ 0 & e^{i\phi} \end{bmatrix}}_{\mathbf{J}_U^{-1}} \underbrace{\begin{bmatrix} H_1' & H_2' \\ V_1' & V_2' \end{bmatrix}\begin{bmatrix} H_1 & e^{i\alpha}H_2 \\ V_1 & e^{i\alpha}V_2 \end{bmatrix}^{-1}}_{\mathbf{J}_T} \underbrace{\begin{bmatrix} e^{i\phi} & 0 \\ 0 & e^{-i\phi} \end{bmatrix}\begin{bmatrix} \cos\theta & -\sin\theta \\ \sin\theta & \cos\theta \end{bmatrix}}_{\mathbf{J}_U}$$

B.H. Park, et al., "Jones matrix analysis for a polarization-sensitive optical coherence tomography system using fiber-optic components," Optics Letters 29(21): 2512-4 (2004).
B.H. Park, et al., "Optic axis determination accuracy for fiber-based polarization-sensitive optical coherence tomography," Optics Letters 30(19): in press (2005).

Optic axis ambiguity

- $\mathbf{J}_C$, $\mathbf{J}_S$, and $\mathbf{J}_T$ are related by unitary transforms and are equivalent (diattenuation and birefringence) except for their coordinate systems (optic axis).

$$\mathbf{J}_C = \begin{bmatrix} P_1 e^{i\eta/2} & 0 \\ 0 & P_2 e^{-i\eta/2} \end{bmatrix} \qquad \mathbf{J}_S = \mathbf{J}_{OA}\mathbf{J}_C\mathbf{J}_{OA}^{-1} \qquad \mathbf{J}_T = \mathbf{J}_{out}\mathbf{J}_S\mathbf{J}_{out}^{-1}$$

- Where the plane of possible optic axes for $\mathbf{J}_S$ is constrained to the QU-plane, the effect of the system fibers in $\mathbf{J}_{out}$ rotates the frame of reference such that the overall plane of possible optic axes of $\mathbf{J}_T$ is rotated off the QU-plane.

- Solving for $\mathbf{J}_U$ finds some rotation that brings the plane of possible optic axes back down onto the QU-plane.

- This process results in two inherent ambiguities in the recovered optic axis that affect all fiber-based PS-OCT systems:
  - An offset caused by a rotation within the plane.
  - An π-ambiguity, or indeterminacy in sign related to the tilt of the pl

- ***Relative optic axes can be compared only within a single image, and not from image to image without a priori knowledge.***

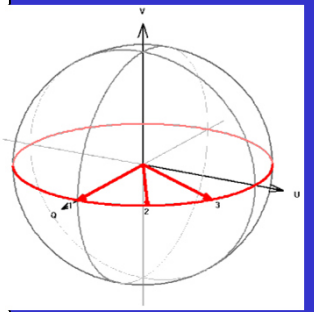

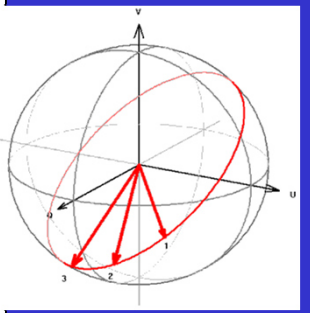

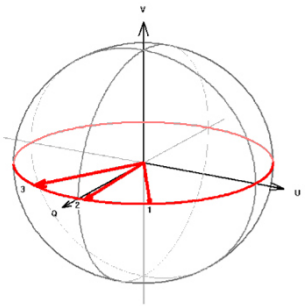

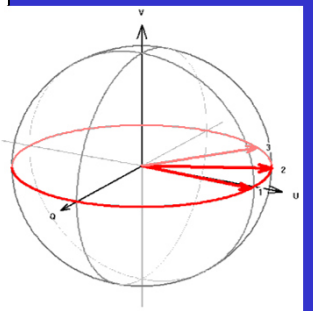

B.H. Park, et al., "Jones matrix analysis for a polarization-sensitive optical coherence tomography system using fiber-optic components," Optics Letters 29(21): 2512-4 (2004).
B.H. Park, et al., "Optic axis determination accuracy for fiber-based polarization-sensitive optical coherence tomography," Optics Letters 30(19): in press (2005).

Birefringence

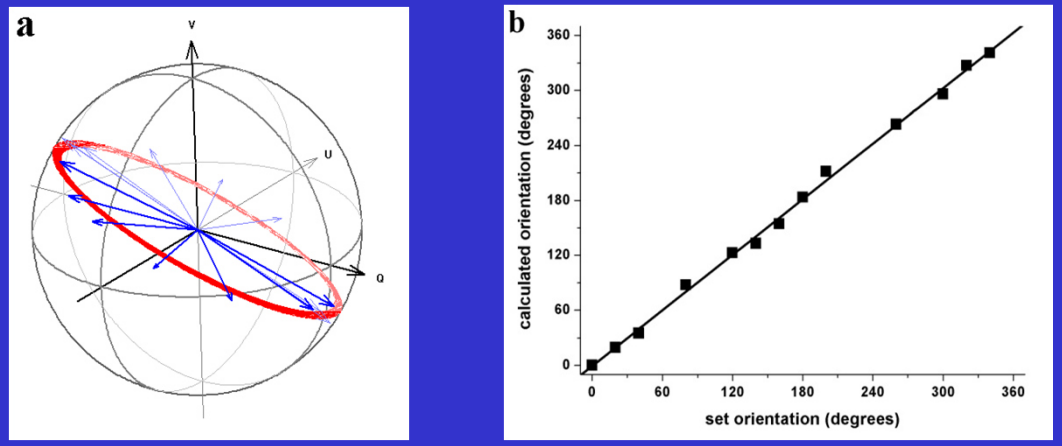

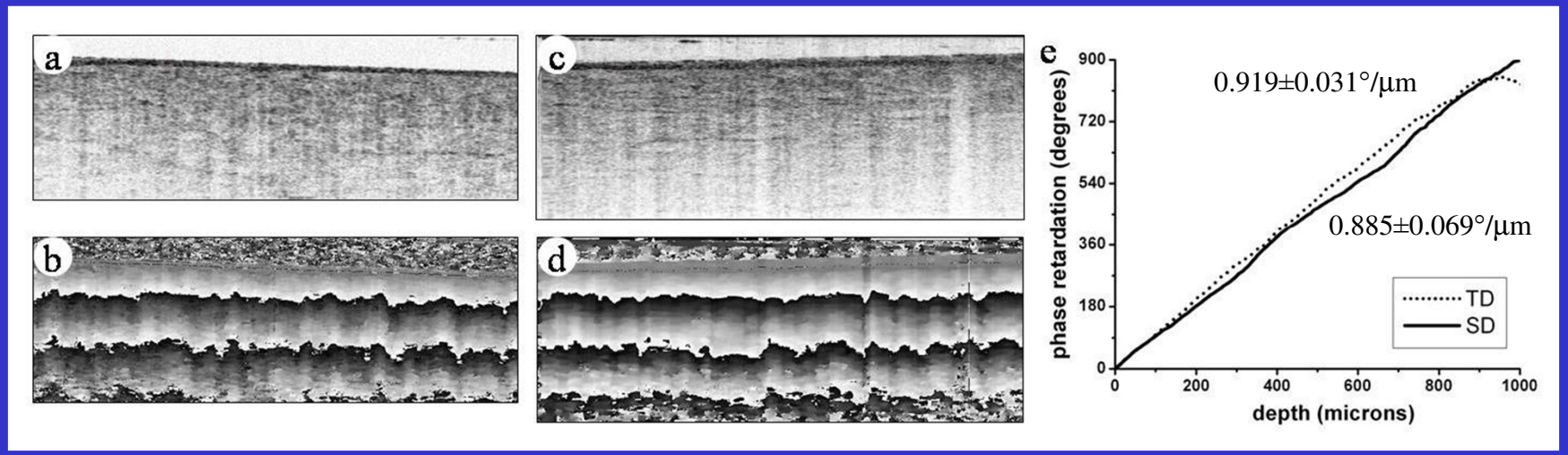

B.H. Park, et al., "Real-time fiber-based multi-functional spectral-domain optical coherence tomography at 1.3 mm," Optics Express 13(11): 3931-3944 (2005).

Phase error vs. SNR

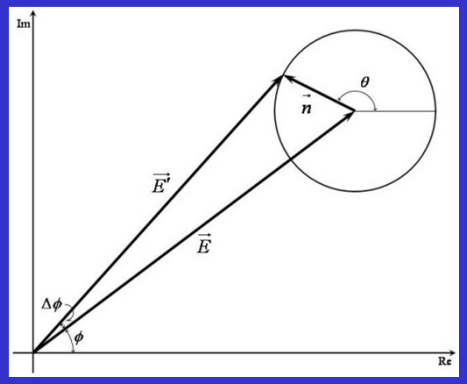

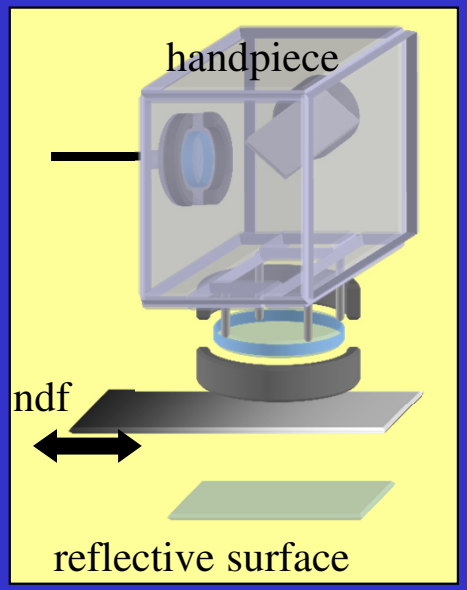

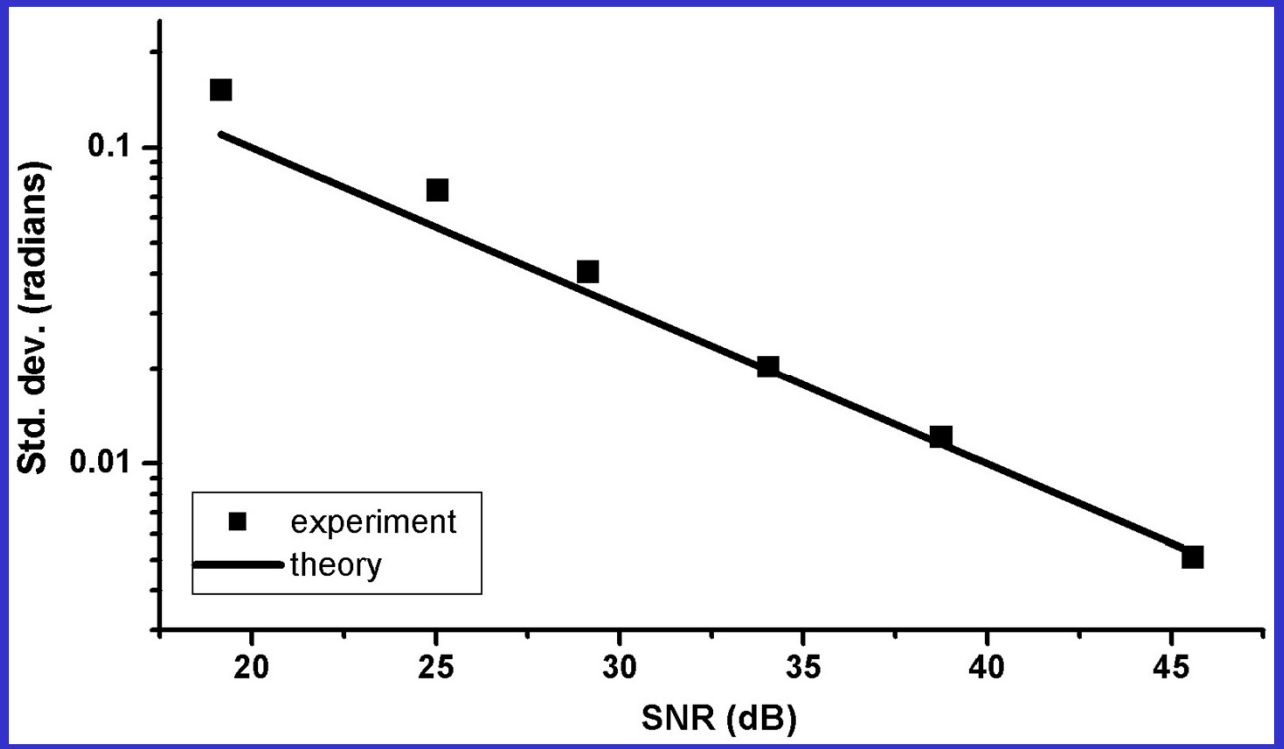

$$\sigma_{\Delta\phi} = \sqrt{2\sigma_{\phi'}^2} = (\mathrm{SNR})^{-1/2}$$

B.H. Park, et al., "Real-time fiber-based multi-functional spectral-domain optical coherence tomography at 1.3 mm," Optics Express 13(11): 3931-3944 (2005).

Cancer degrades the collagen matrix

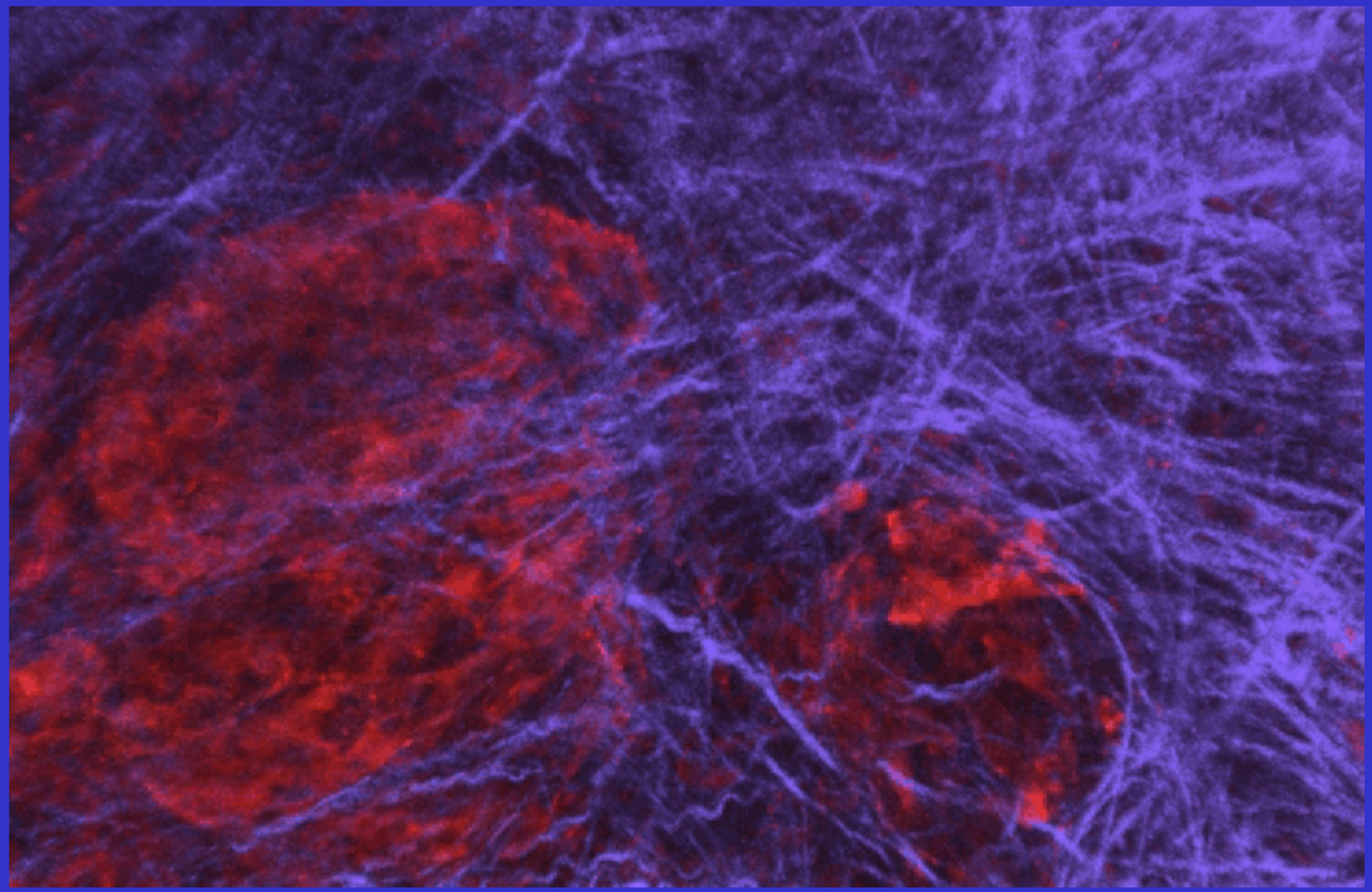

Cancer (red) in collagen matrix (blue)

"PDK1 regulates cancer cell motility by antagonising inhibition of ROCK1 by RhoE." Pinner S, Sahai E. Nat Cell Biol. 2008 Feb;10(2):127-37.

matrix metalloproteinase

PS-OCT endoscopic imaging of the human vocal fold in vivo

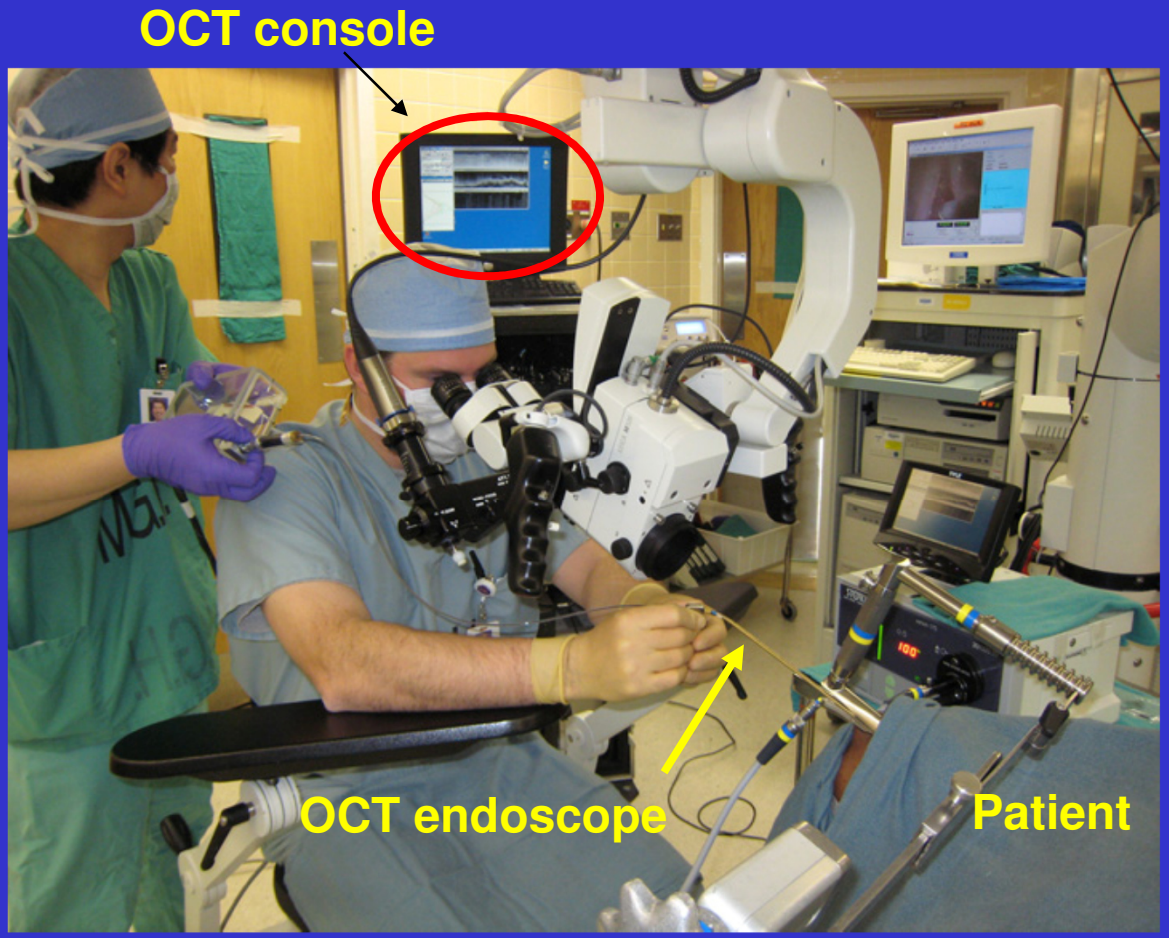

- in awake patients in office or clinic, through endoscope
- under general anesthesa in OR, through suction tube

Vocal Fold imaging: Cancer case

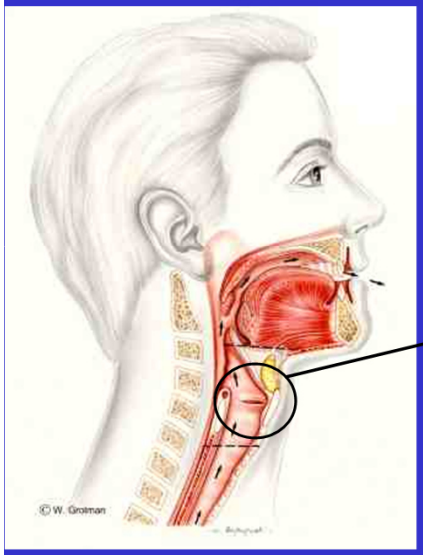

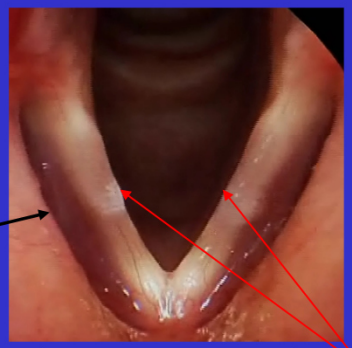

view from top

vocal folds

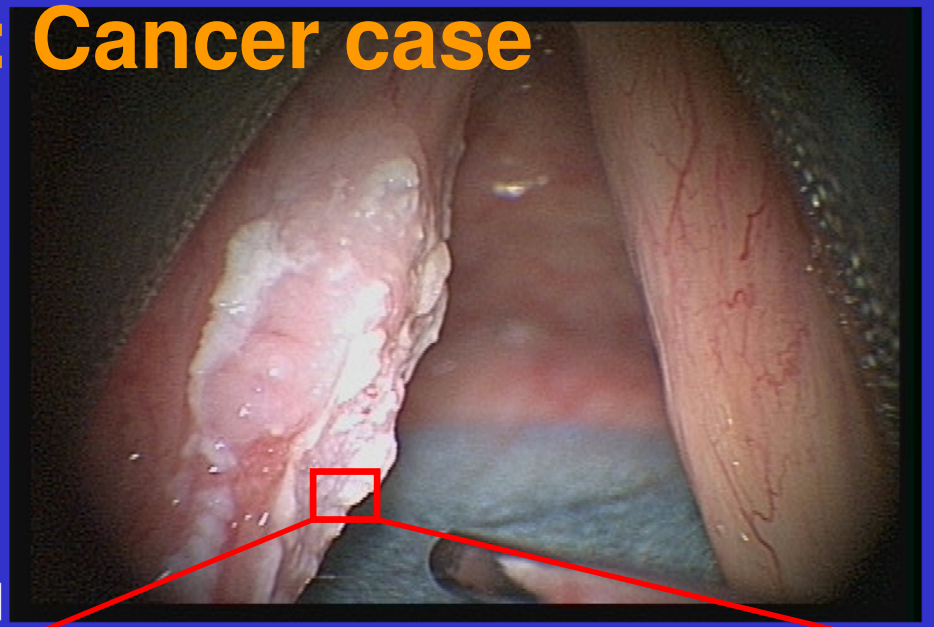

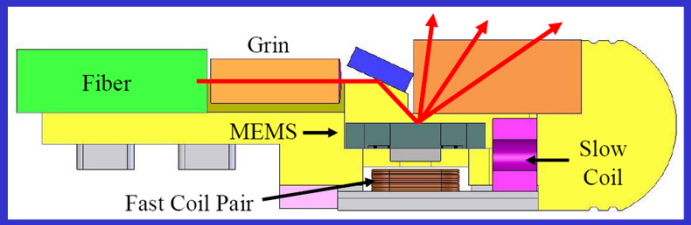

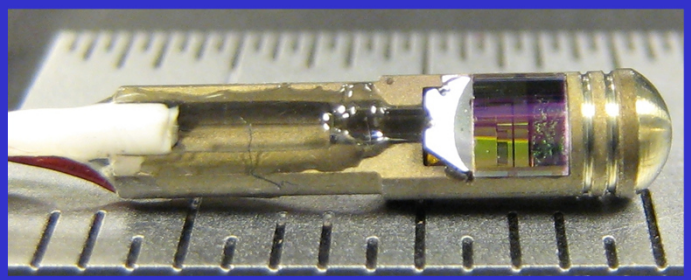

MEMS based scanner

Cancer

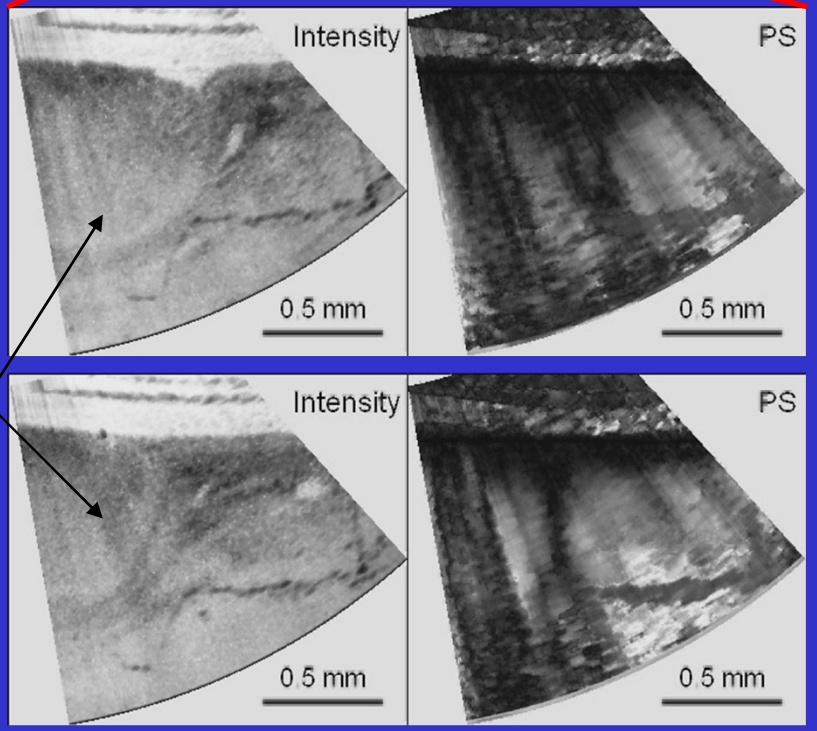

K.H. Kim et al. Optics Express 18 14644 (2010)

OCT structural an PS images

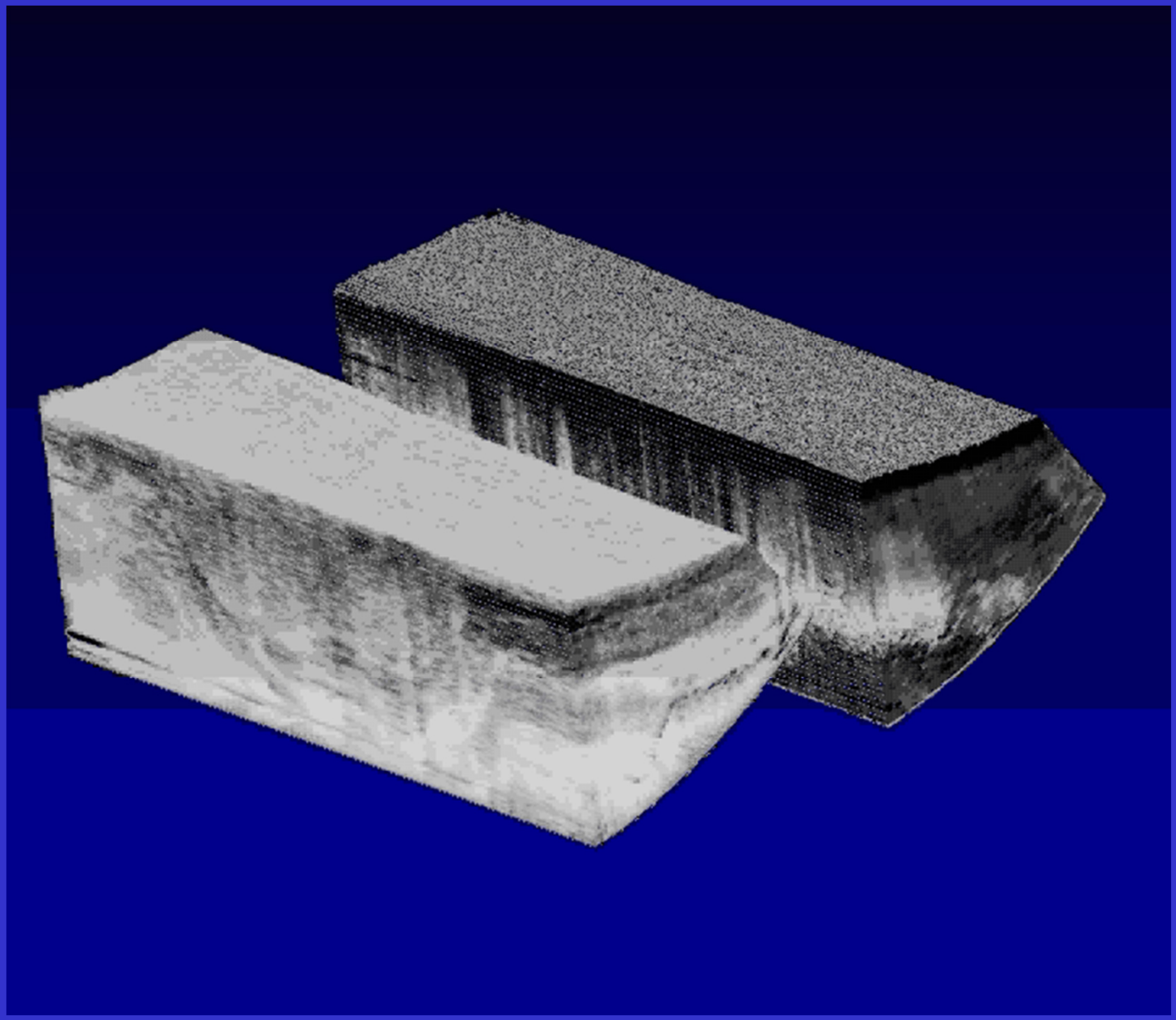

K.H. Kim et al. Optics Express 18 14644 (2010)

PS-OFDI image: mouse cancer model, in-vivo

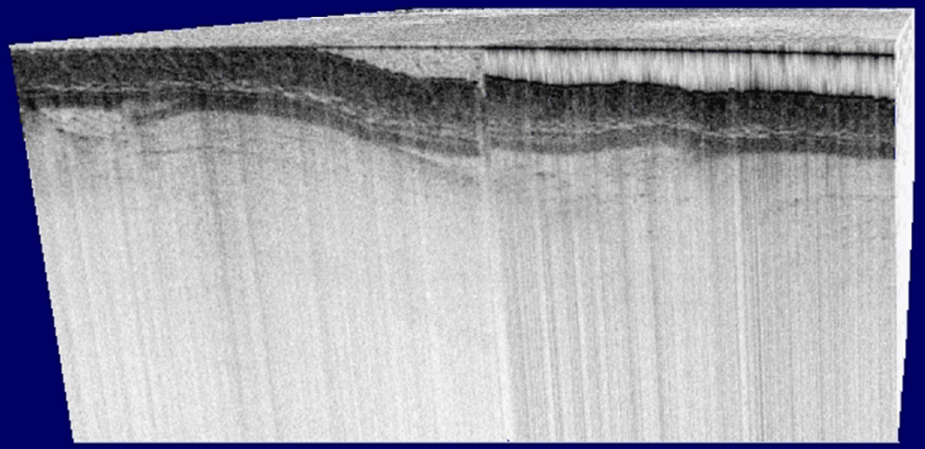

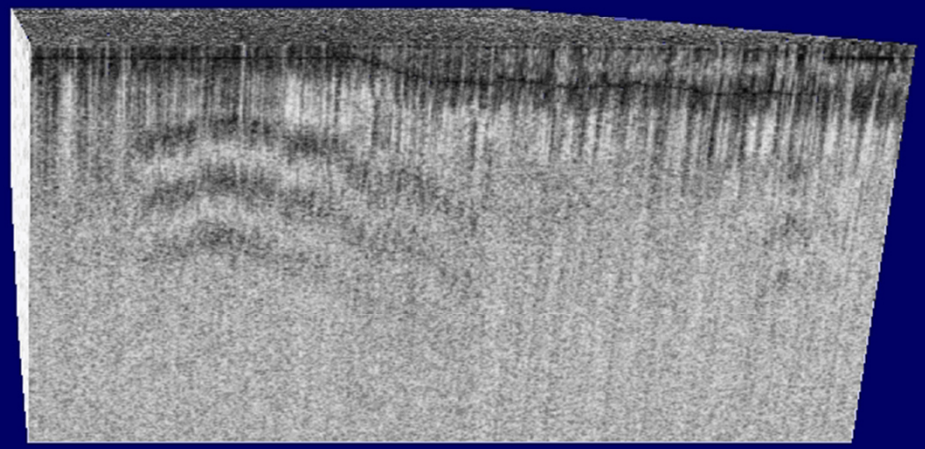

- Injection of cancer cells into the back leg
- Imaging on day 3 after injection
- 10 mm (W) x 10 mm (L) x 2.3 mm (D)

K.H. Kim et al. Optics Express 19 (2) 552 (2011)

Acknowledgement

JFdB group members

Barry Cense
B. Hyle Park
Nader Nassif
Mircea Mujat
Hyungsik Lim
Charles Kerbage
Ki Hean Kim
Martijn de Bruin
Yueli Chen
Mattijs de Groot
Boy Braaf
Bryan Haslam
Koen Vermeer
Arni Sicam

BB and GT Group:

Ray Chan

Andy Yun Group

Edward Lee

Clinical collaborators

Glaucoma: Teresa C. Chen, MD,
AMD: John Loewenstein, MD,
Suzie Chang, MD, Joan Miller, MD
ENT: Steve Zeitel, Jim Burns

Fellow Faculty WODG

Brett E. Bouma, Gary J. Tearney
Andy Yun

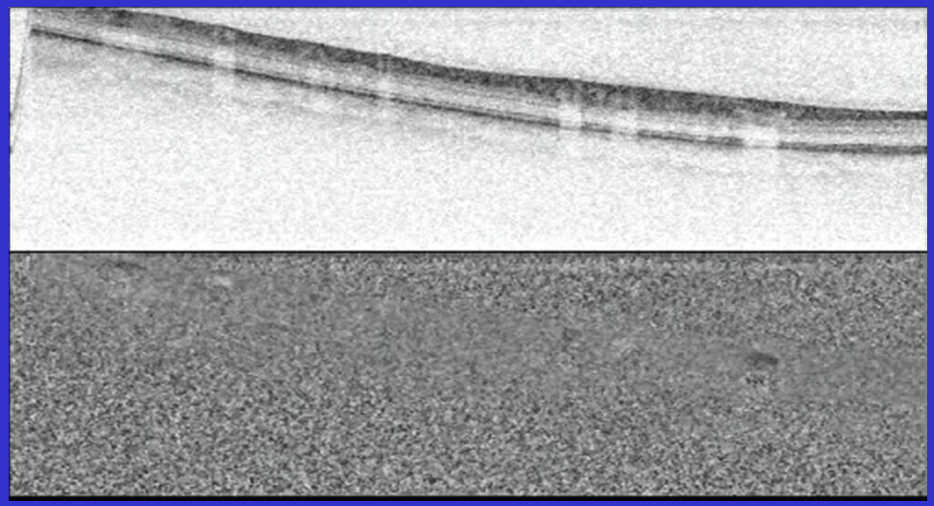

NIH (R01 RR19768, R01 EY14975), CIMIT, Department of Defense (F4 9620-01-1-0014), Gift from Dr. and Mrs. J.S. Chen to the Wellman Center for Photomedicine.